The Dissertation Committee for Yanadet Sripanich
certifies that this is the approved version of the following dissertation:

Seismic anisotropy analysis using Muir-Dellinger parameters

Committee:

Sergey B. Fomel, Supervisor

Paul J. Fowler

Mrinal K. Sen

Kyle T. Spikes

Carlos Torres-Verdin

Seismic anisotropy analysis using Muir-Dellinger parameters

by

Yanadet Sripanich, B.S.Geo.Sci., B.S.Math.

DISSERTATION

Presented to the Faculty of the Graduate School of

The University of Texas at Austin

in Partial Fulfillment

of the Requirements

for the Degree of

DOCTOR OF PHILOSOPHY

THE UNIVERSITY OF TEXAS AT AUSTIN

May 2017

Dedicated to my family

Acknowledgments

When you smile at one, he smiles at you.
So one little smile makes two.
By just cheering heart of love and of care.
Let us smile, and smile, and not forget
Smiles are welcome everywhere.
Smiles — a musical composition by H.M. King Bhumibol Adulyadej of Thailand

---

I owe a great deal to many people whom I have crossed paths with since I started my academic journey in the United States at Brewster Academy, NH, in 2008. Despite my short time there, I am grateful to the people I met and aided me in my hard times settling in the new environment. I acknowledge Chris Brown and Raylene Davis in particular for their tremendous support both academically and mentally. My second stop was at Kent School, CT. It was still one of the toughest years of my life but I was also very fortunate to be surrounded by amazing companions: Andy Chan, Samantha Drayson, Frank Huang, Ched Ramyarupa, and Pakorn Srimongkol to name a few. I'm also grateful to Dr. Kenneth Corey and Dr. Ben Nadire for their mentorship.

I decided to attend the University of Texas at Austin after my first visit to the campus in the Fall of 2008 and I have never regretted that decision. I have spent the most incredible eight years of my life here in Austin and never once hesitated to call

it my second home. Throughout my undergraduate career in the first four years, I have enjoyed state-of-the-art education and being surrounded by like-minded friends who are truly passionate about the Earth and its geology. I especially thank my first geology professor, Dr. Jaime Barnes, for her teachings that ignited my curiosity and passion about geology. I am also thankful to Dr. Elizabeth Catlos, Dr. Bayani Cardenas, Dr. Mark Cloos, Dr. Sergey Fomel, Dr. Omar Ghattas, Dr. Stephen Grand, Dr. Mark Helper, Dr. Matt Hornbach, Dr. Charles Kerans, Dr. Wonsuck Kim, Dr. Luc Lavier, Dr. Sharon Mosher, Dr. Robert Tatham, and Dr. Clark Wilson who helped make my undergraduate time full of knowledge, yet also a lot of fun. In addition, I'd like to give my special thanks to Dr. Chris Bell, Dr. Bill Carlson, and Dr. Mark Cloos whom I learned greatly from during my time in the JSG honors program. Most importantly, I am indebted to Dr. Sergey Fomel, my honors thesis advisor, and Dr. Vladimir Bashkardin, my mentor who introduced me to the world of computational seismology and the unlimited research opportunities in the field that are still ever so captivating.

It is not surprising that I chose to continue my graduate career at UT Austin under the supervision of Dr. Sergey Fomel. It was almost all 'gut' feeling on my part and I cannot be happier that I chose to stay. During my graduate career in the last four years, I have learned greatly from Dr. Björn Engquist, Dr. Victor Eijkhout, Dr. Sergey Fomel, Dr. Omar Ghattas, Dr. Bob Hardage, Thomas Hess, Dr. Kent Milfeld, Dr. Mrinal Sen, and Dr. Kyle Spikes. Being a part of the Texas Consortium of Computaional Seismology (TCCS), I have also enjoyed the companionship of Sean Bader, Lubna Barghouty, Dr. Vladimir Bashkardin, Dr. Yangkang Chen, Luke Decker, Dr. Mehdi Far, Dr. Christina Frederick, Shaunak Ghosh, Sarah Greer, Dr. Jingwei Hu, Dr. Parvaneh Karimi, Dr. Alexander Klokov, Dr. Mark Lai, Dr. Siwei Li, Dmitrii

Merzlikin, Mason Phillips, Dr. Jack Poulson, Kelly Regimbal, Yunzhi Shi, Dr. Xiaolei Song, Dr. Junzhe Sun, Ryan Swindeman, Dr. Xinming Wu, Zhiguang Xue, Yunan Yang, Dr. Hejun Zhu, Dr. Tieyuan Zhu, and many other visiting researchers during my time there. I also extend my gratitude to Karl Schleicher whom I have benefited from his experience in the industry on several occasions. I also appreciate the help from the staff of the Department of Geological Sciences (DGS) and the Bureau of Economical Geology (BEG) whose support cannot go unrecognized. In particular, I thank Philip Guerrero and Jennifer Edwards for their administrative support and companionship. I also thank Jan Braboy, Cathy Brown, Sharon Campos, Poe Chen, Jamie Coggin, Kenneth Edwards, Melissa Garcia, Carlos Garza, Kim LaValley, Eric Potter, Reuben Reyes, Maurine Riess, Jana Robinson, and Joseph Yeh.

I have also significantly benefited from my past summer internships in Houston. Working for two summers at Schlumberger has enhanced my fundamental understanding on seismic ray theory and allowed me to experience research and development in the industrial environment. I am especially grateful to Dr. Chris Chapman, Dr. Richard Coates, Dr. Paul Fowler, Sribharath Kainkaryarm, Dr. Cintia Lapilli, Dr. Dave Nichols, and Alan Teague for being a part of my invaluable experience at Schlumberger. Despite the downturn in the industry, I appreciate the internship opportunity from ExxonMobil and thank their recruiters: Tonya Brahmi and Alana Robinson for such opportunity. I have learned greatly from Dr. John Anderson, Dr. Valeriy Brytik, Dr. William Burnett, Dr. Jonathan Liu, Dr. Rongrong Lu, Dr. Carey Marcinkovich, Dr. Jia Yan, and other colleagues at ExxonMobil.

There are several names that deserve special recognitions and I address them here alphabetically. I thank Dr. Jiubing Cheng for his introduction to the topic of wavefield decomposition. His expertise in the field was instrumental in the success

of our collaborative project. I thank Dr. Joe Dellinger whom I have shared several interesting conversations on seismic anisotropy with. His past experience in the field was crucial in the development of MD parameters in this Ph.D. dissertation. I'm indebted to Dr. Paul Fowler who has been an inspiration ever since the first time we met. His expertise in the field and insightful comments have helped me become a better research scientist. His companionship is something that I will cherish for many years to come. I thank Dr. Ivan Pšenčík for many inspiring discussions on seismic ray theory and anisotropy. His eagerness to provide explanations to my many questions was very helpful to my understanding and led to several important results in this dissertation. I'm indebted to Francis Muir, whose works serve as the foundation of this Ph.D. dissertation. Even though I have never had an opportunity to meet him in person and I never will, I hope that this dissertation sheds some light on his insightful developments that should not be left unrecognized in the past. My research interests have also led me to know Dr. Alexey Stovas, whom I thank for many valuable and useful discussions. My understanding on seismic anisotropy and seismic traveltime inversion has benefited tremendously from his expertise in the field. I thank Dr. Mrinal Sen for many fruitful conversations and his helpful teachings on fundamental seismic anisotropy. I thank Dr. Kyle Spikes for his introduction to rock physics, which has broaden my horizon and excited my interest in the field. Lastly, I thank Statoil Fellowship that has sponsored my Ph.D. research, and my mentor, Dr. Yaping Zhu, for his comments on my work and for the support he has given.

My gratitude also goes to my Ph.D. dissertation committee: Dr. Sergey Fomel, Dr. Paul Fowler, Dr. Mrinal Sen, Dr. Kyle Spikes, and Dr. Carlos Torres-Verdin for evaluating my work and be there with me at the end of my journey at UT Austin.

Judging by the number of times his name appears in the previous paragraphs,

it's almost needless to say that I owe a tremendous amount of gratitude towards my undergraduate and Ph.D. advisor, Dr. Sergey Fomel. He has been there with me since the first day I stepped into the world of researchers. He has shared with me his passion for scientific research, his integrity a researcher should possess, his profound technical knowledge, his courage to undertake the most difficult problems, his skills honed for many years to solve them, and his vision of reproducible research to share his discovery with the world. He has fostered me and my colleagues to be independent thinkers capable of taking on unknown challenges of the future. And for that, he will always be my inspiration and I will forever be grateful that I have had him as my advisor. Thank you, Sergey.

Last but not least, I dedicate this disseration to my family — my beloved parents, Boonmee and Kakkaphong Sripanich, and my brother, Yantarat Sripanich. Their unconditional love and incessant support are priceless to have and the best thing that I could have ever asked for during my long academic journey and in my entire life. Although I didn't explicitly name names because this section would run for many more pages, I am sincerely thankful to my huge Thai family in Austin. I have met many wonderful people here and I hope our paths may cross again. So long, everyone !

YANADET SRIPANICH

The University of Texas at Austin
April 2017

Seismic anisotropy analysis using Muir-Dellinger parameters

Publication No. _____

Yanadet Sripanich, Ph.D.

The University of Texas at Austin, 2017

Supervisor: Sergey B. Fomel

Seismic anisotropy, defined as the dependency of seismic-wave velocities on propagation direction, is an important factor in seismic data analysis. Neglecting anisotropy can lead to significant errors in the subsurface images. Even after decades of considerable research efforts, the topic of anisotropy remains at the center of attention of the research community. In this dissertation, I address the fundamental problem of choosing parameterization to characterize the effects of seismic anisotropy and propose an alternative approach based on the Muir-Dellinger (MD) parameters. I first give their definitions and discuss their properties with respect to the classic qP-wave phase velocity in transversely isotropic (TI) media in the second chapter. I show that, when expressed in terms of MD parameters, the exact expression of phase velocity in this case is controlled by the elliptical background and two anelliptic parameters (q_1 and q_3) defined as the curvature of the qP-wave phase velocity measured along the symmetry axis and its orthogonal. The wide range of possible values for the vertical shear-wave velocity (v_{S0}) expressed under the conventional Thomsen parameterization translates to a considerably narrower range of the slope in the nearly

linear dependence between q_1 and q_3. This discovery suggests a possibility of using such a relationship to characterize the complete stiffness tensor, infer more information about the subsurface directly from qP kinematics, and provide a physical basis for reducing the number of parameters in qP-wave analysis. Based on various experimental measurements of stiffness coefficients reported in the literature, I relate such properties in shales, sandstones, and carbonates with corresponding values of slope. I further investigate this empirical linear relationship in the third chapter and show that it can also gives additional rock physics implications about the type of pore fluids. I provide some supportive evidence of its reality from self-consistent rock physics modeling and Backus averaging for shale samples. In addition, I find that both the 2D MD parameterization and its 3D extension, suitable for studies of qP waves in orthorhombic media, also provide a convenient foundation for the parameter estimation process. I carry out a detailed study on the sensitivity of MD parameters to qP-wave kinematics in comparison with other known anisotropic parameterization schemes in the fourth chapter. In the last chapter, using the MD parameters, I propose novel analytical approximations for qP-wave phase and group velocities in 2D TI and 3D orthorhombic media. The novel approximations are highly accurate and possess an advantage of having similar functional form with reciprocal coefficients, which adds practical convenience to considering both phase (wave) and group (ray) velocities. Finally, I discuss known limitations of the MD parameterization and suggest possible future research topics.

Table of Contents

List of Tables

List of Figures

Chapter 1

Introduction

MOTIVATION AND PROBLEM STATEMENT

In recent years, the oil and gas industry has faced a new challenge of exploration in *unconventional* reservoirs, which include tight-gas sands, gas and oil shales, heavy oil and tar sands, and gas-hydrate deposits (Prasad et al., 2009). These unconventional reservoirs are believed to be associated with approximately two-thirds of worldwide oil and gas reserves (Brendow, 2003). The U.S. alone possesses 10% of proven reserves from oil shales and 90% of total recoverable oil from shales totaling 1.5 trillion barrels of oil (Hepbasli, 2004). In order to economically recover unconventional resources, a complete integrated solution based on knowledge from various exploration-related aspects is necessary. Furthermore, existing techniques appropriate for conventional reservoirs must be modified for effective implementation in unconventional reservoirs.

The most notable difference observed from seismic studies in unconventional reservoirs (e.g, shales) as opposed to conventional reservoirs (e.g, massive sandstones) is the pronounced effects of seismic anisotropy in the former. Seismic anisotropy represents the dependence of seismic-wave velocity on traveling direction. It can be associated with several physical causes and can produce strong effects on seismic reflection data. Previous researchers have shown that careful studies on seismic signatures in anisotropic media can lead to useful implications on natural fracture networks, their orientation, properties, and the type of in-filled fluids (Tsvankin and

Grechka, 2011). These conclusions are invaluable because natural fractures control permeability and can be used in combination with human-induced fractures (results of hydraulic fracturing) for better drainage in the target formation. Therefore, insightful understandings and thorough treatment of seismic anisotropy and its effects is essential to a successful exploration in unconventional reservoirs.

Seismic anisotropy has a long history in the geophysical research community and its importance has been validated several times in different applications (Helbig and Thomsen, 2005). Some historical references in the context of exploration geophysics were provided by Dellinger (1991). Especially in the past few decades, seismic anisotropy has become one of the primary research areas in geophysics thanks to its prominent effects on seismic reflection data and its applications to lithological parameter estimation and seismic imaging technology. Successful handling of seismic anisotropy also benefits from recent advances in seismic acquisition technology such as wide-offset and azimuthal coverage of 3D surveys and acquisition of high-quality multi-component seismic data (Tsvankin et al., 2010).

In this dissertation, I address three major challenges that arise in seismic anisotropy and their corresponding seismic signatures in reflection data under the objective of finding seismic solutions to aid in the understanding of the subsurface especially, unconventional reservoirs. I intend to show that with an appropriate choice of anisotropic parameters that represent the combinations of stiffness tensor coefficients, the behavior of seismic wave propagation in anisotropic media can effectively be captured and some physical characteristics may be inferred. The main objectives of this research can be described as follows:

1. To understand seismic anisotropy and its effects, one must first have an effec-

tive way to characterize them. The current conventional method is based on *Thomsen* parameters (Thomsen, 1986), which characterize the effects of seismic anisotropy through some specific combinations of stiffness tensor coefficients. Dealing with anisotropic parameters (e.g, Thomsen parameters) is convenient not only because they lead to simplified expressions for seismic-wave attributes such as velocity, but also because they can be used to infer rock physics properties of the subsurface. Are there other possible choices of anisotropic parameterization ? Can any of such choices enable us to learn more about the subsurface than others ?

2. Thomsen parameters were proposed with particular emphasis on the vertical direction of wave propagation because many practical subsurface models involve approximately layered media with a vertical symmetry axis. This assumption may lead to possible complications due to the biased definitions when studying modern wide-offset data recorded farther away from the vertical axis. Similar argument holds for Thomsen-styled anisotropic parameters proposed in 3D for characterizing anisotropy induced by fractures. How do Thomsen parameters perform when dealing with information from wide-offset/azimuth ? Do they represent an optimal choice for estimating the subsurface parameters ?

3. Seismic anisotropy controls the variation of phase (wavefront) and group (ray) velocities of the propagating seismic waves with respect to the direction of propagation. Are there other possible choices for anisotropic parameters that can simplify their expressions for practical convenience, yet still maintaining a high level of accuracy ?

The main result of this work is an introduction of a set of anisotropic parame-

ters that may provide answers to these aforementioned questions. In this introductory chapter, I begin with a review of the fundamental concepts behind seismic anisotropy, discuss several important topics related to the presenting work, and end this chapter with an outline of this dissertation.

Finally, although I believe that the mathematical equations presented in this dissertation are correct and that I have properly referenced all relevant publications, I sincerely apologize for any possible errors and exclusions.

FUNDAMENTALS OF SEISMIC ANISOTROPY

In this section, I provide an introduction to seismic anisotropy. I include primarily only information that pertains to the subsequent development of this dissertation and only mention in passing other important concepts that are not directly related to this dissertation. Several classic textbooks are dedicated to a more complete treatment of the subject (e.g, Helbig, 1994; Carcione, 2001; Aki and Richards, 2002; Grechka, 2009; Tsvankin and Grechka, 2011; Tsvankin, 2012; Thomsen, 2014). In mathematical notation, the summation of repeated indices (Einstein notation) is assumed throughout the text unless mentioned otherwise.

Strain, stress, and equation of motion

Seismic waves correspond to the propagation of deformations through an elastic material. When such deformations are caused by some applied forces, the material is said to be strained and produces stress in attempt to restore itself to the unstrained state. Because of the mutual dependence between stress and strain, it can be stated that strains cannot be produced without stresses, and vice versa. The strain tensor

used to describe both changes in the volume and the shape of an arbitrarily small homogeneous cube of the material can be expressed as

$$\epsilon_{ij} = \frac{1}{2}\left(\frac{\partial u_i}{\partial x_j} + \frac{\partial u_j}{\partial x_i}\right) \ , \tag{1.1}$$

where $i, j \in \{1, 2, 3\}$ and u_i denotes the particle displacement with respect to the coordinates x_j. The strain tensor ϵ_{ij} is a unitless second-rank tensor and is also symmetric by definition. Its diagonal members ϵ_{ii} describe the relative elongation or contraction along the x_i axis, and their sum (trace of the strain tensor) denotes dilatation ($\varphi = \epsilon_{11} + \epsilon_{22} + \epsilon_{33}$), which approximately indicates the change in volume. The remaining off-diagonal coefficients control the change in shape from the deformations.

The strains in equation 1.1 are caused by forces applied to the material. The total forces consist of the body forces, f, that are applied throughout the volume and the surface forces, F, that act along the surfaces of the adjacent material elements. The latter is particularly important and is related to stress. Let us consider first the force ΔF_i exerted on the surface element ΔS, whose orientation is characterized by the unit normal $\mathbf{n}$. Therefore, the average force per unit area in the limit of infinitesimal ΔS can be expressed as follows,

$$T_i(\mathbf{n}) = \lim_{\Delta S \to 0} \frac{\Delta F_i}{\Delta S} = \frac{dF_i}{dS} \ , \tag{1.2}$$

where T_i denotes the traction vector that describes the contact force that the adjacent elements at each side of the surface characterized by $\mathbf{n}$ act upon each other. To better describe the state of stress at any given point in the material, it is more convenient to consider tractions acting on the coordinate planes defined by [x_1,x_2], [x_2,x_3], and [x_1,x_3]. This leads to the definition of stress tensor given by

$$\sigma_{ij} = T_i(x_j) \ , \tag{1.3}$$

where the traction along the surface characterized by $\mathbf{n} = n_j$ can simply be computed from

$$T_i(\mathbf{n}) = \sigma_{ij} n_j \ . \tag{1.4}$$

Similar to the strain tensor, the stress tensor is also symmetric but by a different reason. The symmetry of the stress tensor is due to the balance in angular momentum. This proof is provided by, for example, Aki and Richards (2002) and Slawinski (2010).

Let us now consider the Newton's second law of motion given by

$$\iiint_V \rho \frac{\partial^2 u_i}{\partial t^2} dV = \iint_S T_i dS + \iiint_V f_i dV \ , \tag{1.5}$$

where S denotes the surface enclosing volume V. Substituting the expression for traction in equation 1.4 and applying the divergence theorem, we can obtain

$$\iiint_V \rho \frac{\partial^2 u_i}{\partial t^2} dV = \iiint_V \frac{\partial \sigma_{ij}}{\partial x_j} dV + \iiint_V f_i dV \ , \tag{1.6}$$

that can be alternatively written as

$$\iiint_V \rho \frac{\partial^2 u_i}{\partial t^2} - \frac{\partial \sigma_{ij}}{\partial x_j} - f_i dV = 0 \ . \tag{1.7}$$

In order for the integral equation 1.7 to be zero for any arbitrary volume, the integrand must be zero. Hence, this leads to the equation of motion:

$$\rho \frac{\partial^2 u_i}{\partial t^2} = \frac{\partial \sigma_{ij}}{\partial x_j} + f_i \ . \tag{1.8}$$

Under the consideration of infinitesimal volumes, the body forces f_i are negligible and only the effects from the surface forces are significant. In other words, the gravitational effects on the volumes are insignificant in comparison with the effects from elasticity. For further details on the derivation, I refer the reader to the comprehensive summary by Slawinski (2010).

Constitutive relation: Hookean solid

In order to consider the properties of the material and to describe the propagation of seismic waves in such a medium, one has to supplement the equation of motion 1.8 with the constitutive relation that relates stress and strain. The most well-known relation for linear elasticity is referred to as Hooke's law and can be written as

$$\sigma_{ij} = c_{ijkl}\epsilon_{kl} \ , \tag{1.9}$$

where c_{ijkl} denotes the fourth-rank stiffness tensor that describe the properties of the considered material. In view of the symmetry of both strain and stress tensors, the stiffness tensor possesses the following property:

$$c_{ijkl} = c_{jikl} = c_{ijlk} \ , \tag{1.10}$$

which reduces the number of independent elements from $3^4 = 81$ to 36 parameters. Due to these symmetries, the stiffness tensor is commonly written as a 6×6 stiffness matrix under the Voigt notation with translation of indices as follows:

$$11 \to 1, \quad 22 \to 2, \quad 33 \to 3, \quad 23 \to 4, \quad 13 \to 5, \text{ and } \quad 12 \to 6 \ . \tag{1.11}$$

Therefore, the constitutive relation can be rewritten as

$$\begin{bmatrix} \sigma_{11} \\ \sigma_{22} \\ \sigma_{33} \\ \sigma_{23} \\ \sigma_{13} \\ \sigma_{12} \end{bmatrix} = \begin{bmatrix} c_{11} & c_{12} & c_{13} & c_{14} & c_{15} & c_{16} \\ c_{21} & c_{22} & c_{23} & c_{24} & c_{25} & c_{26} \\ c_{31} & c_{32} & c_{33} & c_{34} & c_{35} & c_{36} \\ c_{41} & c_{42} & c_{43} & c_{44} & c_{45} & c_{46} \\ c_{51} & c_{52} & c_{53} & c_{54} & c_{55} & c_{56} \\ c_{61} & c_{62} & c_{63} & c_{64} & c_{65} & c_{66} \end{bmatrix} \begin{bmatrix} \epsilon_{11} \\ \epsilon_{22} \\ \epsilon_{33} \\ 2\epsilon_{23} \\ 2\epsilon_{13} \\ 2\epsilon_{12} \end{bmatrix} \ . \tag{1.12}$$

Note the factor of 2 in front of the last three strain components. Alternatively, one may choose to work with stiffness matrix under the Kelvin notation, which can be

expressed as

$$\begin{bmatrix} \sigma_{11} \\ \sigma_{22} \\ \sigma_{33} \\ \sqrt{2}\sigma_{23} \\ \sqrt{2}\sigma_{13} \\ \sqrt{2}\sigma_{12} \end{bmatrix} = \begin{bmatrix} c_{11} & c_{12} & c_{13} & \sqrt{2}c_{14} & \sqrt{2}c_{15} & \sqrt{2}c_{16} \\ c_{21} & c_{22} & c_{23} & \sqrt{2}c_{24} & \sqrt{2}c_{25} & \sqrt{2}c_{26} \\ c_{31} & c_{32} & c_{33} & \sqrt{2}c_{34} & \sqrt{2}c_{35} & \sqrt{2}c_{36} \\ \sqrt{2}c_{41} & \sqrt{2}c_{42} & \sqrt{2}c_{43} & c_{44} & c_{45} & c_{46} \\ \sqrt{2}c_{51} & \sqrt{2}c_{52} & \sqrt{2}c_{53} & c_{54} & c_{55} & c_{56} \\ \sqrt{2}c_{61} & \sqrt{2}c_{62} & \sqrt{2}c_{63} & c_{64} & c_{65} & c_{66} \end{bmatrix} \begin{bmatrix} \epsilon_{11} \\ \epsilon_{22} \\ \epsilon_{33} \\ \sqrt{2}\epsilon_{23} \\ \sqrt{2}\epsilon_{13} \\ \sqrt{2}\epsilon_{12} \end{bmatrix} . \tag{1.13}$$

Despite an almost exclusive use of the Voigt notation (equation 1.12) in the geophysical literature, some advantages from using the Kelvin notation have been noted by Dellinger et al. (1998) and Chapman (2004).

An additional symmetry of the stiffness tensor can be obtained from the definition of the strain energy expressed as

$$W = \frac{1}{2} c_{ijkl} \epsilon_{ij} \epsilon_{kl} \ , \tag{1.14}$$

which denotes the total work (or energy) expended in straining the material. This potential energy is a defining property of an elastic medium, which allows the strained medium to regain its equilibrium state. Because the total work only depends on the states before and after the deformation and has to evaluate to the same quantity W regardless of the integration path, it follows that

$$c_{ijkl} = c_{klij} \ . \tag{1.15}$$

Therefore, there are only 21 independent parameters in the stiffness tensor. When a viscoelastic medium is of consideration, the constitutive relation (equation 1.9) will also involve an additional term with the derivative of strain ϵ with respect to time (Carcione, 2001). Moreover, it is also possible to consider the material to be non-linear elastic, which leads to an additional dependence of stiffness coefficients on

stress. The strain energy in this case can be written as

$$W_{non-linear} = W + \frac{1}{6} c_{ijklmn} \epsilon_{ij} \epsilon_{kl} \epsilon_{mn} \ , \tag{1.16}$$

which involves a sixth-rank tensor in addition to the strain energy W from the linear elasticity (equation 1.14). A consideration of non-linear elasticity is crucial to the analysis of stress-induced seismic anisotropy. Some references on this topic were provided by Rasalofosaon (1998) and Mavko et al. (2009). In this dissertation, I focus only on linear elasticity and adopt the Voigt notation in equation 1.12 when discussing the stiffness tensor and its components.

Material symmetry

In the previous section, it has been shown there are 21 independent stiffness coefficients that can be used to specify the property of the medium. The notion of symmetry classes used in exploration seismology were originally developed in crystal acoustics. Some historical references and more detailed descriptions were provided by Fedorov (1968), Musgrave (1970), Auld (1973), and Helbig (1994). Some of the interesting properties of the stiffness tensor such as its eigentensors were discussed by Backus (1970), Cowin (1989), and Mehrabadi and Cowin (1990). In the most general case, all 21 parameters are used and the resulting medium is called triclinic and said to have the lowest symmetry. The fewer number of the independent parameters, the higher symmetry a medium will exhibit. In seismic exploration, only triclinic (18 or 21), monoclinic (12 or 13), orthorhombic (9), and transversely isotropic (5) symmetries are usually relevant.

In this dissertation, I primarily focus on two particular symmetries: transversely isotropic and orthorhombic (orthotropic) media. Transverse isotropy is the

most commonly used anisotropic model in seismic data analysis. It is sometimes referred to as 'polar' anisotropy, as its effects are measured with respect to the 'polar' angle from the symmetry axis (Figure 1.1(a)). By definition, a transversely isotropic solid is invariant under any rotations around this symmetry axis. Some references on applications of this symmetry in global and exploration seismology were provided by Anderson (1989), Aki and Richards (2002), and Thomsen (2014). In the context of seismic exploration, transverse isotropy is generally ascribed to fine layering, and its effects can be observed in both conventional and unconventional reservoirs. In Voigt notation, the stiffness matrix for a transversely isotropic model with vertical symmetry axis (VTI) can be written as

$$c_{ij}^{TI} = \begin{bmatrix} c_{11} & c_{11}-2c_{66} & c_{13} & 0 & 0 & 0 \\ c_{11}-2c_{66} & c_{11} & c_{13} & 0 & 0 & 0 \\ c_{13} & c_{13} & c_{33} & 0 & 0 & 0 \\ 0 & 0 & 0 & c_{55} & 0 & 0 \\ 0 & 0 & 0 & 0 & c_{55} & 0 \\ 0 & 0 & 0 & 0 & 0 & c_{66} \end{bmatrix}, \tag{1.17}$$

which involves five independent stiffness coefficients: c_{11}, c_{33}, c_{13}, c_{55}, and c_{66}. Only the first four of these coefficients are important for the studies of qP waves that I will primarily focus in this dissertation.

Recently, orthorhombic symmetry have gained popularity due to its prominent relevance to the effects of anisotropy observed in unconventional reservoirs (Figure 1.1(b)). Examples of orthorhombic media include orthogonally fractured rocks and thin fractured layers with cracks orthogonal to the layering (Schoenberg and Helbig, 1997). There are three symmetry planes in an orthorhombic model and in these planes, the seismic waves exhibit similar behavior as in TI media. The stiffness tensor

of an orthorhombic medium in Voigt notation can be written as

$$c_{ij}^{ORT} = \begin{bmatrix} c_{11} & c_{12} & c_{13} & 0 & 0 & 0 \\ c_{12} & c_{22} & c_{23} & 0 & 0 & 0 \\ c_{13} & c_{23} & c_{33} & 0 & 0 & 0 \\ 0 & 0 & 0 & c_{44} & 0 & 0 \\ 0 & 0 & 0 & 0 & c_{55} & 0 \\ 0 & 0 & 0 & 0 & 0 & c_{66} \end{bmatrix} , \tag{1.18}$$

which involves nine independent stiffness coefficients: c_{11}, c_{22}, c_{33}, c_{23}, c_{13}, c_{12}, c_{44}, c_{55}, and c_{66}. Unlike the case of TI media, all nine coefficients are relevant in consideration of qP waves.

Any rotations of the coordinate frame results in a change of apparent stiffness tensor as (e.g, Helbig, 1994):

$$c'_{i'j'k'l'} = \mathcal{R}_{i'i}\mathcal{R}_{j'j}\mathcal{R}_{k'k}\mathcal{R}_{l'l}c_{ijkl} , \tag{1.19}$$

where $\mathcal{R}$ is a rotation matrix given by

$$\mathcal{R}_{ij} = \frac{\partial x'_i}{\partial x_j} . \tag{1.20}$$

This operation can lead to a change in apparent symmetry of the same material under different choices of coordinate system. Bond transformation allows one to accomplish similar rotations on the stiffness matrix under Voigt notation. A concise description of Bond transformation was given by Chapman (2004). Throughout this dissertation, I assume that the reference coordinate frame matches with the symmetry planes and both stiffness matrices of TI and orthorhombic media can be expressed exactly as in equations 1.17 and 1.18.

Elastic wave equation

Equipped with the constitutive relation (Hooke's law) in equation 1.9, we can now return to the equation of motion (equation 1.8). Substituting both Hooke's law

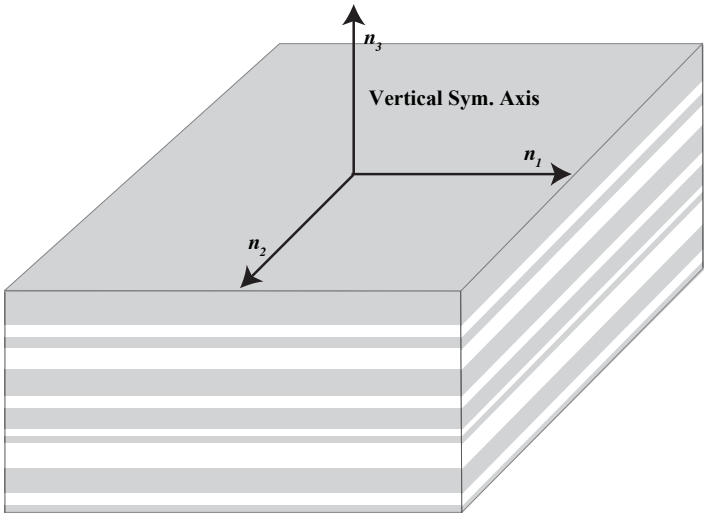

(a)

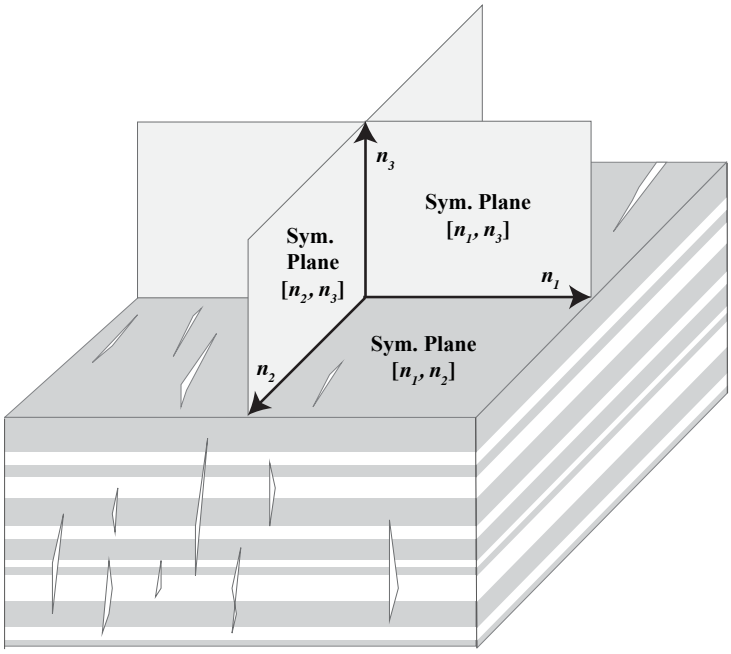

(b)

Figure 1.1: Illustrations showing (a) an example of transversely isotropic medium with vertical symmetry axis (VTI) and (b) an example of orthorhombic medium. disser-intro/. TI1,ortho1

and the definition of strain tensor to the equation of motion, we arrive at the elastic wave equation,

$$\rho \frac{\partial^2 u_i}{\partial t^2} = \frac{\partial}{\partial x_j} \left(c_{ijkl} \frac{\partial u_k}{\partial x_l} \right) \ , \tag{1.21}$$

which represents a system of second-order partial differential equations (PDEs) that governs the propagation of displacement vector u_i given the property of the medium c_{ijkl}. Alternatively, one may choose to consider a coupled system of first-order PDEs as follows:

$$\rho \frac{\partial v_i}{\partial t} = \frac{\partial \sigma_{ij}}{\partial x_j} \ , \tag{1.22}$$

$$\frac{\partial \sigma_{ij}}{\partial t} = c_{ijkl} \frac{\partial v_k}{\partial x_l} \ , \tag{1.23}$$

where $v_i = \frac{\partial u_i}{\partial t}$ denotes the velocity vector. The latter system involves only c_{ijkl} but not its spatial derivatives, which might be indeterminate. It can also be rearranged to form yet another second-order system in stress instead of displacement that can be expressed as

$$\frac{\partial^2 \sigma_{ij}}{\partial t^2} = c_{ijkl} \ \frac{\partial}{\partial x_l} \left(\frac{1}{\rho} \frac{\partial \sigma_{km}}{\partial x_m} \right) \ . \tag{1.24}$$

It is important to emphasize that the numerical implementation of equation 1.21 is often done under the assumption that the material, specified by c_{ijkl} and density ρ, is spatially locally homogeneous and the term involving spatial derivatives of c_{ijkl} can be safely dropped. This assumption is exact when the medium is truly homogeneous but is only approximate when the medium is heterogeneous (e.g, Cheng and Kang, 2014; Du et al., 2014). Equation 1.21 under this assumption can be expressed as

$$\rho \frac{\partial^2 u_i}{\partial t^2} = c_{ijkl} \frac{\partial^2 u_k}{\partial x_l \partial x_j} \ . \tag{1.25}$$

A recent development by Sun et al. (2016) sheds some light on the importance of the previously dropped term for seismic modeling in heterogeneous anisotropic media. In the following text, I start by considering elastic waves in a homogeneous anisotropic medium that are governed by equation 1.25. I will visit the exact equation 1.21 for elastic waves in heterogeneous anisotropic media again during a later discussion on its high-frequency solution.

Plane waves and the Christoffel equation

Let us consider first a homogeneous anisotropic medium and describe the solution to the associated elastic wave equation 1.25 by a vectorial transient plane wave given by

$$u_i = A_i F\big(t - T(\mathbf{x})\big) \ , \tag{1.26}$$

where A_i is an amplitude vector and F denotes an analytical waveform at time $T(\mathbf{x})$. Substituting the plane-wave solution 1.26 into equation 1.25 with an assumption that $F'' \neq 0$ leads to

$$\frac{c_{ijkl}}{\rho} p_j p_l A_k - A_i = 0 \ , \tag{1.27}$$

where $p_j = \frac{\partial T}{\partial x_j}$ denotes the slowness vector in the direction of wavefront normal (phase direction). Equation 1.27 is commonly referred to as the Christoffel equation, where the term $\Gamma_{ik} = \frac{c_{ijkl}}{\rho} p_j p_l$ is called the Christoffel matrix. An alternative formulation of equation 1.27 can be written as

$$\left[\frac{c_{ijkl}}{\rho} n_j n_l - v_{phase}^2 \delta_{ik}\right] A_k = 0 \ , \tag{1.28}$$

where n_j denotes the unit phase direction and v_{phase} denotes the phase velocity. It follows from the definition of the Christoffel matrix that it is symmetric and because of the symmetries 1.10 and 1.15 of the stiffness tensor, it is also positive-definite.

This fact turns the Christoffel equation 1.27, or equivalently equation 1.28, into an eigenvalue-eigenvector problem with the following properties:

1. There are three positive eigenvalues that correspond to the phase velocities squared v^2_{phase} of the three possible elastic waves: qP, qS1, and qS2. I use the notation of qS1 to represent the faster secondary (shear) waves and qS2 for the slower ones.

2. The phase velocities v^2_{phase} of all elastic waves depend on the phase direction (n_i) that the waves propagate.

3. In transversely isotropic media, one shear-wave is always polarized in the isotropy plane orthogonal to the symmetry axis and this wave is referred to as qSH waves. The other shear wave (qSV) is polarized in the plane that contains the symmetry axis. Both qSV and qSH waves have the same velocity along the direction of the symmetry axis but can be different otherwise.

4. In other lower-symmetry media, the convention on phase velocities—$v_{qP} \geq v_{qS1} \geq v_{qS2}$—is used to distinguish different wave modes at any given phase direction. Even though the first equality in this convention is theoretically possible, it is an oddity and is not normally observed (Grechka, 2009). On the other hand, the second equality is commonly observed and gives rise to shear-wave singularities (Crampin and Yedlin, 1981; Crampin, 1984, 1991). When both shear waves do not propagate with the same velocity, they create the shear-wave splitting phenomenon.

5. The eigenvectors correspond to the polarization vectors (A_i) and they are mutually orthogonal to one another due to the symmetry of Christoffel matrix.

They are generally different from the phase direction but there exists a special circumstance where the polarization vector of qP waves can be the same as the phase direction (Helbig, 1994).

Rays and high-frequency solutions

In the last section, it is shown that the Christoffel equation 1.27 governs the elastic wave propagation in homogeneous anisotropic media. What happens when the medium is heterogeneous ? Let us go back to the elastic wave equation 1.21 and suppose that we are propagating waves that have sufficiently high frequencies so that the medium can be deemed approximately locally homogeneous. The most popular method of studying these high-frequency waves is the ray series method, where the solution to the elastic wave equation can be approximated as

$$u_i = F\big(t - T(\mathbf{x})\big) \sum_{n=0}^{\infty} \frac{A^{(n)}(x_i)}{(-i\omega)^n} \ . \tag{1.29}$$

Equation 1.29 is similar to the plane-wave solution in equation 1.26 if only the term $n = 0$ is considered. This simplified solution is referred to as the zeroth-order ray approximation and can sufficiently describe the kinematics of elastic waves. Higher-order terms are important for accurate computations of frequency-dependent amplitudes.

Substituting the zeroth-order ray approximation, which is similar to the plane-wave solution as before, into the elastic wave equation 1.21, we can derive (Červený, 2001):

$$N_i \frac{\partial^2 F}{\partial t^2} - M_i \frac{\partial F}{\partial t} + L_i F = 0 \ , \tag{1.30}$$

where

$$N_i = c_{ijkl} A_k \frac{\partial T}{\partial x_l} \frac{\partial T}{\partial x_j} - \rho A_i \ , \tag{1.31}$$

$$M_i = c_{ijkl} \frac{\partial A_k}{\partial x_l} \frac{\partial T}{\partial x_j} + \frac{\partial}{\partial x_j} \left(c_{ijkl} A_k \frac{\partial T}{\partial x_l} \right) \ , \tag{1.32}$$

$$L_i = \frac{\partial}{\partial x_j} \left(c_{ijkl} \frac{\partial A_k}{\partial x_l} \right) \ . \tag{1.33}$$

If one consider the waveform F to be time-harmonic plane waves given by $F(t) = \exp[-i\omega t]$, then equation 1.30 becomes

$$-N_i \omega^2 + M_i \omega + L_i = 0 \ . \tag{1.34}$$

It is clear that under the high-frequency assumption, the terms $N_i\omega^2$ and $M_i\omega$ dominate. To ensure that equation 1.30 is satisfied, we put

$$N_i = 0 \qquad \text{and} \qquad M_i = 0 \ . \tag{1.35}$$

The last term associated with L_i is only important in the analysis of high-order ray approximation and we choose to neglect it at the present. The former condition $N_i = 0$ leads to the same Christoffel equation 1.27 as in the case of homogeneous anisotropic media, while the latter condition $M_i = 0$ leads to the transport equation that describes the variation of wavefront amplitudes associated with the derivatives of A_k. Therefore, under the high-frequency approximation, the kinematics of the solution to the elastic wave equation in heterogeneous media can be described by the same Christoffel equation for a homogeneous media with properly specified local medium parameters. Two comprehensive books by Červený (2001) and Chapman (2004) provide further details on this topic.

Equipped with this knowledge, we can now proceed to study the kinematics (e.g, traveltime) of any wave mode as it travels through the medium using ray tracing

instead of directly solving the elastic wave equation (equation 1.25) numerically as mentioned in the previous section. Using ray tracing, one approaches wave propagation problem by tracking the movement of individual points on the wavefront, which is governed by the Christoffel equation 1.27. Let us recast the problem into another formulation with simpler notation. The Christoffel equation, in essence, relates the derivatives of traveltime T to the phase velocity v_{phase} of any particular wave mode of interest. The velocity is also dependent upon the propagation direction. Therefore, we can write

$$|\nabla T|^2 = |\mathbf{p}|^2 = s^2_{phase}(\mathbf{x}, \mathbf{n}) = \frac{1}{v^2_{phase}(\mathbf{x}, \mathbf{n})} \ , \tag{1.36}$$

where $\mathbf{p}$ is the phase slowness vector with the magnitude s_{phase}. The phase velocity squared $v^2_{phase} = 1/s^2_{phase}$ of the wave mode m is given by

$$v^2_{phase} = \frac{c_{ijkl}}{\rho} n_j n_l A^{(m)}_i A^{(m)}_k \ , \tag{1.37}$$

and is dependent on both spatial location $\mathbf{x}$ and the phase direction $\mathbf{n} = \frac{\nabla T}{|\nabla T|}$. $A^{(m)}_i$ denotes the unit polarization vectors of the wave mode m. The particular formulation in equation 1.36 is referred to as anisotropic eikonal equation, which reduces to the isotropic eikonal equation when the phase velocity is independent of phase direction.

Differentiating the anisotropic eikonal equation 1.36 with respect to some parameter ς that varies along the ray, we have

$$2\mathbf{p}\frac{d\mathbf{p}}{d\varsigma} = 2s(\mathbf{x}, \mathbf{n}) \left(\nabla_x s \frac{d\mathbf{x}}{d\varsigma} + \nabla_p s \frac{d\mathbf{p}}{d\varsigma} \right) \ , \tag{1.38}$$

which can split into the following ray tracing system:

$$\begin{aligned} \frac{d\mathbf{x}}{d\varsigma} &= \mathbf{p} - s\nabla_p s \ , \\ \frac{d\mathbf{p}}{d\varsigma} &= s\nabla_x s \ . \end{aligned} \tag{1.39}$$

Several other choices of equivalently valid ray tracing system were reported and discussed by Červený (2001). From equation 1.39, it follows that

$$\frac{\partial \mathbf{n}}{\partial \mathbf{p}} = \frac{1}{|\mathbf{p}|}(\mathbf{I} - \mathbf{n}\mathbf{n}^T) \ , \tag{1.40}$$

where $\mathbf{I}$ is an identity matrix. Therefore, we can compute the change in traveltime T along the ray from

$$\begin{aligned} \frac{dT}{d\varsigma} &= \nabla T \cdot \frac{d\mathbf{x}}{d\varsigma} \ , \\ &= \mathbf{p} \cdot (\mathbf{p} - s\nabla_p s) \ , \\ &= \mathbf{p} \cdot (\mathbf{p} - (\mathbf{I} - \mathbf{n}\mathbf{n}^T)\nabla_n s) \ , \\ &= \mathbf{p} \cdot \mathbf{p} - s\mathbf{n}^T(\mathbf{I} - \mathbf{n}\mathbf{n}^T)\nabla_n s \ , \\ &= \mathbf{p} \cdot \mathbf{p} = s^2 \ . \end{aligned} \tag{1.41}$$

Finally, the general ray (group) velocity, denoting the derivative of $\mathbf{x}$ with respect to time, can be expressed as

$$\mathbf{v}_{group} = \frac{d\mathbf{x}}{dT} = v_{phase}\mathbf{n} + (\mathbf{I} - \mathbf{n}\mathbf{n}^T)\nabla_n v_{phase} \ . \tag{1.42}$$

It represents the velocity at which a point (blob of energy) on the wavefront propagates and is generally different from the phase velocity (v_{phase}) in the direction of the wavefront normal ($\mathbf{n}$). Hence, the group velocity plot mimics the shape of the traveling wavefront. The formula in equation 1.42 for group velocity is general and can be applied to any anisotropic media.

From phase to group

Consider Figure 1.2 where I plot group velocity (equation 1.42) in a transversely isotropic medium. The plot mimics the wavefront emanating from a point

source in the middle of the figure. The wavefront represents a constant phase surface —i.e, a set of points at the same stage of the wavelet— and the energy riding such surface travels directly along a radial line from the source (Dellinger, 1991). We can clearly see the difference between the two directions.

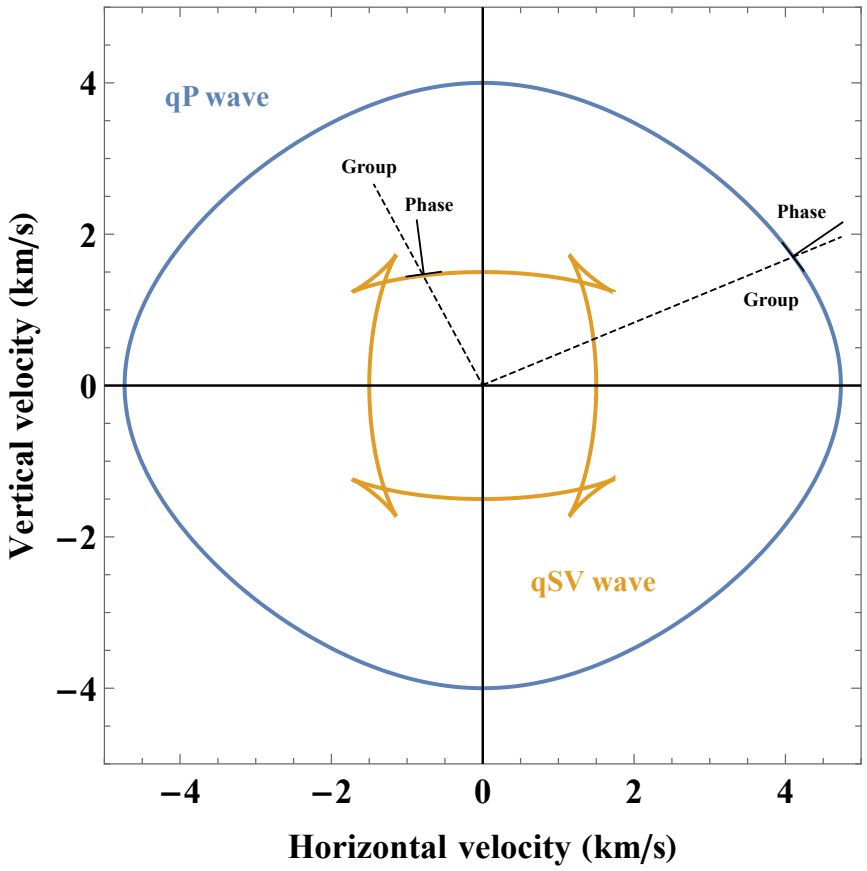

Figure 1.2: A group velocity plot, which mimics a wavefront emanating from a point source in the middle of the figure in a transversely isotropic medium. The energy (group) travels straight out from the source. The phase direction points along the wavefront normal and is different from the energy (group) velocity. It is also possible for energy to travel with multiple velocities as shown by the triplications on the qSV wavefront. disser-intro/. groupvs15

A schematic diagram in Figure 1.3 that shows the geometrical relationship between phase and group velocities. Here, I follow Dellinger (1991) and use elliptical

group velocity as an example. Because group velocity represents a wavefront created by a point source ($\star$), the tangent line to any point on the group velocity curve represents a plane wave radiated from the point source. Since a plane wave travels in the direction of its normal, a solid line drawn from the source to meet the tangent line at right angle indicates the plane-wave propagation (phase) direction and its length indicates the phase velocity. Therefore, the locus of such intersections maps out the phase-velocity curve.

A second line (dashed) can be drawn from the source to the intersection point of the tangent line and the group velocity surface. It represents the shortest direction in which the energy can travel from the source to that position and denotes the group direction. Its length corresponds to the magnitude of the group velocity. Using this relationship, one can consider two right triangles—ABC and ACD—and relates the phase velocity to the group velocity, and vice versa.

To demonstrate the last point, let us first consider $\triangle ABC$ and the general expression for group velocity (equation 1.42) as shown in Figure 1.4. The first term in the right-hand side denotes the phase-velocity vector $v_{phase}\mathbf{n}$. The second term can be separated into two parts: $\nabla_n v_{phase}$ and $\mathbf{n}\mathbf{n}^T\nabla_n v_{phase}$. The former is simply the gradient of the phase-velocity curve, which is orthogonal to the curve itself. The latter is the projection of this gradient onto the phase direction $\mathbf{n}$. Subtracting the two leads to the component of $\nabla_n v_{phase}$ that lives in the plane defined by the phase direction $\mathbf{n}$. This particular plane also contains the tangent line to the group-velocity curve that we discussed previously. Therefore, despite its somewhat complicated derivation, the general group velocity 1.42 holds a simple geometrical meaning.

We can also attempt to convert group velocity to phase velocity. Let us now

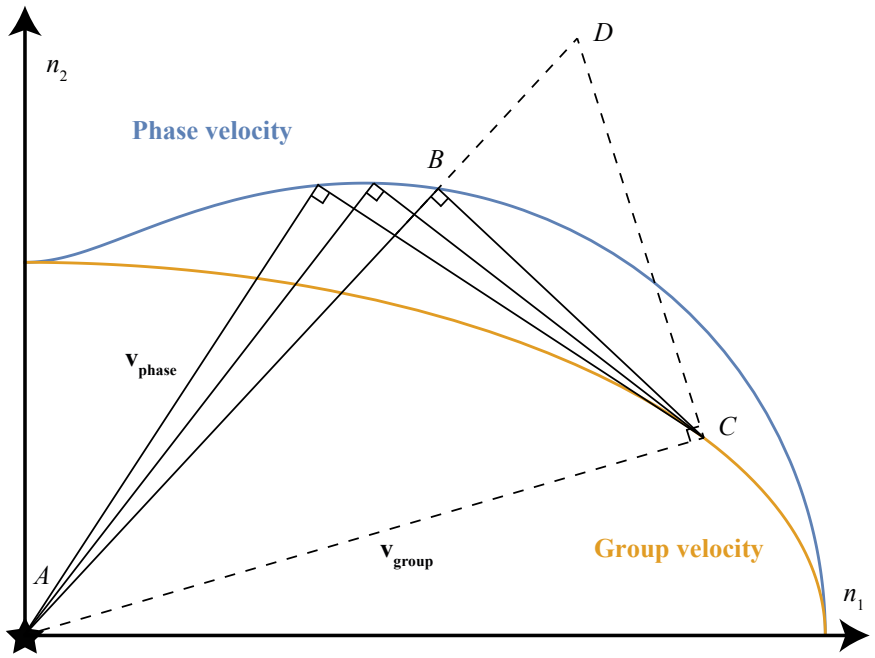

Figure 1.3: A diagram showing geometrical relationship between phase and group velocities. In this example, group velocity is an ellipse. disser-intro/. phaseandgroup

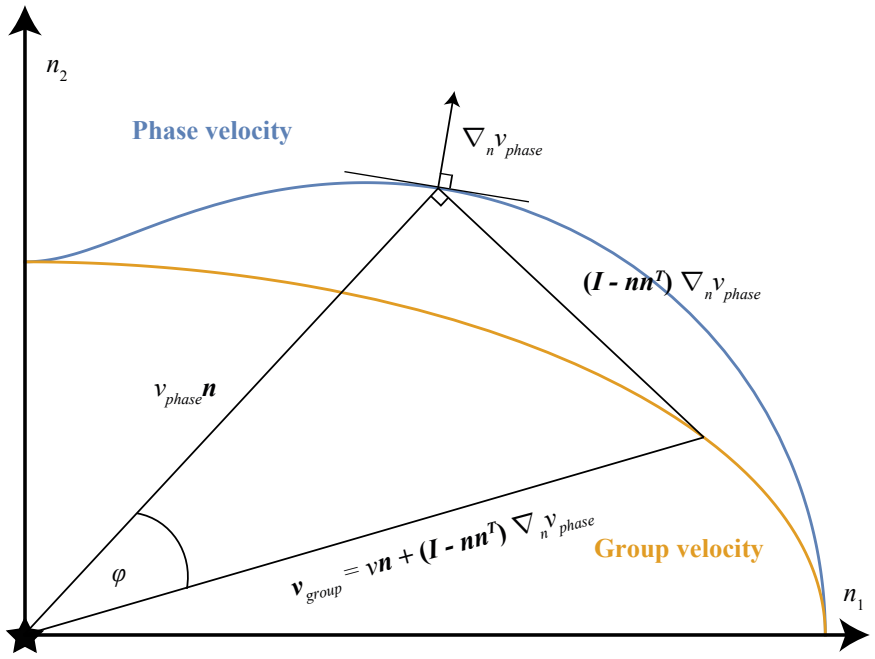

Figure 1.4: A diagram showing geometrical relationship when converting from phase velocity to group velocity. disser-intro/. phasetogroup

consider $\triangle ACD$ as shown in Figure 1.5. Proceeding in a similar fashion as before, we arrive at

$$\cos\varphi = \angle CAD = \frac{v_{group}}{|v_{group}\mathbf{N} + (\mathbf{I} - \mathbf{N}\mathbf{N}^T)\nabla_N v_{group}|} \ , \tag{1.43}$$

where I use the capital $\mathbf{N}$ to denote the group direction. From Figure 1.4, we also know that

$$\cos\varphi = \angle BAC = \frac{v_{phase}}{v_{group}} \ . \tag{1.44}$$

Therefore, we can compute the phase velocity from the group velocity using the following expression:

$$\mathbf{v}_{phase} = v_{phase}\mathbf{n} = \left(\frac{v_{group}^2}{|v_{group}\mathbf{N} + (\mathbf{I} - \mathbf{N}\mathbf{N}^T)\nabla_N v_{group}|} \right) \mathbf{n} \ , \tag{1.45}$$

where the unit phase direction n can be found from

$$\mathbf{n} = \frac{v_{group}\mathbf{N} + (\mathbf{I} - \mathbf{N}\mathbf{N}^T)\nabla_N v_{group}}{|v_{group}\mathbf{N} + (\mathbf{I} - \mathbf{N}\mathbf{N}^T)\nabla_N v_{group}|} \ . \tag{1.46}$$

Equation 1.46 also implies that one can obtain the phase direction $\mathbf{n}$ by starting from the group direction $\mathbf{N}$ and stepping in the direction of the projected group-velocity gradient as shown in Figure 1.5.

Now, let us return to the general expression for group velocity (equation 1.42) and rewrite it in terms of the phase slowness (s_{phase}) and the group slowness (s_{group}),

$$\frac{\mathbf{N}}{s_{group}} = \frac{1}{s_{phase}^2} \left(s_{phase}\mathbf{n} - (\mathbf{I} - \mathbf{n}\mathbf{n}^T)\nabla_n s_{phase} \right) \ . \tag{1.47}$$

With a simple algebraic manipulation, we arrive at

$$s_{group}\mathbf{N} = \left(\frac{s_{phase}^2}{|s_{phase}\mathbf{n} - (\mathbf{I} - \mathbf{n}\mathbf{n}^T)\nabla_n s_{phase}|} \right) \mathbf{N} \ , \tag{1.48}$$

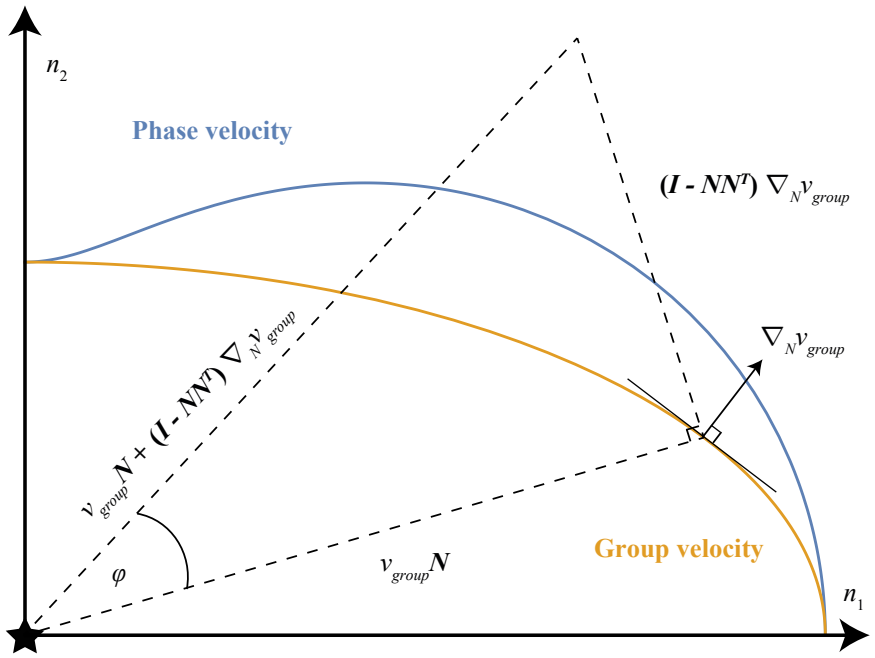

Figure 1.5: A diagram showing geometrical relationship when converting from group velocity to phase velocity. disser-intro/. grouptophase

where

$$\mathbf{N} = \frac{s_{phase}\mathbf{n} - (\mathbf{I} - \mathbf{n}\mathbf{n}^T)\nabla_n s_{phase}}{|s_{phase}\mathbf{n} - (\mathbf{I} - \mathbf{n}\mathbf{n}^T)\nabla_n s_{phase}|} \ , \tag{1.49}$$

Equation 1.48 has a strikingly similar mathematical pattern to equation 1.45 except the minus sign in front of $\mathbf{I} - \mathbf{n}\mathbf{n}^T$, which controls the direction of the projected gradient but does not affect the total magnitude of its summation with the term $s_{phase}\mathbf{n}$. This fact implies that one can obtain the group direction $\mathbf{N}$ by starting from the phase direction n and stepping in the opposite direction of the projected slowness gradient, which agrees with the observation we made earlier from equation 1.46. This finding results in the phase velocity and the group slowness being 'polar reciprocals', which can also be proved for the case of phase slowness and group velocity as well. Some historical references on this topic were provided by Dellinger (1991).

Because of this interesting symmetry, one can look at, for example, the phase-slowness curve and make some implications about the wavefront in a straightforward manner. I show in the next section that this approach is particularly useful for detecting triplications on the wavefront. Figure 1.6 shows the corresponding phase slowness to the wavefront (group velocity) in Figure 1.2. Notice the triplications on the qSV wavefront that are related to the concave part of the phase-slowness curve. Finally, it is important to note that this symmetry between the polar reciprocals also holds in 3D and all the presented schematics depict the situation in the plane that contains both phase and group-velocity vectors of interest.

Triplications

The polar reciprocity between the group velocity and the phase slowness enables us to analyze a condition for the occurrence of triplications on the wavefront. It can be inferred from the reciprocity that the group direction is always perpendicular to the phase-slowness curve and the phase direction is always perpendicular to the group-velocity curve. An alternative proof of this fact was given by Claerbout (1985) from the definition of the group velocity in the frequency domain:

$$\mathbf{v}_{group} = \nabla_k \omega \ , \tag{1.50}$$

where ω is the angular frequency, $\mathbf{k}$ is the spatial frequency and they can be related to the phase velocity as $v_{phase} = \omega/|\mathbf{k}|$. A graph of the dispersion relation $\omega(\mathbf{k})$ is commonly shown with the axes k_i/ω for some constant ω. It is obvious that the group velocity, by definition, represents the gradient of the dispersion relation, hence the group direction is perpendicular to the surface of constant ω displayed in the $\mathbf{k}$ space. This surface is simply a plot of the phase slowness $s_{phase} = |\mathbf{k}|/\omega$.

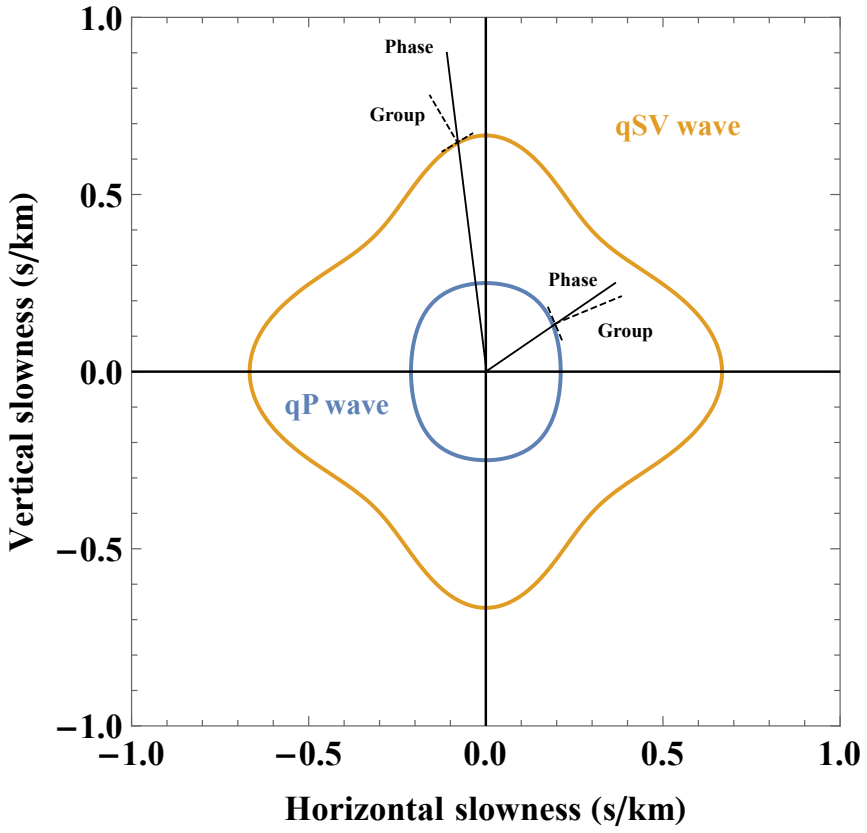

Figure 1.6: A phase-slowness plot corresponding to the group-velocity plot in Figure 1.2. Note the triplications on the qSV wavefront that are associated with the concave part of the phase-slowness curve. disser-intro/. phasevs15

Because the group velocity is perpendicular to the phase-slowness surface, it can be observed that if the phase-slowness surface has a concavity, then there exists multiple values of the phase slowness that map to the same group direction. This phenomenon is present on the qSV wavefront in Figure 1.2 and the concavity is shown in Figure 1.6. Apart from the concavity, some triplications can also be associated with saddle-shaped areas. Several analytical conditions for different kinds of triplications exist and I refer the reader to the the following works for further details (Musgrave, 1970; Dellinger, 1991; Vavryčuk, 2003). One may also compute a numerical Gaussian curvature and use it as an indicator of a concavity on the phase-slowness surface (Ivanov and Stovas, 2016).

Energy constraints and anomalous polarizations

Let us now return to the stiffness matrices of transversely isotropic and orthorhombic media that I will be working with throughout this dissertation. In this section, I discuss their energy constraints and additional conditions to prevent anomalous polarizations.

To ensure that the strain energy of an elastic material is positive, equation 1.17 must be positive-definite, which is equivalent to having positive determinants for all its leading principal minors and the matrix itself (Slawinski, 2010). Let us first notice that the VTI stiffness in equation 1.17 consists of two submatrices:

$$\begin{bmatrix} c_{11} & c_{11}-2c_{66} & c_{13} & 0 & 0 & 0 \\ c_{11}-2c_{66} & c_{11} & c_{13} & 0 & 0 & 0 \\ c_{13} & c_{13} & c_{33} & 0 & 0 & 0 \\ 0 & 0 & 0 & 0 & 0 & 0 \\ 0 & 0 & 0 & 0 & 0 & 0 \\ 0 & 0 & 0 & 0 & 0 & 0 \end{bmatrix} \quad \text{and} \quad \begin{bmatrix} 0 & 0 & 0 & 0 & 0 & 0 \\ 0 & 0 & 0 & 0 & 0 & 0 \\ 0 & 0 & 0 & 0 & 0 & 0 \\ 0 & 0 & 0 & c_{55} & 0 & 0 \\ 0 & 0 & 0 & 0 & c_{55} & 0 \\ 0 & 0 & 0 & 0 & 0 & c_{66} \end{bmatrix}, \tag{1.51}$$

where rows and columns of zero can be disregarded in computation of determinants

of principal minors. Therefore, it is sufficient to only consider

$$\begin{bmatrix} c_{11} & c_{11}-2c_{66} & c_{13} \\ c_{11}-2c_{66} & c_{11} & c_{13} \\ c_{13} & c_{13} & c_{33} \end{bmatrix} \quad \text{and} \quad \begin{bmatrix} c_{55} & 0 & 0 \\ 0 & c_{55} & 0 \\ 0 & 0 & c_{66} \end{bmatrix} , \tag{1.52}$$

There are seven principal minors associated with the first submatrix but only five of them are independent:

1. $\det\big(\begin{bmatrix} c_{11} \end{bmatrix}\big) > 0$, which implies that $c_{11} > 0$.

2. $\det\big(\begin{bmatrix} c_{33} \end{bmatrix}\big) > 0$, which implies that $c_{33} > 0$.

3. $\det\left(\begin{bmatrix} c_{11} & c_{11}-2c_{66} \\ c_{11}-2c_{66} & c_{11} \end{bmatrix}\right) > 0$, which implies that $c_{11} > c_{66} > 0$.

4. $\det\left(\begin{bmatrix} c_{11} & c_{13} \\ c_{13} & c_{33} \end{bmatrix}\right) > 0$, which implies that $c_{11}c_{33} > c_{13}^2$.

5. $\det\left(\begin{bmatrix} c_{11} & c_{11}-2c_{66} & c_{13} \\ c_{11}-2c_{66} & c_{11} & c_{13} \\ c_{13} & c_{13} & c_{33} \end{bmatrix}\right) > 0$, which implies that $c_{33}(c_{11}-c_{66}) > c_{13}^2$.

Similar analysis on the second submatrix can be done and leads to the conditions that $c_{55} > 0$ and $c_{66} > 0$. Because $c_{66} > 0$, the condition 5 from the analysis of the first submatrix is stronger than condition 4. In summary, the energy constraints for TI media can be expressed as (Dellinger, 1991; Helbig, 1994):

$$c_{11} > c_{66} > 0, \quad c_{33} > 0, \quad c_{55} > 0, \text{ and } c_{13}^2 < c_{33}(c_{11}-c_{66}) \ . \tag{1.53}$$

An additional constraint can be imposed on the TI model to prevent it from having anomalous polarizations, which implies that qP waves are no longer the fastest waves in some directions. I refer the reader to comprehensive studies on this phenomenon by Helbig and Schoenberg (1987) and Dellinger (1991). In TI media, the appropriate condition to prevent anomalous polarizations is

$$c_{13} + c_{55} > 0 \ . \tag{1.54}$$

Similar analysis can be done on an orthorhombic model (equation 1.18), whose two corresponding submatrices are

$$\begin{bmatrix} c_{11} & c_{12} & c_{13} \\ c_{12} & c_{22} & c_{23} \\ c_{13} & c_{23} & c_{33} \end{bmatrix} \quad \text{and} \quad \begin{bmatrix} c_{44} & 0 & 0 \\ 0 & c_{55} & 0 \\ 0 & 0 & c_{66} \end{bmatrix} . \tag{1.55}$$

Consequently, the energy constraints for orthorhombic media can be expressed as (Helbig, 1994):

$$\begin{aligned} & c_{11} > 0, \quad c_{22} > 0, \quad c_{33} > 0, \quad c_{44} > 0, \quad c_{55} > 0, \quad c_{66} > 0 \ , \\ & c_{11}c_{33} > c_{13}^2, \quad c_{22}c_{33} > c_{23}^2, \quad c_{11}c_{22} > c_{12}^2 \ , \\ & 2c_{12}c_{23}c_{13} + c_{11}c_{22}c_{33} > c_{13}^2 c_{22} + c_{23}^2 c_{11} + c_{12}^2 c_{33} \ . \end{aligned} \tag{1.56}$$

Additional conditions to prevent anomalous polarizations are (Stovas, 2017):

$$c_{23} + c_{44} > 0, \quad c_{13} + c_{55} > 0, \quad \text{and} \quad c_{12} + c_{66} > 0 \ . \tag{1.57}$$

Exact phase velocities

Based on the Christoffel equation 1.27, we can derive the exact phase velocities for qP waves in TI and orthorhombic media that I later use in subsequent chapters. Throughout the rest of the text I treat the elements of stiffness matrix $c_{ij} = c_{ijkl}/\rho$ as density-normalized quantities.

The exact phase velocity of qP waves in TI media has the following expression (Gassmann, 1964; Berryman, 1979):

$$\begin{aligned} v_{qP}^2(\theta) \quad = \quad & \frac{1}{2}[(c_{11} + c_{55})n_1^2 + (c_{33} + c_{55})n_3^2] + \\ & \frac{1}{2}\sqrt{[(c_{11} - c_{55})n_1^2 - (c_{33} - c_{55})n_3^2]^2 + 4(c_{13} + c_{55})^2 n_1^2 n_3^2} \ , \end{aligned} \tag{1.58}$$

where $n_1 = \sin\theta$, $n_3 = \cos\theta$, and θ is the phase angle measured from the symmetry axis. As the analog of equation 1.58, qP waves have the following explicit expression

for phase velocity in orthorhombic media (Schoenberg and Helbig, 1997; Tsvankin, 1997, 2012):

$$v_{qP}^2 = 2\sqrt{\frac{-d}{3}}\cos(\frac{\nu}{3}) - \frac{a}{3} \ , \tag{1.59}$$

where

$$\begin{aligned}
\nu &= \arccos\left(\frac{-q}{2\sqrt{(-d/3)^3}}\right) \ , \\
q &= 2\left(\frac{a}{3}\right)^3 - \frac{ab}{3} + c \ , \quad d = -\frac{a^2}{3} + b \ , \\
a &= -(G_{11} + G_{22} + G_{33}) \ , \\
b &= G_{11}G_{22} + G_{11}G_{33} + G_{22}G_{33} - G_{12}^2 - G_{13}^2 - G_{23}^2 \ , \\
c &= G_{11}G_{23}^2 + G_{22}G_{13}^2 + G_{33}G_{12}^2 - G_{11}G_{22}G_{33} - 2G_{12}G_{13}G_{23} \ ,
\end{aligned}$$

and

$$\begin{aligned}
G_{11} &= c_{11}n_1^2 + c_{66}n_2^2 + c_{55}n_3^2 \ , \\
G_{22} &= c_{66}n_1^2 + c_{22}n_2^2 + c_{44}n_3^2 \ , \\
G_{33} &= c_{55}n_1^2 + c_{44}n_2^2 + c_{33}n_3^2 \ , \\
G_{12} &= (c_{12} + c_{66})n_1n_2 \ , \\
G_{13} &= (c_{13} + c_{55})n_1n_3 \ .
\end{aligned}$$

Here, $n_1 = \sin\theta\cos\phi$, $n_2 = \sin\theta\sin\phi$, $n_3 = \cos\theta$, θ is zenith phase angle (measured from n_3), and ϕ is azimuthal phase angle (measured from n_1) in the local orthorhombic frame of reference where the axes n_1, n_2, and n_3 are intersections of the corresponding planes of symmetry. In both media, the corresponding group-velocity expressions can be determined from equation 1.42.

DEFINITIONS OF ANISOTROPIC PARAMETERIZATIONS

When dealing with seismic anisotropy and its effects, it is more preferable to work with anisotropic parameters, which represent combinations of elastic moduli (stiffness coefficients) believed to characterize the most important seismic-wave signatures in anisotropic media. These useful parameters allow complex formulas to be expressed in a concise manner with the complexity hidden inside the notation and can be related to some physical properties. I discuss the concept of anisotropic parameterization in this section. A summary table for the anisotropic parameterization schemes that I consider is shown in Table 1.1. Muir-Dellinger parameters serve as the foundation of this dissertation and will be discussed in details in Chapter 2.

TI parameterizations	Orthorhombic parameterizations
Thomsen parameters (Thomsen, 1986)	Tsvankin parameters (Tsvankin, 1997)
Alkhalifah parameters (Alkhalifah, 1998, 2000a, 2003)	
Chapman-Miller-Fowler parameters (Chapman and Miller, 1996; Fowler, 2015)	
Muir-Dellinger parameters (Muir and Dellinger, 1985; Sripanich and Fomel, 2015)	

Table 1.1: Different TI parameterizations and their extensions to orthorhombic media.

Thomsen-Tsvankin parameters

In the current geophysical community, the conventional anisotropic parameterization is Thomsen's parameterization, which was proposed by Thomsen (1986).

The set of TI parameters under Thomsen's notation include:

$$
\begin{aligned}
v_{P0} = \sqrt{c_{33}} \quad , \quad v_{S0} = \sqrt{c_{55}} \\
\epsilon = \frac{c_{11} - c_{33}}{2c_{33}} \quad , \quad \gamma = \frac{c_{66} - c_{55}}{2c_{55}} \\
\delta = \frac{(c_{13} + c_{55})^2 - (c_{33} - c_{55})^2}{2c_{33}(c_{33} - c_{55})} \ ,
\end{aligned}
\tag{1.60}
$$

where c_{ij} denotes density-normalized stiffnesses and v_{P0} and v_{S0} denote the velocities of qP and qS waves along the symmetry axis. In the case of VTI media, the symmetry axis is simply the vertical direction. Additionally, ϵ, δ, and γ are dimensionless parameters that govern the directional dependency of velocity. Parameters ϵ and γ control the velocities of qP and qSH waves orthogonal to the symmetry axis; δ influences intermediate velocities between the symmetry axis and its orthogonal for qP and qSV waves. The parameter γ can be neglected in consideration of qP and qSV waves. In practice, parameter $f = 1 - v_{S0}^2/v_{P0}^2$ may be used instead of v_{S0}.

Tsvankin (1997) extended the Thomsen parameters (equation 1.60) to orthorhombic media by recognizing the similarity of the Christoffel equation in the three symmetry planes in orthorhombic media to that of TI media. The extended parameters include:

$$
\begin{aligned}
v_{P0} = \sqrt{c_{33}} \quad , \quad v_{S0} = \sqrt{c_{55}} \ , \\
\epsilon_1 = \frac{c_{22} - c_{33}}{2c_{33}} \ , \quad \epsilon_2 = \frac{c_{11} - c_{33}}{2c_{33}} \ , \\
\gamma_1 = \frac{c_{66} - c_{44}}{2c_{44}} \ , \quad \gamma_2 = \frac{c_{66} - c_{55}}{2c_{55}} \ , \\
\delta_1 = \frac{(c_{23} + c_{44})^2 - (c_{33} - c_{44})^2}{2c_{33}(c_{33} - c_{44})} \ , \\
\delta_2 = \frac{(c_{13} + c_{55})^2 - (c_{33} - c_{55})^2}{2c_{33}(c_{33} - c_{55})} \ , \\
\delta_3 = \frac{(c_{12} + c_{66})^2 - (c_{11} - c_{66})^2}{2c_{11}(c_{11} - c_{66})} \ ,
\end{aligned}
\tag{1.61}
$$

where the subscript denotes the normal to the plane of interest. Thomsen-Tsvankin parameters have led to many successes in the analysis of the kinematics and dynamics (e.g, amplitudes) of reflection data in anisotropic media. However, as pointed out by Fowler (2015), scheme 1.61 has an undesirable property of variance with respect to different choices of coordinate labeling, which results from the emphasis on the vertical symmetry axis. This is apparent from having v_{P0} and v_{S0} as separate parameters and missing ϵ_3 and γ_3 for the $[x_1, x_2]$ plane. This choice may be troublesome because it may lead to a convergence to a wrong local minimum during anisotropic parameter estimation because there are six equally valid sets of parameters depending on the choices of local coordinate labeling (Fowler, 2015).

A connection to Weak Anisotropy (WA) parameters

WA parameters consist of twenty-one members and are derived from first-order perturbation of the qP and qS phase velocities with respect to reference isotropic background velocities α and β for P and S waves (Pšenčík and Gajewski, 1998; Pšenčík and Farra, 2007; Farra and Pšenčík, 2013; Farra et al., 2016). The number of considered WA parameters can be reduced when the assumptions on the type of wave and the kind of an anisotropic model are made. In consideration of orthorhombic symmetry, WA parameters are composed of nine parameters that include

$$\begin{aligned}
\epsilon_x &= \frac{c_{11}-\alpha^2}{2\alpha^2}\ ,\ \delta_x = \frac{c_{13}+2c_{55}-\alpha^2}{\alpha^2}\ ,\ \gamma_x = \frac{c_{55}-\beta^2}{2\beta^2}\ , \\
\epsilon_y &= \frac{c_{22}-\alpha^2}{2\alpha^2}\ ,\ \delta_y = \frac{c_{23}+2c_{44}-\alpha^2}{\alpha^2}\ ,\ \gamma_y = \frac{c_{44}-\beta^2}{\beta^2}\ , \\
\epsilon_z &= \frac{c_{33}-\alpha^2}{2\alpha^2}\ ,\ \delta_z = \frac{c_{12}+2c_{66}-\alpha^2}{\alpha^2}\ ,\ \gamma_z = \frac{c_{66}-\beta^2}{\beta^2}\ ,
\end{aligned} \tag{1.62}$$

where α and β are reference P and S velocities of the isotropic background. Other advantages of WA parameters include being linear with respect to c_{ij}, free from a

variance under coordinate transformation, and being able to relate to other Thomsen-Tsvankin parameterization scheme with a proper specification of reference velocity. To elaborate on the last point, I point out that by setting $\alpha = v_{P0}$ and $\beta = v_{S0}$, WA parameters in this case can be related to Thomsen-Tsvankin parameters (equation 1.61) (Farra et al., 2016). The δ_i from this process denotes the linearized Thomsen-Tsvankin δ_i. This simple relation stems from the fact that at heart, the Thomsen-Tsvankin parameters are associated with perturbation of stiffnesses from some reference background similar to the fundamental concept behind the derivation of WA parameters, and therefore, can be regarded as specifications of WA parameters.

Alkhalifah parameters

Another approach parameterizes using the normal moveout velocity v and the anelliptic parameter η that govern the behavior of qP reflection traveltime. The Taylor expansion of reflection traveltime around zero offset can be expressed as

$$t^2(x) \approx t_0^2 + \frac{x^2}{v^2} - \frac{2\eta x^4}{v^4 t_0^2} + \cdots \ , \tag{1.63}$$

where t_0 denotes reflection traveltime along the vertical axis and x is offset. The normal moveout velocity v governs the second-order derivative of traveltime at zero offset, while the anelliptic parameter η appears in the fourth-order (quartic) term. Alkhalifah parameters are particularly useful for velocity analysis and the implementation of pseudoacoustic wave equations (Alkhalifah and Tsvankin, 1995; Alkhalifah,

1998, 2000a). In TI media, the set includes:

$$
\begin{aligned}
v_{P0} &= \sqrt{c_{33}} \quad , \quad v_{S0} = \sqrt{c_{55}} \\
v &= \sqrt{\frac{c_{13}(c_{13}+2c_{55})+c_{33}c_{55}}{c_{33}-c_{55}}} \ , \\
\eta &= \frac{c_{11}(c_{33}-c_{55})}{2c_{13}(c_{13}+2c_{55})+2c_{33}c_{55}} - \frac{1}{2} \ ,
\end{aligned}
\tag{1.64}
$$

and they are appropriate for qP and qSV waves. They can be extended to orthorhombic media as follows (Alkhalifah, 2003):

$$
\begin{aligned}
v_{P0} &= \sqrt{c_{33}} \quad , \quad v_{S1} = \sqrt{c_{44}} \ , \\
v_{S2} &= \sqrt{c_{55}} \quad , \quad v_{S3} = \sqrt{c_{66}} \ , \\
v_1 &= \sqrt{\frac{c_{23}(c_{23}+2c_{44})+c_{33}c_{44}}{c_{33}-c_{44}}} \ , \\
v_2 &= \sqrt{\frac{c_{13}(c_{13}+2c_{55})+c_{33}c_{55}}{c_{33}-c_{55}}} \ , \\
\eta_1 &= \frac{c_{22}(c_{33}-c_{44})}{2c_{23}(c_{23}+2c_{44})+2c_{33}c_{44}} - \frac{1}{2} \ , \\
\eta_2 &= \frac{c_{11}(c_{33}-c_{55})}{2c_{13}(c_{13}+2c_{55})+2c_{33}c_{55}} - \frac{1}{2} \ , \\
\eta_3 &= \frac{c_{22}(c_{11}-c_{66})}{2c_{12}(c_{12}+2c_{66})+2c_{11}c_{66}} - \frac{1}{2} \ .
\end{aligned}
\tag{1.65}
$$

Note that, in this study, we follow Stovas (2015) and replace δ_3 in the original proposition by Alkhalifah (2003) with η_3. Similar to the Thomsen-Tsvankin parameters, the emphasis is put on the vertical direction with missing v_3 for the $[x_1, x_2]$ plane. Thus, the parameterization suffers from the same problem of variance from a change in coordinate labeling (Fowler, 2015).

Chapman-Miller-Fowler parameters

Fowler (2015) extended the TI parameterization of Chapman and Miller (1996) and Schoenberg and de Hoop (2000) and proposed the following TI parameters:

$$
\begin{aligned}
&w_{P1} = c_{11} \quad , \quad w_{P3} = c_{33} \ , \\
&w_{S1} = c_{55} \quad , \quad w_{S3} = c_{66} \ , \\
&w_{PA} = c_{13} + 2c_{55} \quad \text{or} \quad \xi = \frac{1}{2}\left(\frac{w_{PA}^2}{w_{P1}w_{P3}} - 1\right) \ .
\end{aligned}
\tag{1.66}
$$

where w_{PA} is derived from the qP-wave phase velocity squared at 45° under first-order perturbation of stiffnesses. This parameter can also be substituted by a dimensionless anellipticity parameter ξ if desired. The corresponding orthorhombic extension of equation 1.66 is given as follows (Fowler, 2015):

$$
\begin{aligned}
w_{P1} = c_{11} \quad , \quad w_{P2} = c_{22} \quad , \quad w_{P3} = c_{33} \ , \\
w_{S1} = c_{44} \quad , \quad w_{S2} = c_{55} \quad , \quad w_{S3} = c_{66} \ , \\
w_{PA1} = c_{23} + 2c_{44} \quad , \quad w_{PA2} = c_{13} + 2c_{55} \ , \\
w_{PA3} = c_{12} + 2c_{66} \ ,
\end{aligned}
\tag{1.67}
$$

where the associated dimensionless anellipticity parameters are

$$
\begin{aligned}
&\xi_1 = \frac{1}{2}\left(\frac{w_{PA1}^2}{w_{P2}w_{P3}} - 1\right) \quad , \quad \xi_2 = \frac{1}{2}\left(\frac{w_{PA2}^2}{w_{P1}w_{P3}} - 1\right) \ , \\
&\xi_3 = \frac{1}{2}\left(\frac{w_{PA3}^2}{w_{P1}w_{P2}} - 1\right) \ .
\end{aligned}
\tag{1.68}
$$

This scheme is free from the variance from different choices of coordinate labeling thanks to the symmetric definitions of parameters associated with the elliptic part of the phase velocity (w_{Pi}) and the anelliptic part (w_{PAi}) pinned at 45° in each of the symmetry planes, or equivalently the dimensionless ξ_i parameters.

It is worth mentioning that the derivation of CMF parameters also stems from the concept of perturbation of stiffnesses from some reference background similar to the fundamental concept behind the derivation of WA parameters. However, the CMF parameters are defined based on an approximation of phase velocity squared and hence the unit of velocity squared in all parameters. On the other hand, the WA parameters are defined to indicate the relative change of phase velocity (equation 1.62) with respect to the background and thus, they are dimensionless. To further explain this point, let us consider the expression for the first-order approximation of phase velocity squared for qP waves in TI media (Pšenčík and Gajewski, 1998):

$$V^2_{phase}(\mathbf{n}) \approx \alpha^2(1 + 2\epsilon_x n_1^4 + 2\epsilon_z n_3^4 + 2\delta_x n_1^2 n_3^2) \ , \tag{1.69}$$

where $n_1 = \sin\theta$, $n_3 = \cos\theta$, and θ is the phase angle measured from the symmetry axis. ϵ_x, ϵ_z, and δ_x are WA parameters given in equation 1.62. Equation 1.69 can be rewritten in the following form (Pšenčík and Gajewski, 1998):

$$V^2_{phase}(\mathbf{n}) \approx c_{11} n_1^4 + c_{33} n_3^4 + 2(c_{13} + 2c_{55}) n_1^2 n_3^2 \ , \tag{1.70}$$

which shows that this approximation is independent of the reference velocity α. It is clear that the CMF parameters (equation 1.66) are related to the coefficients of equation 1.70 and are defined differently from WA parameters. The importance of the similar combinations of c_{ij} was noticed by Chapman and Pratt (1992) in the context of traveltime tomography in weakly anisotropic media. The same argument holds for the case of orthorhombic symmetry as well. Using this framework, it appears to be plausible to extend CMF parameters to lower-symmetry media including monoclinic and triclinic media.

Pseudoacoustic approximation

When only qP waves are of interest, the so-called *pseudoacoustic approximation* can be adopted. Under this approximation, the effects of qS-wave parameter on qP-wave velocity are neglected within the limits of seismic resolution (Alkhalifah, 1998; Fowler, 2003). Therefore, the number of dependent anisotropic parameters for qP-wave analysis in TI and orthorhombic media reduces to three and six, respectively. This reduction in the total number of dependent parameters cannot be done directly to the stiffnesses c_{ij} but is only applicable when considering some anisotropic parameterization. Different conditions to define this pseudoacoustic approximation exist for different parameterizations and are summarized later in Tables 2.2 and 2.3. Note that Thomsen parameters in TI and Tsvankin parameters in orthorhombic media were originally proposed without considering pseudoacoustic simplifications. Both phase and group velocities of qP waves can be shown to depend only on v_{P0}, ϵ, and δ under weak-anisotropy approximation without invoking pseudoacoustic approximation (Tsvankin, 2012). However, one can still use pseudoacoustic approximation when considering Thomsen-Tsvankin parameters by setting $v_{S0} = 0$ in TI media and $v_{S0} = \gamma_1 = \gamma_2 = 0$ in orthorhombic media.

To elaborate on this concept, let us consider a similar experiment of Fowler (2003) based on an example model with parameters $c_{11} = 22.4\ km^2/s^2$, $c_{13} = 13.18\ km^2/s^2$, $c_{33} = 16\ km^2/s^2$, and varying c_{55} from 0 to $6.76\ km^2/s^2$. I plot the qP-wave phase velocity with the given model parameters in Figure 1.7(a) and it is apparent that the qP phase velocity varies significantly with the change in c_{55}. Alternatively, I convert the exact formula of qP phase velocity expressed in terms of c_{ij} (equation 1.58) to Thomsen parameters (equation 2.12) and repeat the same experiment. The corresponding model parameters under Thomsen notation are given by $v_{P0} = 4$

km/s, $\epsilon = 0.2$, $\delta = -0.05$, and varying v_{S0} from 0.0 to 2.6 km/s. The resultant plot is shown in Figure 1.7(b) and it can be observed that the qP velocity in this case is almost insensitive to the change in v_{S0}. Figure 1.8 show the effects of varying v_{S0} from 0 to 2.6 km/s on the phase velocity of both qP and qSV waves. The virtual insensitivity of qP-wave phase velocity to the change in v_{S0} is observed, whereas the qSV phase velocity varies significantly. A similar observation can be made in the case of group velocity in Figure 1.9. Notice the diamond-shaped qSV wavefront that appears when setting v_{S0} to 0. This remaining qSV wave in 'acoustic' media was studied in details by Grechka et al. (2004).

In other words, under pseudoacoustic approximation, the relevant effect of vertical qS-wave velocity ($v_{S0} = \sqrt{c_{55}}$) on qP-wave velocity is included inside the retained anisotropic parameters such as δ, η, v_{PA}, and q_i in different schemes. This results in an approximate apparent insensitivity of qP-wave velocity to the remaining stand-alone qS-wave velocity term $v_{S0} = \sqrt{c_{55}}$ (Fowler, 2003). In practice, v_{S0} is normally set to zero as this process leads to more simplified expressions, although other choices can be valid as long as the value remains relatively small relative to the qP-wave velocity.

In general, pseudoacoustic approximation is advantageous when only qP waves are of consideration as it allows for seismic modeling and imaging of scalar qP waves with correct kinematics based on fewer number of dependent parameters (Alkhalifah, 1998, 2003). It is also beneficial for parameter estimation process with qP waves, where only three (TI) or six (orthorhombic) parameters as opposed to four and nine have to be inverted. However, some stability issues in seismic modeling of qP waves due to the assumption of setting $v_{S0} = 0$ were reported and discussed in, for example, Fowler et al. (2010), Bakker and Duveneck (2011), Zhang et al. (2011), Bube et al.

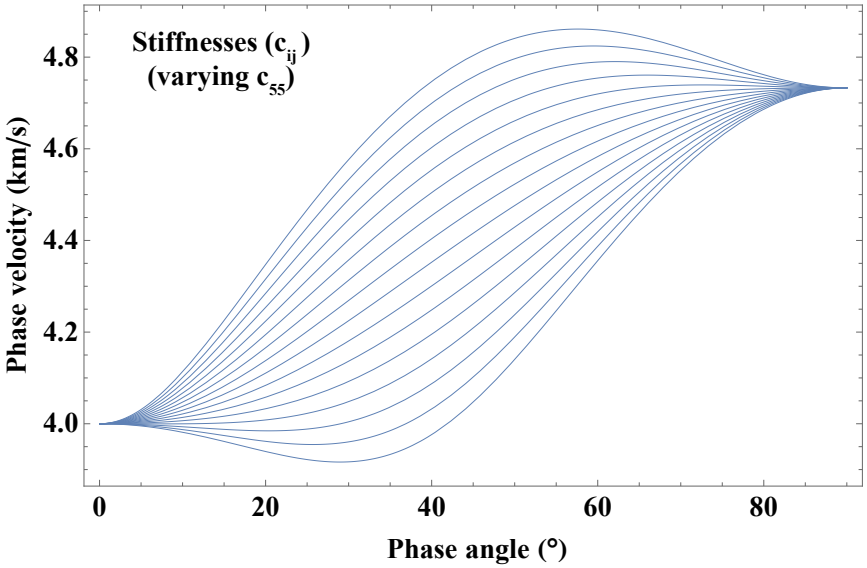

(a)

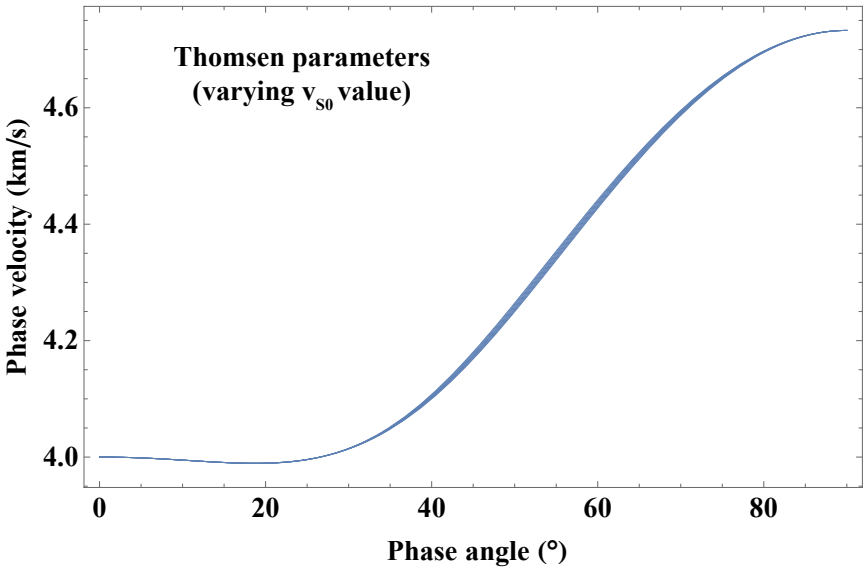

(b)

Figure 1.7: (a) A noticeable variation of qP-wave phase velocity under the change in c_{55}. (b) Insensitivity of qP-wave phase velocity under Thomsen parameterization to the change in v_{S0}. disser-intro/. cij-c55,thomsen-vs

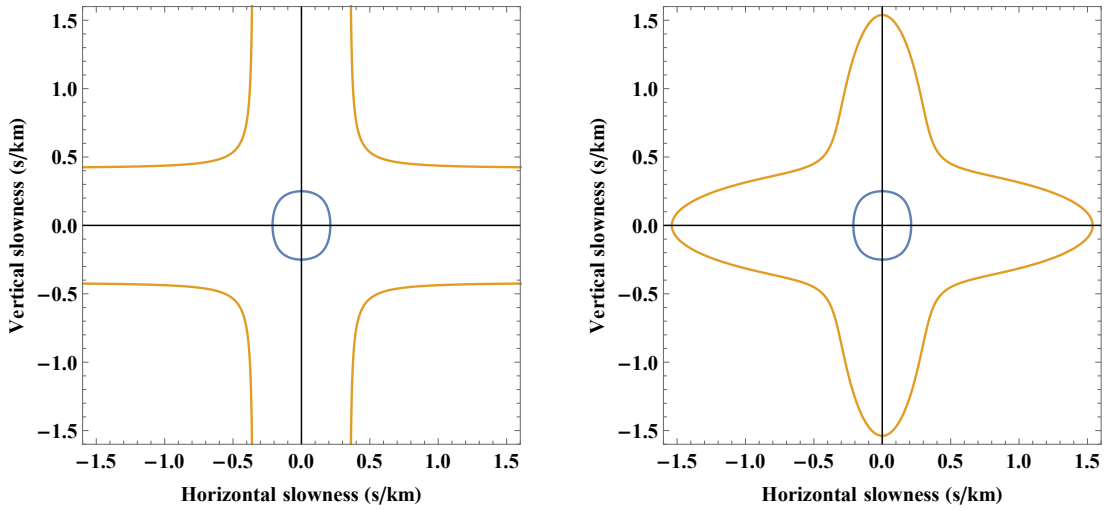

(a) (b)

(c) (d)

Figure 1.8: Illustrations showing the effects of varying v_{S0} on the phase slowness of qP (blue) and qSV (orange) waves in an example TI media from Figure 1.2 that has the parameters: $v_{P0} = 4\ km/s$, $\epsilon = 0.2$, and $\delta = -0.05$. The v_{S0} is (a) 0, (b) 0.65, (c) 1.3, and (d) 2.6 km/s disser-intro/. phasevs0,phasevs065,phasevs13,phasevs26

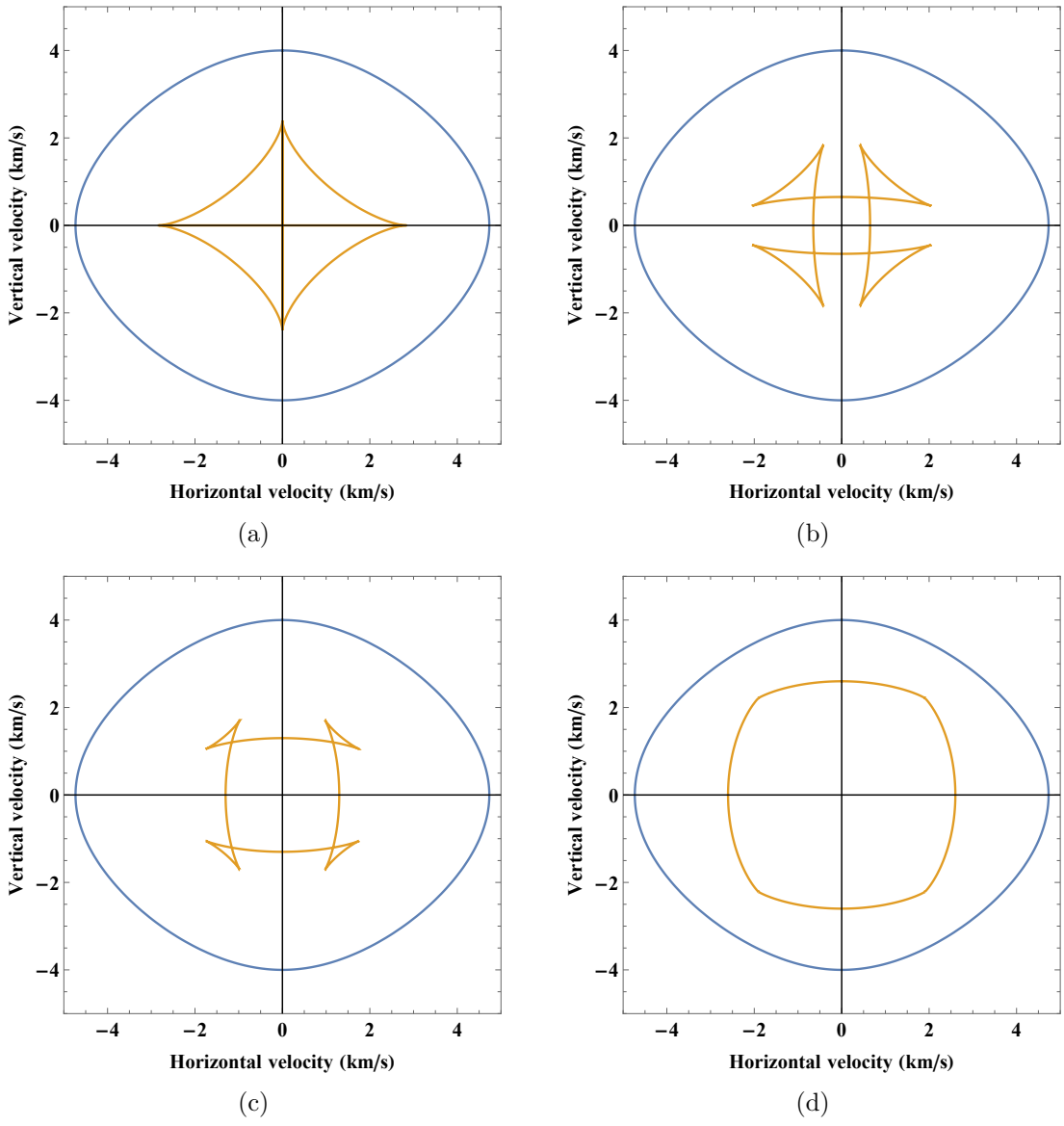

Figure 1.9: Illustrations showing the effects of varying v_{S0} on the group velocity (wavefront) of qP (blue) and qSV (orange) waves in an example TI media from Figure 1.2 that has the parameters: $v_{P0} = 4\ km/s$, $\epsilon = 0.2$, and $\delta = -0.05$. The v_{S0} is (a) 0, (b) 0.65, (c) 1.3, and (d) 2.6 km/s disser-intro/. groupvs0,groupvs065,groupvs13,groupvs26

(2012a), and Bube et al. (2012b).

THESIS OUTLINE

The dissertation is organized according to the following outline:

- **Chapter 1: Introduction**

  Chapter 1 introduces the research objectives of this work. It also contains a review on the fundamentals of seismic anisotropy and the thesis outline.

- **Chapter 2: Muir-Dellinger parameters and their empirical linear relationship**

  I begin Chapter 2 by introducing the Muir-Dellinger parameters and their empirical linear relationship. I show how to incorporate several important assumptions including elliptical anisotropy and pseudoacoustic approximation in MD notation, and provide expressions to convert to/from MD parameters with respect to other anisotropic parameterizations. I demonstrate that the empirical linear relationship can be used to indicate rock type based on the degree of anisotropy as captured by its slope value. I conclude the chapter with an analysis of qP-wave phase velocity in TI media (equation 1.58) under the MD parameterization.

- **Chapter 3: The linear relationship from rock physics modeling**

  Chapter 3 contains an investigation of the empirical linear relationship for shale samples. I show that it can also be used to infer about the type of pore fluids. I use self-consistent rock physics modeling method and Backus averaging to provide some evidence in support of its existence. I use wide-ranging values of

mineral compositions for shale samples to help make the results of my numerical experiments more impartial.

- **Chapter 4: Sensitivity analysis with respect to qP kinematics**

  I investigate the sensitivity qP-wave velocities and traveltime to different anisotropic parameterizations under different ranges of aperture in hopes of finding the most desirable scheme for the parameter inversion process. I use an approximation of the Hessian as the basic construction of my experiment and use the corresponding condition number as a theoretical indicator of the inversion's efficacy. I provide both 2D and 3D examples on one-hundred samples for testing conclusions from these model-dependent experiments.

- **Chapter 5: Anelliptic approximations for qP velocities**

  Chapter 5 addresses a challenging problem of finding analytical approximations for phase and group velocities for qP waves in transversely isotropic and orthorhombic media. The phase velocity is important for numerical seismic modeling and can be expressed in a more or less manageable form. The group velocity, on the other hand, is significantly more complex and plays a crucial role in seismic ray tracing. I take an advantage of the reciprocal property of MD parameters in the phase and group domain and propose analytical approximations for both velocities that have similar functional form for practical convenience but can still maintain a high level of accuracy. I test my proposed approximations on many benchmark models to verify their effectiveness.

- **Chapter 6: Conclusion**

  Chapter 6 completes the dissertation by summarizing major technical contributions and discusses the known limitations of MD parameterization. I end this

chapter with some suggestions on possible future areas of research with MD parameters.

Chapter 2

Muir-Dellinger parameters and their empirical linear relationship

The goal of this chapter is to introduce the readers to the Muir-Dellinger parameters and discuss their properties. The main advantage of the Muir-Dellinger parameters lies in the fact that they present an alternative way of capturing the qP kinematics that allows one to make rock physics implications such as lithology and the type of pore fluids directly without needing multi-component data nor amplitude variation with offset (AVO) analysis. I discuss the basics behind the Muir-Dellinger parameters in this chapter and continue on to its applications for distinguishing the type of pore fluids in Chapter 3.

Most importantly, this chapter serves as an honorary tribute to the original work of Francis Muir and Dr. Joe Dellinger that is almost lost through time.

INTRODUCTION

Seismic anisotropy is defined as the dependence of seismic velocities on the direction of wave propagation and is the large-scale manifestation of ordered, small-scale heterogeneities relative to the seismic wavelength (Thomsen, 2014). Anisotropy can be

Parts of this chapter were first published in Sripanich, Y., S. Fomel, P. Fowler, A. Stovas, and K. Spikes, 2016, Muir-Dellinger parameters for analysis of anisotropic signatures: 17th International Workshop on Seismic Anisotropy (IWSA). This work was done under the supervision of Dr. Sergey Fomel.

ascribed to different physical causes including alignment of platelet-shaped clay minerals in sedimentary rocks (e.g., shales), fractures—a compliant planar inhomogeneity, and fine layering (Grechka, 2009). In the conventional analysis of seismic anisotropy and its effects on seismic reflection data, geophysicists commonly adopt the *Thomsen parameters* (Thomsen, 1986), which represent combinations of elastic moduli (stiffness coefficients) believed to govern the most important seismic-wave signatures in anisotropic media (Tsvankin, 2012). These parameters allow complex formulas to be expressed in a concise manner with the complexity hidden inside the notation. Thomsen parameterization is shown in equation 1.60 for transversely isotropic media with vertical symmetry axis (VTI). Its extension to orthorhombic media was proposed by Tsvankin (1997) (equation 1.61). Thomsen-Tsvankin parameters have led to many advancements in the analysis of seismic anisotropy based on both the kinematic and dynamic (amplitudes) signatures of qP and qS waves (Rüger, 2002; Tsvankin, 2012; Thomsen, 2014). Another related approach uses parameterization through normal moveout velocity v and the time-processing parameter η (Alkhalifah and Tsvankin, 1995; Alkhalifah, 1998, 2000a, 2003), which is particularly useful for velocity analysis and the implementation of pseudoacoustic wave equation to study qP-wave kinematics.

MUIR-DELLINGER PARAMETERS

In this dissertation, I analyze an alternative set of anisotropic parameters that allows for a possibility of making direct rock physics implications such as lithology and/or pore fluids from qP-wave kinematics. The basis for my construction is the Muir-Dellinger parameters, originally developed by Muir and Dellinger (1985) for studying qP waves. They were later completed for TI media by Fomel (2004) and extended

to orthorhombic media by Sripanich and Fomel (2015), respectively. Their sensitivity with respect to qP phase velocity, group velocity, and traveltime are analyzed in Chapter 4 in comparison with several other anisotropic parameterizations. For analysis of qP waves in TI media, the set consists of four parameters: $w_1 = c_{11}/\rho$, $w_3 = c_{33}/\rho$, q_1, and q_3. The first two constitute the qP-wave velocity squared along the symmetry axis (n_3) and its orthogonal (n_1). The remaining two (q_1 and q_3) are anelliptic parameters that govern the deviation from an elliptical phase velocity and are defined as follows:

$$q_1 = \frac{c_{55}(c_{11} - c_{55}) + (c_{55} + c_{13})^2}{c_{33}(c_{11} - c_{55})} , \tag{2.1}$$

$$q_3 = \frac{c_{55}(c_{33} - c_{55}) + (c_{55} + c_{13})^2}{c_{11}(c_{33} - c_{55})} . \tag{2.2}$$

They can be found from fitting the curvatures of phase velocity along the n_1 axis and the n_3 axis as denoted by the subscript (Fomel, 2004). By fitting instead with the curvatures of group slowness at similar locations, one can obtain

$$Q_1 = \frac{1}{q_1} , \tag{2.3}$$

$$Q_3 = \frac{1}{q_3} , \tag{2.4}$$

which indicates the reciprocity between phase velocity and group slowness as discussed in Chapter 1 and the reciprocal property of q_i in MD parameterization. I use this property as the basis for proposing approximate phase and group velocities with MD parameters in Chapter 5. If I consider instead expressions for $q_1 - 1$ and $q_3 - 1$, the numerator of both expressions is given by

$$f = (c_{55} + c_{13})^2 - (c_{33} - c_{55})(c_{11} - c_{55}) , \tag{2.5}$$

which is related to the description of anellipticity previously considered by several researchers (Carrion et al., 1992; Vernik and Nur, 1992; Schoenberg, 1994; Alkhalifah

and Tsvankin, 1995; Fowler, 2003).

Sripanich and Fomel (2015) showed that there existed an empirical linear correlation between q_1 and q_3 found from laboratory measurements on stiffnesses (c_{ij}) in TI media for different rock types: shales, sandstones, and carbonates. This correlation can be used to reduce the number of dependent parameters in velocity approximations for qP waves from four to three in TI and from nine to six in orthorhombic media, while still maintaining a high level of approximation accuracy. In principle, this reduction in number of parameters is applicable to any expression of different anisotropic kinematic signatures.

The empirical linear relationship

The Muir-Dellinger parameters (w_1, w_3, q_1, and q_3) were suggested by Fomel (2004) and originated in the work of Muir and Dellinger (1985) in the context of qP velocities approximations in TI media. The empirically linear relationship between q_1 and q_3 was observed by Sripanich and Fomel (2015) and takes the form

$$q_1 - 1 = \left(\frac{1 - c_{55}/c_{33}}{1 - c_{55}/c_{11}}\right)(q_3 - 1) \ , \tag{2.6}$$

where the slope parameter $s = (1-c_{55}/c_{33})/(1-c_{55}/c_{11})$ can be related to the v_{S0}/v_{P0} ratio and ϵ in Thomsen's notation as follows:

$$\frac{v_{S0}^2}{v_{P0}^2} = \frac{(s-1)(1+2\epsilon)}{s-(1+2\epsilon)} \ . \tag{2.7}$$

Figure 2.1 shows the plot of equation 2.6 with the data collected from various sources of laboratory measurements in the literature (Jones and Wang, 1981; Vernik and Nur, 1992; Johnston and Christensen, 1995; Hornby, 1998; Vernik and Liu, 1997; Jakobsen and Johansen, 2000; Domnesteanu et al., 2002; Wang, 2002; Dewhurst et al.,

2011; Sone, 2012). All measurements were conducted on different core samples from various geographical locations in the world and done under different conditions. Nevertheless, one can observe a nearly linear relationship from Figure 2.1 with the best-fit slope value approximately 0.85. Analogous linear trends with varying slope values were observed for samples of other rock types including sandstones (Figure 2.2) and carbonates (Figure 2.3). The results suggest that q_1 and q_3 exhibit a linear relationship that appears to depend primarily on lithology, regardless of the geographical location of the samples. The resultant best-fit slopes of the sandstone and carbonate samples are closer to unity especially for carbonate samples, which is indicative of a smaller anisotropy. Such relationship cannot be observed from Thomsen parameters (Haven and Batzle, 2014). Therefore, the empirical linear relationship may serve as a mean to distinguish the rock type based solely on the information from qP-wave kinematics.

Figures 2.4 and 2.5 show plots similar to the empirical linear relationship from shale samples (Figure 2.1) but is now color-coded with the values of ϵ and δ in Thomsen's notation. One can observe a general trend of the slope value that varies with ϵ — the smaller the slope is, the larger ϵ becomes. This is not surprising as this observation can be inferred from the very definition of the slope in equation 2.6. The variation with respect to δ is less apparent as is to be expected because δ is controlled also by c_{13}, which is not present in the definition of the linear slope.

As a consequence of this discovery, one can use the empirical linear relationship as a reasonable way to reduce the number of parameters in qP-wave analysis instead of using assumptions such as pseudoacoustic approximation (Alkhalifah, 1998) and elliptical anisotropy (Helbig, 1983; Schoenberg et al., 1996) because it was an observation based on physical measurements. I later show that this relationship allows

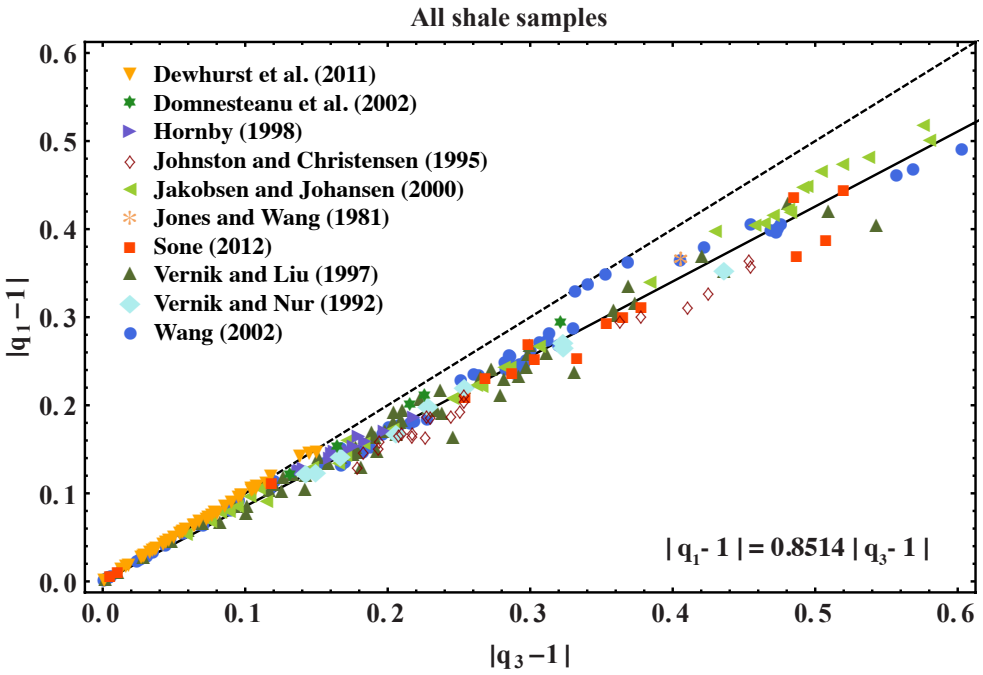

Figure 2.1: Plot of the linear relationship (equation 2.6) between q_1 and q_3 based on the laboratory measurements of shale samples from multiple sources under various conditions. The dashed line denotes the line of slope = 1. One can observe a strong correlation between the two parameters with the linear slope deviating most from unity in comparison to those from sandstone samples 2.2 and carbonate samples 2.3. disser-MD/. shalerelationship

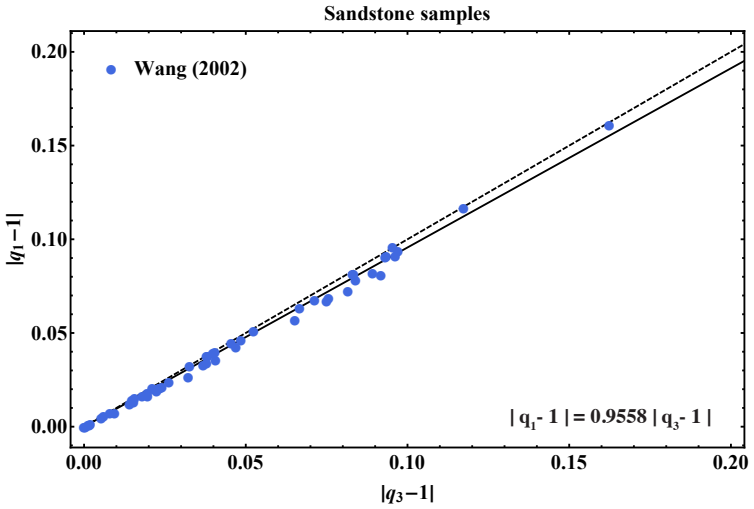

Figure 2.2: Plot of the linear relationship (equation 2.6) between q_1 and q_3 based on the laboratory measurements of sandstone samples from Wang (2002). The dashed line denotes the line of slope = 1. One can observe a strong correlation between the two parameters. disser-MD/. sandrelationship

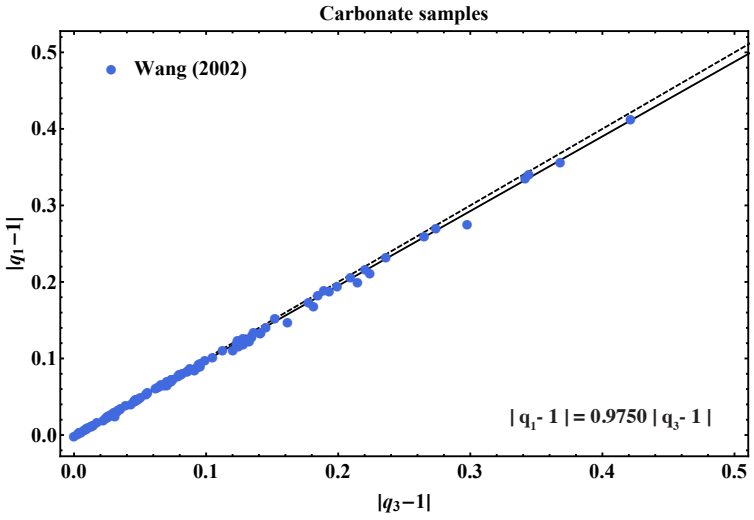

Figure 2.3: Plot of the linear relationship (equation 2.6) between q_1 and q_3 based on the laboratory measurements of carbonate samples from Wang (2002). The dashed line denotes the line of slope = 1. One can observe a strong correlation between the two parameters with the highest linear slope closest to unity among the three cases. disser-MD/. carbrelationship

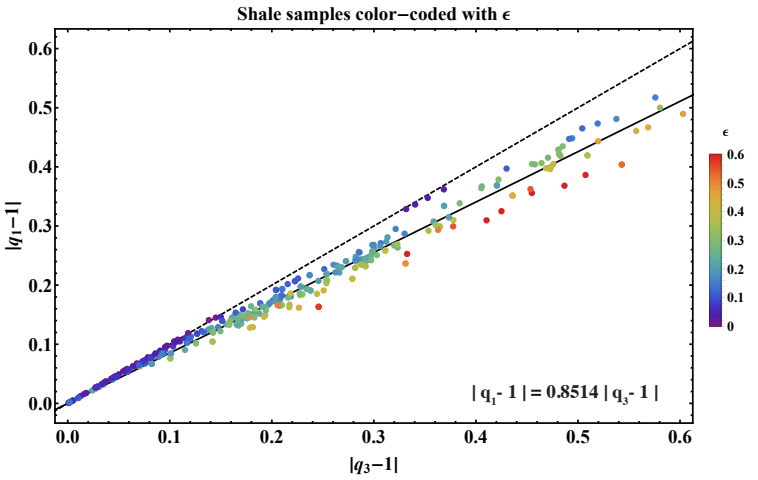

Figure 2.4: Plot of the linear relationship (equation 2.6) between q_1 and q_3 based on the laboratory measurements of shale samples similar to Figure 2.1 but is color-coded with the value of ϵ. disser-MD/. shalerelationship-coloreps

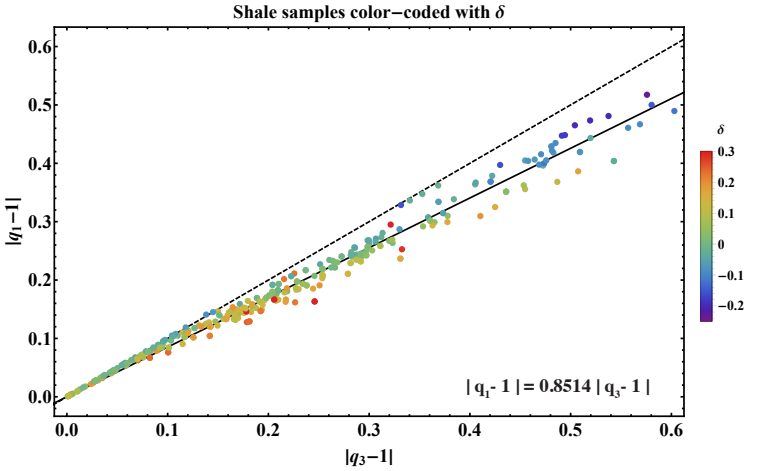

Figure 2.5: Plot of the linear relationship (equation 2.6) between q_1 and q_3 based on the laboratory measurements of shale samples similar to Figure 2.1 but is color-coded with the value of δ. disser-MD/. shalerelationship-colordelta

one to translate a wide range of possible vertical shear-wave velocity v_{S0} values under Thomsen notation to a much smaller range of variation of the linear slope. I will also further analyze this linear relationship in Chapter 3 in the context of rock physics.

Extension to 3D orthorhombic media

Because the in-symmetry-plane qP-wave propagation in orthorhombic media behaves identically to the case of TI media (Tsvankin, 2012), it is possible to extend the Muir-Dellinger parameters from 2D to 3D appropriately for studies in orthorhombic media. The full set of orthorhombic parameters in 3D includes $w_1 = c_{11}/\rho$, $w_2 = c_{22}/\rho$, $w_3 = c_{33}/\rho$, q_{21}, q_{31}, q_{12}, q_{32}, q_{13}, and q_{23}, where q_{ij} denotes the anelliptic parameters derived from fitting the phase velocity curvatures along the n_i axis in the symmetry plane defined by the n_j axis. For example, in plane [n_1,n_3], I consider q_{12} and q_{32} because I can find q either by fitting along the n_1 or n_3 axis with n_2 as the axis defining the symmetry plane. The expressions for the 3D anelliptic parameters are as follows (Sripanich and Fomel, 2014a, 2015):

$$q_{21} = \frac{c_{44}(c_{22}-c_{44})+(c_{44}+c_{23})^2}{c_{33}(c_{22}-c_{44})}\,, \tag{2.8}$$

$$q_{31} = \frac{c_{44}(c_{33}-c_{44})+(c_{44}+c_{23})^2}{c_{22}(c_{33}-c_{44})}\,, \tag{2.9}$$

$$q_{13} = \frac{c_{66}(c_{11}-c_{66})+(c_{66}+c_{12})^2}{c_{22}(c_{11}-c_{66})}\,, \tag{2.10}$$

$$q_{23} = \frac{c_{66}(c_{22}-c_{66})+(c_{66}+c_{12})^2}{c_{11}(c_{22}-c_{66})}\,. \tag{2.11}$$

Expressions for q_{12} and q_{32} are equivalent to expressions for q_1 and q_3 in equations 2.1 and 2.2. Unlike some other parameterizations, the Muir-Dellinger parameters in orthorhombic media put no emphasis on any particular direction and thus, avoid the undesirable property of strong variance under different coordinate labeling

important in the parameter estimation problem (Fowler, 2015; Sripanich et al., 2016). A schematic illustration of the fitting locations for MD parameters in a 3D orthorhombic model is shown in Figure 2.6. A conversion table between MD parameters and other orthorhombic parameterizations schemes is shown in Table 2.1.

The linear relationship in equation 2.6 can be appropriately extended for parameter reduction in the [n_1,n_3] and [n_2,n_3] planes in the case of orthorhombic media with vertical symmetry axis (VOR) if similar underlying physical cause of anisotropy (alignment of shale constituents) as in the case of 2D VTI media is assumed (Sripanich and Fomel, 2014b, 2015). However, for the [n_1,n_2] plane, even though the seismic wave also exhibits transversely isotropic behavior, it originates in a possible different physical cause (fractures). Sripanich and Fomel (2015) proposed to simply set $q_{13} = q_{23}$, which is equivalent to a VTI pseudoacoustic approximation (Alkhalifah, 1998; Fomel, 2004).

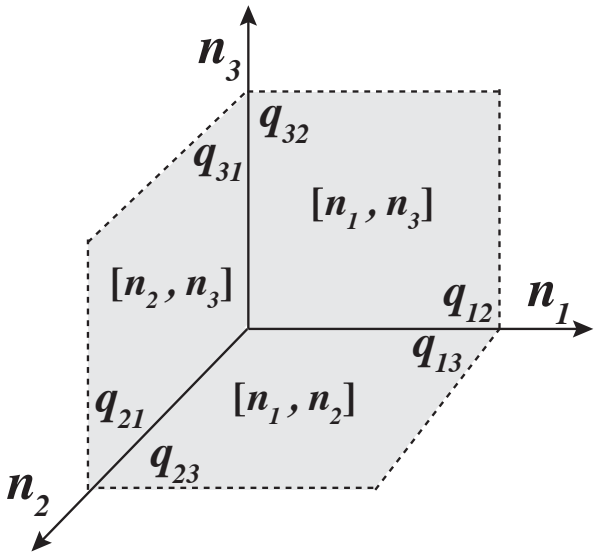

Figure 2.6: A 3D plot of the fitting locations of Muir-Dellinger parameters in an orthorhombic model reproduced from Sripanich and Fomel (2015). Each grey plane denotes one of the three symmetry planes in an orthorhombic model. One can observe symmetric definitions of parameter in 3D that are free from variation with the choice of coordinate labeling. disser-MD/. fittingnotation

PHASE VELOCITY EXPRESSION IN TI MEDIA

The exact phase velocity of qP waves in TI media has the well-known expression as shown in equation 1.58. Under Thomsen parameterization (equation 1.60), it translates to (Thomsen, 1986, 2014),

$$v_{qP}^2 = v_{P0}^2\left[1 + \epsilon \sin^2\theta + D(\theta)\right] \ , \tag{2.12}$$

where

$$D(\theta) = \frac{1}{2}\left(1 - \frac{v_{S0}^2}{v_{P0}^2}\right)\left[\left(1 + \frac{4(2\delta - \epsilon)}{1 - v_{S0}^2/v_{P0}^2}\sin^2\theta\cos^2\theta + \frac{4\epsilon(1 - v_{S0}^2/v_{P0}^2 + \epsilon)}{(1 - v_{S0}^2/v_{P0}^2)^2}\sin^4\theta\right)^{1/2} - 1\right] . \tag{2.13}$$

Assuming weak anisotropy where ϵ and δ are small, Thomsen (1986) showed that equation 2.12 can be linearized to

$$v_{qP}(\theta) \approx v_{P0}\left(1 + \delta\sin^2\theta\cos^2\theta + \epsilon\sin^4\theta\right) \ , \tag{2.14}$$

where it becomes apparent that ϵ and δ govern the qP-wave phase velocity in different ranges of θ and it is valid to consider only three independent controlling parameters v_{P0}, ϵ, and δ for qP phase and group velocities. Despite having a simple functional form, approximation 2.14, may not provide sufficient accuracy for some practical purposes in comparison with other three-parameter non-linear velocity approximations (Fowler, 2003; Fomel, 2004; Sripanich and Fomel, 2015). I address this topic in Chapter 5 of this dissertation.

Figures 1.7(b) and 2.7 shows plots of similar experiment as in Figure 1 of Fowler (2003), where an example model with parameters $v_{P0} = 4\ km/s$, $\epsilon = 0.2$, $\delta = -0.05$, and a varying v_{S0} was used to demonstrate the relative insensitivity of qP-wave velocity to v_{S0} when the effects from c_{13} and c_{55} are captured through Thomsen's δ. Here, I vary the v_{S0} in a range from 0.0 to 2.6 km/s. The benchmark qP-wave

From Muir-Dellinger	To Muir-Dellinger
Tsvankin (1997):	
$v_{P0} = \sqrt{w_3}$ $v_{S0} = \sqrt{\frac{(q_{12}-q_{32})w_1w_3}{w_1(1-q_{32})-w_3(1-q_{12})}}$ $\epsilon_1 = \frac{1}{2}\left(\frac{w_2}{w_3}-1\right)$ $\epsilon_2 = \frac{1}{2}\left(\frac{w_1}{w_3}-1\right)$ $\delta_1 = \frac{1}{2}\left(\frac{q_{31}w_2}{w_3}-1\right)$ $\delta_2 = \frac{1}{2}\left(\frac{q_{32}w_1}{w_3}-1\right)$ $\delta_3 = \frac{1}{2}\left(\frac{q_{13}w_2}{w_1}-1\right)$ $\gamma_1 = \frac{(q_{32}-1)(q_{13}-q_{23})w_1w_2+(q_{13}-q_{12}+q_{32}-q_{23}+q_{23}q_{12}-q_{13}q_{32})w_2w_3+(q_{23}-1)(q_{32}-q_{12})w_1w_3}{2w_3(q_{12}-q_{32})[(q_{23}-1)w_1-(q_{13}-1)w_2]}$ $\gamma_2 = \frac{(q_{31}-1)(q_{13}-q_{23})w_1w_2+(q_{13}+q_{21}-q_{31}-q_{23}+q_{23}q_{31}-q_{21}q_{13})w_1w_3+(q_{13}-1)(q_{21}-q_{31})w_2w_3}{2w_3(q_{21}-q_{31})[(q_{23}-1)w_1-(q_{13}-1)w_2]}$	$w_1 = v_{P0}^2(1+\epsilon_2)$ $w_2 = v_{P0}^2(1+\epsilon_1)$ $w_3 = v_{P0}^2$ $q_{32} = \frac{1+2\delta_2}{1+2\epsilon_2}$ $q_{12} = \frac{(v_{P0}^2-v_{S0}^2)(1+2\delta_2)+2v_{S0}^2\epsilon_2}{v_{P0}^2(1+2\epsilon_2)-v_{S0}^2}$ $q_{31} = \frac{1+2\delta_1}{1+2\epsilon_1}$ $q_{21} = \frac{v_{P0}^2(1+2\gamma_2)(1+2\delta_1)-v_{S0}^2(1+2\gamma_1)(1+2\delta_1-2\epsilon_1)}{v_{P0}^2(1+2\gamma_2)(1+2\epsilon_1)-v_{S0}^2(1+2\gamma_1)}$ $q_{13} = \frac{(1+2\delta_3)(1+2\epsilon_2)}{1+2\epsilon_1}$ $q_{23} = \frac{v_{P0}^2(1+2\delta_3)(1+2\epsilon_2)+v_{S0}^2(1+2\gamma_1)(-1-2\delta_3+2\epsilon_1-4\epsilon_2-4\delta_3\epsilon_2)}{(1+2\epsilon_2)\left(v_{P0}^2(1+2\epsilon_1)-v_{S0}^2(1+2\gamma_1)\right)}$
Alkhalifah (2003):	
$v_{P0} = \sqrt{w_3}$ $v_{S1} = \sqrt{\frac{(q_{21}-q_{31})w_2w_3}{(1-q_{31})w_2-(1-q_{21})w_3}}$ $v_{S2} = \sqrt{\frac{(q_{12}-q_{32})w_1w_3}{(1-q_{32})w_1-(1-q_{12})w_3}}$ $v_{S3} = \sqrt{\frac{(q_{13}-q_{23})w_1w_2}{(1-q_{23})w_1-(1-q_{13})w_2}}$ $v_1 = \sqrt{q_{31}w_2}$ $v_2 = \sqrt{q_{32}w_1}$ $\eta_1 = \frac{1}{2}\left(\frac{1}{q_{31}}-1\right)$ $\eta_2 = \frac{1}{2}\left(\frac{1}{q_{32}}-1\right)$ $\eta_3 = \frac{1}{2}\left(\frac{1}{q_{13}}-1\right)$	$w_1 = v_2^2(1+2\eta_2)$ $w_2 = v_1^2(1+2\eta_1)$ $w_3 = v_{P0}^2$ $q_{32} = \frac{1}{1+2\eta_2}$ $q_{12} = \frac{v_{P0}^2(v_2^2-v_{S2}^2)+2v_2^2v_{S2}^2\eta_2}{v_{P0}^2(v_2^2(1+2\eta_2)-v_{S2}^2)}$ $q_{31} = \frac{1}{1+2\eta_1}$ $q_{21} = \frac{v_{P0}^2(v_1^2-v_{S1}^2)+2v_1^2v_{S1}^2\eta_1}{v_{P0}^2(v_1^2(1+2\eta_1)-v_{S1}^2)}$ $q_{13} = \frac{v_2^2(1+2\delta_3)(1+2\eta_2)}{v_1^2(1+2\eta_1)}$ $q_{23} = \frac{-v_2^2v_{S3}^2(1+2\eta_2)(1+2\eta_3)+v_1^2(1+2\eta_1)[v_2^2(1+2\eta_2)+2v_{S3}^2\eta_3]}{v_2^2(1+2\eta_2)(1+2\eta_3)[v_1^2(1+2\eta_1)-v_{S3}^2]}$
Fowler (2015):	
$w_{P1} = w_1$ $w_{P2} = w_2$ $w_{P3} = w_3$ $w_{S1} = \frac{(q_{21}-q_{31})w_2w_3}{(1-q_{31})w_2-(1-q_{21})w_3}$ $w_{S2} = \frac{(q_{12}-q_{32})w_1w_3}{(1-q_{32})w_1-(1-q_{12})w_3}$ $w_{S3} = \frac{(q_{13}-q_{23})w_1w_2}{(1-q_{23})w_1-(1-q_{13})w_2}$ $\xi_1 = \frac{1}{2}\left(\frac{[(q_{21}-q_{31})w_2w_3+\sqrt{(q_{21}-1)(q_{31}-1)(q_{31}w_2-q_{21}w_3)(w_2-w_3)w_2w_3}]^2}{w_2w_3[(1-q_{21})w_3-(1-q_{31})w_2]^2}-1\right)$ $\xi_2 = \frac{1}{2}\left(\frac{[(q_{12}-q_{32})w_1w_3+\sqrt{(q_{12}-1)(q_{32}-1)(q_{32}w_1-q_{12}w_3)(w_1-w_3)w_1w_3}]^2}{w_1w_3[(1-q_{12})w_3-(1-q_{32})w_1]^2}-1\right)$ $\xi_3 = \frac{1}{2}\left(\frac{[(q_{23}-q_{13})w_1w_2+\sqrt{(q_{13}-1)(q_{23}-1)(q_{13}w_2-q_{23}w_1)(w_2-w_1)w_1w_2}]^2}{w_1w_2[(1-q_{13})w_2-(1-q_{23})w_1]^2}-1\right)$	$w_1 = w_{P1}$ $w_2 = w_{P2}$ $w_3 = w_{P3}$ $q_{32} = \frac{(1+2\xi_2)w_{P1}w_{P3}+w_{P3}w_{S2}-2w_{S2}\sqrt{w_{P1}w_{P3}(1+2\xi_2)}}{w_{P1}(w_{P3}-w_{S2})}$ $q_{12} = \frac{(1+2\xi_2)w_{P1}w_{P3}+w_{P1}w_{S2}-2w_{S2}\sqrt{w_{P1}w_{P3}(1+2\xi_2)}}{w_{P3}(w_{P1}-w_{S2})}$ $q_{31} = \frac{(1+2\xi_1)w_{P2}w_{P3}+w_{P3}w_{S1}-2w_{S1}\sqrt{w_{P2}w_{P3}(1+2\xi_1)}}{w_{P2}(w_{P3}-w_{S1})}$ $q_{21} = \frac{(1+2\xi_1)w_{P2}w_{P3}+w_{P2}w_{S1}-2w_{S1}\sqrt{w_{P2}w_{P3}(1+2\xi_1)}}{w_{P3}(w_{P2}-w_{S1})}$ $q_{13} = \frac{(1+2\xi_3)w_{P1}w_{P2}+w_{P1}w_{S3}-2w_{S3}\sqrt{w_{P1}w_{P2}(1+2\xi_3)}}{w_{P2}(w_{P1}-w_{S3})}$ $q_{23} = \frac{(1+2\xi_3)w_{P1}w_{P2}+w_{P2}w_{S3}-2w_{S3}\sqrt{w_{P1}w_{P2}(1+2\xi_3)}}{w_{P1}(w_{P2}-w_{S3})}$

Table 2.1: Conversion table to and from Muir-Dellinger parameters with respect to different parameterizations in orthorhombic media.

phase velocity in this test is computed with $v_{S0} = 1\ km/s$. It can clearly be seen that despite a large variation in v_{S0} from 0.0 to 2.6 km/s, the accuracy of the approximated qP-wave phase velocity is barely affected and only has the maximum error of 0.8 % in this particular model. This observation justifies the use of pseudoacoustic approximation and its overall success in approximating qP-wave kinematics despite some implementation drawbacks that may occur when setting $v_{S0} = 0$ (Fowler et al., 2010; Bakker and Duveneck, 2011; Zhang et al., 2011; Bube et al., 2012a,b).

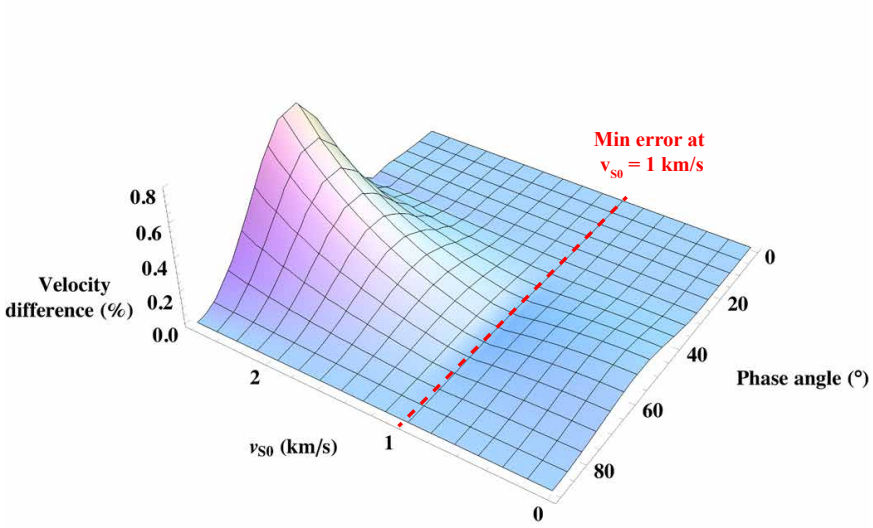

Figure 2.7: qP-wave phase velocity errors under Thomsen parameterization with the variation of v_{S0}. qP-wave phase velocity is virtually insensitive to the change in v_{S0} with the maximum error of only 0.8 %. Other parameters of the model include $v_{P0} = 4\ km/s$, $\epsilon = 0.2$, and $\delta = -0.05$. disser-MD/. thomsen-vs-3d

Alternatively, under MD parameterization scheme, the exact phase velocity of qP waves becomes:

$$v_{qP}^2(\theta) = \frac{1}{2}(w_1 \sin^2\theta + w_3 \cos^2\theta + a) + \frac{1}{2}\sqrt{(w_1 \sin^2\theta + w_3 \cos^2\theta - a)^2 + 4 w_1 w_3 b \sin^2\theta \cos^2\theta}\ , \tag{2.15}$$

where

$$a = \frac{(q_1 - q_3)w_1 w_3}{w_3(q_1 - 1) - w_1(q_3 - 1)} \quad \text{and} \quad b = \frac{(q_1 - 1)(q_3 - 1)(w_3 - w_1)}{w_3(q_1 - 1) - w_1(q_3 - 1)} \ .$$

Equation 2.15 reveals an explicit connection between qP phase velocity and the elliptical reference $w_1 \sin^2\theta + w_3 \cos^2\theta$, where the deviations are governed by a and b. Note the similar denominator and the factors $q_1 - 1$ and $q_3 - 1$ in their expressions. This result suggests that the qP phase velocity in TI media is primarily controlled by an elliptical reference, the magnitude of q_1 and q_3 relative to unity and their difference. Again, the factors $q_1 - 1$ and $q_3 - 1$ are again similar to what some previous researchers consider as anellipticity (equation 2.5).

From data samples used in Figure 2.1, the mean average values of q_1 and q_3 are 0.8314 and 0.8024, respectively. Assuming $q_1 = q_3$ results in $a = v_{S0}^2 = 0$ and $b = q_1 - 1 = q_3 - 1$ and reduces equation 2.15 to the pseudoacoustic phase-velocity approximation studied by Alkhalifah (1998). Therefore, the common practice of setting $v_{S0} = 0$ under pseudoacoustic approximation is equivalent to setting $q_1 = q_3$ under MD parameterization and implies equal curvature parameters along vertical and horizontal axes in VTI media, or equivalently the symmetry axis and its orthogonal in any TI media. Assuming $q_1 = q_3 = 1$ reduces equation 2.15 to $w_1 \sin^2\theta + w_3 \cos^2\theta$ and results in elliptical anisotropy.

Similarly to the case of Thomsen parameters, I conduct the same experiment and observe that the computed velocity is virtually insensitive to the changing slope with the minimum error at slope = 0.9813 at all angles (Figure 2.8). This slope value corresponds to the exact value of $v_{S0} = 1\ km/s$ used to generate the benchmark qP-wave phase velocity in the first place. Another interesting note from this experiment is that under Thomsen parameterization, the range of variation of v_{S0} from 0.0 to 2.6

km/s translates to a much smaller range of slope from 0.827 to 1. This observation supports the presence of the empirical linear relationship (Figures 2.1-2.3) despite many possible values of c_{55} from different samples of measurement. Additionally, under MD parameterization, there exists a slope parameter with value slightly smaller than unity that can result in minimal error in three-parameter velocity approximation at all possible angles and the most optimal value will correspond to the true value of c_{55} of the model considered. I provide a further analysis on the insensitivity of the exact phase velocity to the change in slope using the derivative $\frac{\partial v_{qP}^2}{\partial s}$ in Appendix A.

In other words, this finding indicates that based on real rock physics measurements, qP-wave kinematics under MD parameterization are captured in such a way that two of the four governing parameters become approximately linearly dependent on each other, and one may use such empirical relationship to reduce the number of involving parameters in qP-wave analyses down to three with high fidelity. It is worth emphasizing this concept is different from the one used in the weak-anisotropy approximation, where parameters reduction is due to the effect from v_{S0} being second-order and is neglected when approximating qP-wave velocities (Thomsen, 1986; Tsvankin, 2012). It is also different from the pseudoacoustic approximation, where v_{S0} is assumed to have negligible effects on qP-wave velocities and often simply set to zero to achieve parameter reduction. This choice may, however, lead to stability problems in seismic modeling process (Fletcher et al., 2009; Bakker and Duveneck, 2011; Bube et al., 2012b). Different conditions to define the pseudoacoustic approximation for different parameterizations are summarized in Tables 2.2 and 2.3.

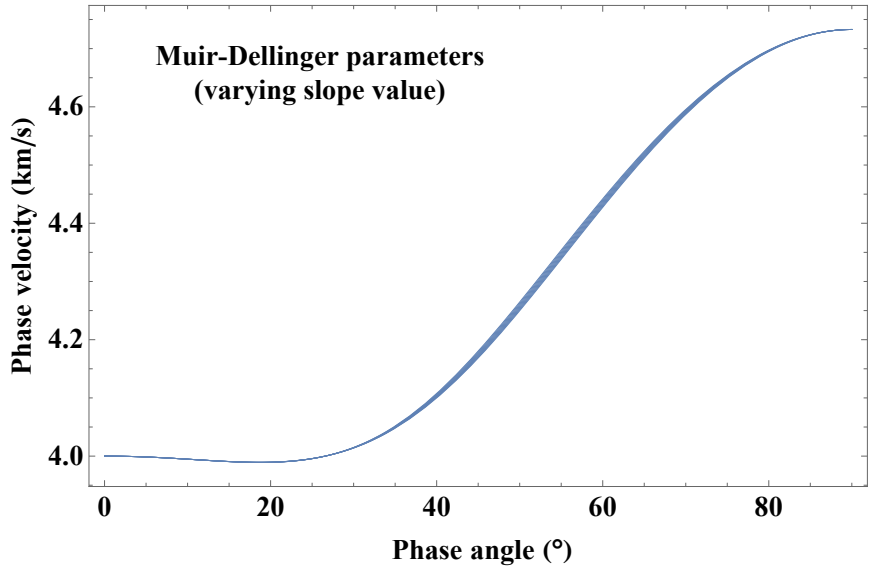

(a)

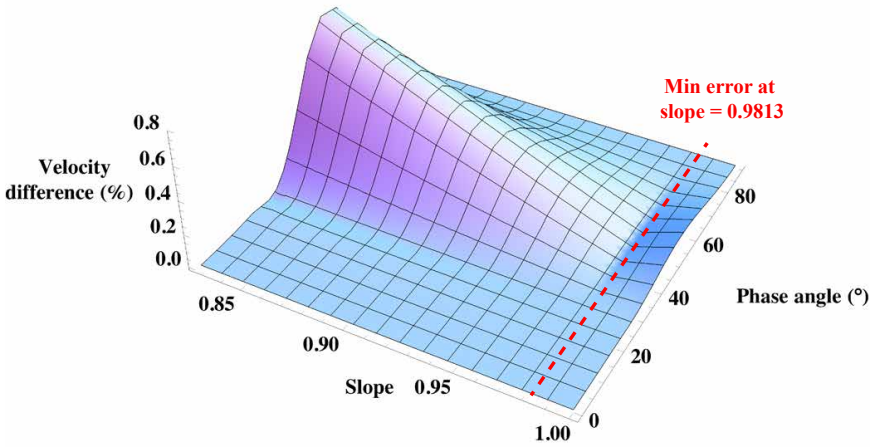

(b)

Figure 2.8: (a) Approximated qP-wave phase velocity under the change of v_{S0} from 0.0 to 2.6 km/s, which correspond to the change in slope from 0.827 to 1. (b) qP-wave phase velocity errors under MD parameterization with the same variation of slope. qP-wave phase velocity is virtually insensitive to the change in slope. disser-MD/. md-slope,md-slope-3d

Schemes	Parameters	Elliptical Ani.	Pseudoacoustic Approx.
Thomsen	v_{P0}, v_{S0}, ϵ, and δ	$\epsilon = \delta$	$v_{S0} = 0$
Alkhalifah	v_{P0}, v_{S0}, v and η	$\eta = 0$	$v_{S0} = 0$
Chapman-Miller-Fowler	w_{P1}, w_{P3}, ξ and w_{S1}	$\xi = \frac{w_{S1}}{w_{P1}w_{P3}}\left(w_{S1} - \frac{w_{P1}}{2} - \frac{w_{P3}}{2} \pm \sqrt{(w_{S1} - w_{P1})(w_{S1} - w_{P3})}\right)$	$w_{S1} = 0$
Muir-Dellinger	w_1, w_3, q_1 and q_3	$q_1 = q_3 = 1$	$q_1 = q_3$

Table 2.2: Comparison of four-parameter parameterization schemes for qP-wave anisotropic parameters in TI media with conditions for elliptical anisotropy and pseudoacoustic approximation.

Schemes	Parameters	Pseudoacoustic Approx.
Tsvankin	v_{P0}, v_{S0}, δ_3,	$v_{S0} = 0$
	ϵ_1, δ_1, γ_1,	$\gamma_1 = 0$
	ϵ_2, δ_2, γ_2	$\gamma_2 = 0$
Alkhalifah	v_{P0}, v_{S1}, v_{S2},	$v_{S1} = 0$
	v_{S3}, v_1, v_2,	$v_{S2} = 0$
	η_1, η_2, η_3	$v_{S3} = 0$
Chapman-Miller-Fowler	w_{P1}, w_{P2}, w_{P3},	$w_{S1} = 0$,
	w_{S1}, w_{S2}, w_{S3},	$w_{S2} = 0$
	ξ_1, ξ_2, ξ_3	$w_{S3} = 0$
Muir-Dellinger	w_1, w_2, w_3,	$q_{21} = q_{31}$,
	q_{12}, q_{21}, q_{13},	$q_{12} = q_{32}$
	q_{31}, q_{23}, q_{32}	$q_{13} = q_{23}$

Table 2.3: Comparison of nine-parameter parameterization schemes for qP-wave anisotropic parameters in orthorhombic media with conditions for pseudoacoustic approximation.

DISCUSSION

I emphasize that the Muir-Dellinger parameters studied here are specifically designed for analysis of qP-wave kinematics. In TI media, they only consist of four parameters as opposed to the total of five parameters required to study the full elastic behaviors of qP, qSV, and qSH waves. In orthorhombic media, however, MD parameterization consists of nine parameters, which is similar to total number of necessary parameters to describe all elastic waves, although they should only be used to study qP waves. In light of this statement, it can be shown that in the limit of isotropy, the MD parameters in TI media become

$$\lim_{\text{isotropy}} [w_1, w_3, q_1, q_3] = [v_P^2, v_P^2, 1, 1] \ , \tag{2.16}$$

where they specify only the compressional-wave velocity (v_P) but are independent of the shear-wave velocity (v_S) in isotropic media. Moreover, an attempt to compute the vertical shear-wave velocity v_{S0} under Thomsen notation in TI media from MD space will yield the indeterminacy,

$$\lim_{\text{isotropy}} a = v_{S0}^2 = \frac{0}{0} \ , \tag{2.17}$$

because v_{S0} also governs the vertical velocity of both qSV and qSH waves. Similar results can be obtained for v_{S1}, v_{S2}, and v_{S3} in the case of orthorhombic media. Therefore, the MD parameters described here are only appropriate for use with qP waves, not qS waves. As a result, the applicability of MD parameters to study converted waves, reflection/transmission coefficients, and amplitude variation with offset (AVO) may be limited.

As pointed out by Sripanich and Fomel (2015) and discussed in this chapter, the observed empirical linear relationship might provide additional constraints on the

subsurface lithology from known quantities in seismic processing (equation 2.7) with different slope values corresponding to different rock types. Further investigations on this linear relationship are needed to address its applicability in other practical aspects of seismic anisotropy, for example, constructing effective shale models from well data (Quirein et al., 2014; Murphy et al., 2015). Moreover, it is important to keep in mind that the empirical linear relationship (Figure 2.1) was observed based on rock physics measurements with the assumption of transverse isotropy (TI). Its applicability to orthotropy may be limited since the causes of anisotropy in orthorhombic media can be different from those in TI media. For example, an orthorhombic medium can be constructed from multiple sets of fractures embedded in an isotropic background, which is different from the alignment of platelet minerals or layering in TI media. Experimental measurements of real samples with the presence of fractures beyond TI assumption are essential to the verification of the current linear relationship and the extent of its applicability.

Additionally, the compiled laboratory measurements in Figures 2.1-2.3 were taken from various studies based on different techniques for measuring stiffness coefficients. Aside from the effect of the type of fluid infill at the time of measurement that I will investigate in Chapter 3, another notable effect can be from the type of measured velocities (phase or group) in different experimental setups. In the current dataset, I make use of the reported stiffness coefficients by the original authors and assume that appropriate procedure was applied in the conversion process from measured velocities to stiffnesses.

Finally, the dependence of the laboratory stiffness measurements on pressure was not considered in Figures 2.1-2.3. Future research opportunity exists for investigating the plausible variation of the slope parameter with respect to effective pressure

at the time of measurement.

CONCLUSIONS

I analyze the Muir-Dellinger parameters and show that they have several interesting characteristics that may provide new insights about the behavior of qP waves in TI media. Particularly, the empirical linear relationship between two anelliptic parameter q_1 and q_3 can serve as a basis for parameter reduction and an indicator of the degree of anisotropy. It may also provide additional insights to subsurface lithology. I will provide some supportive evidence of its existence and its possible relevance to the type of pore fluids in Chapter 3. Muir-Dellinger parameters also have symmetric definitions with no orientation aliases when extended to orthorhombic media and are suitable for use in parameter estimation problems. This point will further be addressed in details in Chapter 4.

ACKNOWLEDGMENTS

I appreciate the comments from Q. Hao and Y. Ivanov. I thank the sponsors of the Texas Consortium for Computational Seismology (TCCS), the Exploration and Development Geophysics Education and Research Forum (EDGER), and the Rock Seismic Research project (ROSE) for financial support. I also acknowledges the additional support from the Statoil Fellows Program at the University of Texas at Austin.

Chapter 3

The linear relationship from rock physics modeling

In this chapter, I provide a further analysis of the empirical linear relationship in shale samples based on self-consistent rock physics modeling and Backus averaging. The results provide some supportive evidence of the existence of the observed linear dependence and show that it may also provide more insights towards distinguishing the type of pore fluids.

INTRODUCTION

We see from Chapter 2 that the Muir-Dellinger parameters possess a unique property that two of the parameters (q_1 and q_3) have an approximately linear relationship based on rock physics measurements that varies with rock type. However, the used rock physics data can also be significantly affected by the type of fluid infill at the time of measurement. Figures 3.1-3.3 show plots of the same type for shale samples as in Figure 2.1 but categorized by the type of infill fluids of the measured samples. One can observe that the average slope value increases when the stiffness of the pores increases. In other words, the values are closer to unity, i.e., deviate less from isotropy, when the pores are brine-saturated (Figure 3.2). For softer pores, e.g., dry with vanishing

Parts of this chapter were first published in Sripanich, Y., S. Fomel, P. Fowler, A. Stovas, and K. Spikes, 2016, Muir-Dellinger parameters for analysis of anisotropic signatures: 17th International Workshop on Seismic Anisotropy (IWSA). This work was done under the supervision of Dr. Sergey Fomel.

stiffness (Figure 3.1), the average slope values deviate the most from unity, which suggests a higher degree of anellipticity. In the case of synthetic formation fluid infill (Figure 3.3), the average value of slope is higher than that of the dry pore case but can be in the same or slightly lower range than that of the brine-saturated case. Hence, given prior knowledge of shale lithology, there is also a possibility of using the slope of this linear correlation to make an implication about the type of fluid infills.

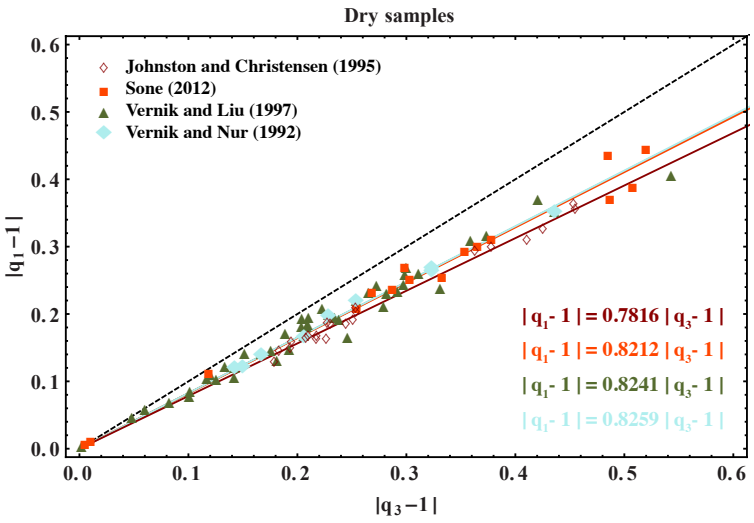

Figure 3.1: Plot of the linear relationship (equation 2.6) between q_1 and q_3 based on the laboratory measurements on dry shale samples from multiple sources. The dashed line denotes the line of slope = 1. mdshales/. dry

Seeking a deeper understanding to the empirical linear relationship, I analyze it by means of the self-consistent rock physics modeling and Backus averaging particularly for shale samples. The first method constitutes a rock physics approach to model elastic anisotropy of shale based on the knowledge of its mineral composition and averaged orientation distribution function of clay platelets (Sayers, 2005). I supplement the results from rock physics modeling with a simple Backus average of several mineral constituents of the mineral framework (Backus, 1962). I assume that

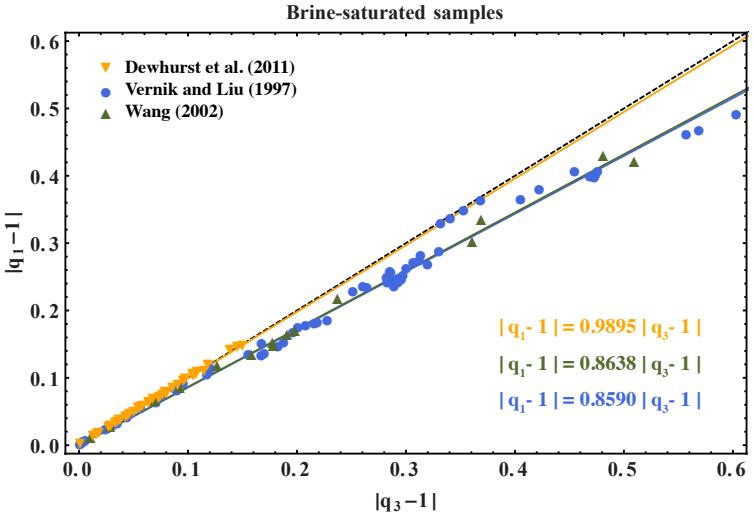

Figure 3.2: Plot of the linear relationship (equation 2.6) between q_1 and q_3 based on the laboratory measurements on brine-saturated shale samples from multiple sources. The dashed line denotes the line of slope = 1. The average slope is higher than what observed from the dry samples. mdshales/. brine

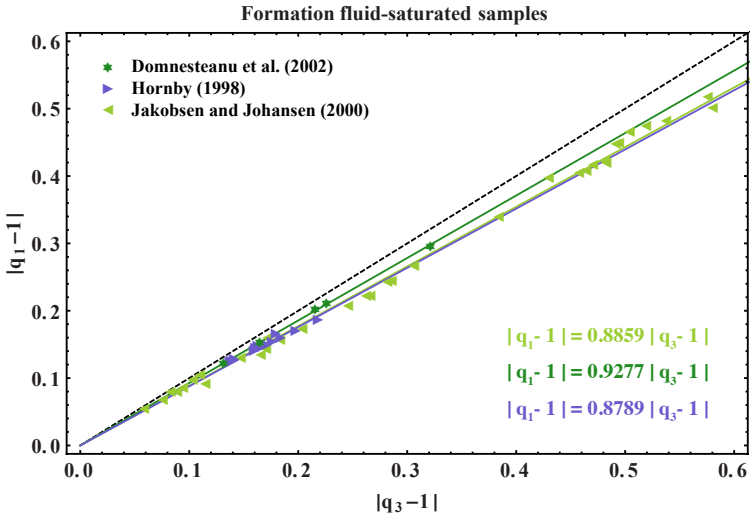

Figure 3.3: Plot of the linear relationship (equation 2.6) between q_1 and q_3 based on the laboratory measurements on formation fluid-saturated shale samples from multiple sources. The dashed line denotes the line of slope = 1. The average slope is higher than that of the dry pore but can be in the same or slightly lower range than that of the brine-saturated case. mdshales/. ff

the Backus averaging is valid in this case because of the small size of each mineral grain compared to the frequency range used in the laboratory. The results show a change in the linear relationship with respect to the change in the volume proportion for different mineral constituents and provide some supportive evidence for the empirically observed linear trend.

SELF-CONSISTENT ROCK PHYSICS MODELING

To further investigate the apparent linear relationship between anelliptic parameters q_1 and q_3, I first utilize the self-consistent approximation (SCA), which is sometimes referred to as the first-order coherent potential approximation (CPA), to model elastic moduli of shales based on the knowledge of mineral composition and average orientation distribution. The SCA has a long history in modeling of multi-phase materials (Hill, 1965; Budiansky, 1965; Wu, 1966; Willis, 1977). The modern version, which does not single out a matrix phase, for effective isotropic composite material is due to Berryman (1980a,b), while the anisotropic counterpart has been studied by other researchers (Hornby et al., 1994; Jakobsen et al., 2000; Johansen et al., 2004; Jakobsen et al., 2003; Bandyopadhyay, 2009; Vasin et al., 2013). I use the anisotropic self-conistent approximation to analyze the linear relationship and is given by the following formula (Jakobsen et al., 2000):

$$\mathbf{C}^* = \left[\sum_{n=1}^{N} v_n \mathbf{C}_n \mathbf{Q}_n\right] \left[\sum_{m=1}^{N} v_m \mathbf{Q}_m\right]^{-1} , \tag{3.1}$$

where

$$\mathbf{Q}_n = [\mathbf{I} + \mathbf{G}_n(\mathbf{C}^*, \alpha_n)(\mathbf{C}_n - \mathbf{C}^*)]^{-1} , \tag{3.2}$$

$\mathbf{C}^*$ and $\mathbf{C}_n$ denote the stiffness tensors in the matrix notation of the effective material and of the n-th phase respectively. v_n represents the volume fraction of the n-th phase.

$\mathbf{G}_n$ denotes the response of a single ellipsoidal inclusion of the n-th phase embedded in an unbounded matrix of the effective (as yet unknown) material having the elastic stiffness $\mathbf{C}^*$. The explicit formulas for $\mathbf{G}_n$ as a function of any background matrix for a specified aspect ratio of an inclusion type are given by Mura (1987). In the case of SCA, the background matrix is equivalent to the unknown effective material $\mathbf{C}^*$, and the aspect ratio (α_n) corresponds to the aspect ratio of each phase of inclusion.

The matrix $\mathbf{G}_n$ has been denoted differently and is not to be confused with matrix $\mathbf{G}_d^{(rs)}$ corresponding to the two-point interaction between the r-th set and the s-th of inclusions showing the effect of spatial distributions of inclusions (Ponte Castañeda and Willis, 1995; Jakobsen et al., 2003). This interaction term only appears when the higher-order CPA or the optical potential approximation (OPA) are considered. Note that matrix notation in equations 3.1 and 3.2 as opposed to the full tensor notation is permissible thanks to the symmetry of the present parameters. This leads to more straightforward expressions suitable for computer programming.

Because of the implicit nature of the SCA scheme (equation 3.1), it has to be solved iteratively. The stopping criterion is when the change in the resultant effective stiffness tensor is smaller than some specified tolerance level. In this study, I choose the following values for average mineral composition for the framework of shales:

$$\begin{aligned} \text{quartz} + \text{clay} + \text{calcite} &= 80\% \ , \\ \text{pyrite} + \text{kerogen} &= 15\% \ , \\ \text{orthoclase} + \text{plagioclase} + \text{dolomite} &= 5\% \text{ (split equally)} \ . \end{aligned} \tag{3.3}$$

These percentages are given out of the total mineral framework, which amounts to only 95% of the entire sample. The porosity in is set to be 5% with vanishing stiffness in the case of dry pores, with the mixture of 70% water and 30% gas in the case of

wet pores, and with 100% water in the case of brine-saturated pores. The result from this step is then corrected for average orientation distribution following the method proposed by Johansen et al. (2004) as described in Appendix B.

The results from the SCA before/after correction are shown in Figures 3.4–3.9 for dry pore case, water/gas-filled pore case and brine-filled pore case with the standard deviation of the Gaussian orientation distribution function (ODF) being $\pi/9$. Moreover, because of the constraints in equation 3.3, I can show the results easily as plots instead of multi-D data. The percentage of calcite can be found from 80% - quartz (%) - clay (%). The results after ODF correction always lead to an increase in the range of possible slope values.

Figures 3.5–3.9 show the ranges of resultant slopes after ODF correction with the dry pores case corresponding to the lowest slope values and the brine-saturated pores case corresponding to the highest. This observation agrees with those seen from the laboratory measurements shown in Figures 3.1 and 3.2. Note that the case of a mixture between water and gas in Figures 3.6 and 3.7 is hypothetical because it was not observed in the laboratory samples. I assume that the values should lie between the two extreme cases of dry and brine-saturated pores. I can observe from the results that despite the significant changes in mineral proportion —especially quartz, clay, and calcite— the slope values vary slowly. Their average is determined largely by the type of fluid infills. This partly justifies the global linear trend from different shale samples subjected to various conditions and the average slope value shown in Figure 2.1. Moreover, the change in proportion of minor minerals such as pyrite with large stiffness coefficients does not lead to a significant effect in the slope values.

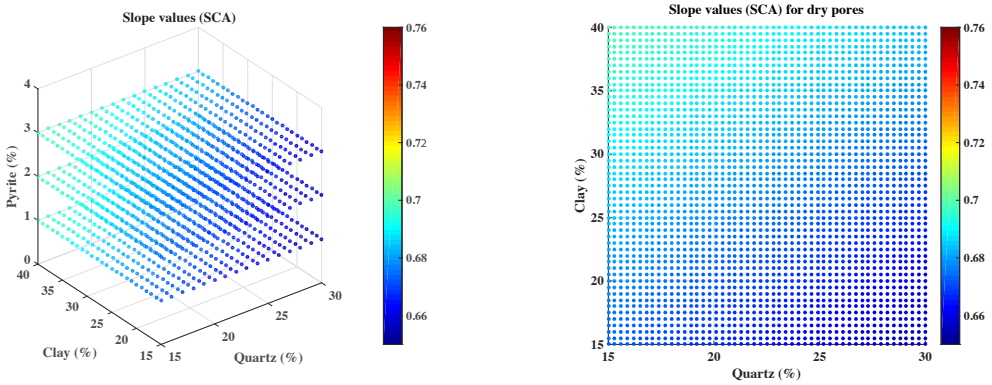

(a) (b)

Figure 3.4: (a) Results of self-consistent modeling for shale composition in equation 3.3 for dry pores without ODF correction. The effect from small variations of pyrite and kerogen appears to be negligible and in (b) they are fixed at 2%, and 13%, respectively. The slope values before correction have the maximum of approximately 0.68 that increases after the correction (Figure 3.5). mdshales/. scadry,scadrypy2

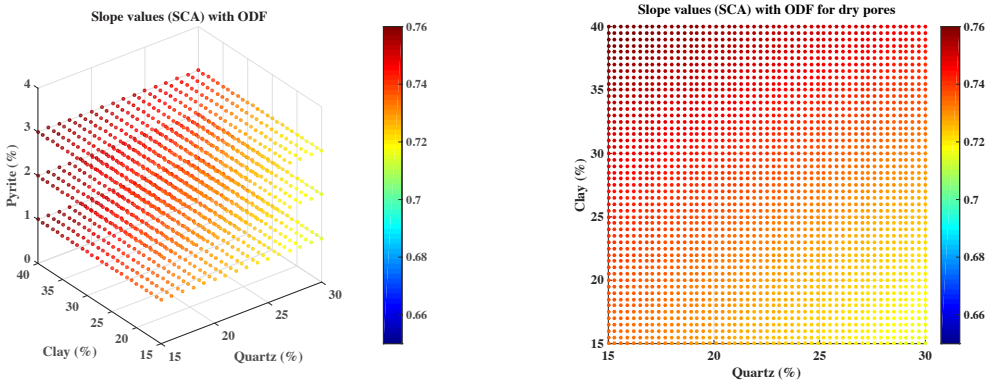

(a) (b)

Figure 3.5: (a) Results of self-consistent modeling for shale composition in equation 3.3 for dry pores with ODF correction. The effect from small variations of pyrite and kerogen appears to be negligible and in (b) they are fixed at 2%, and 13%, respectively. The slope values after correction have the maximum of approximately 0.75. Though slightly lower, this number generally agrees with what observed in the laboratory measurements in Figure 3.1. mdshales/. scadryODF,scadryODFpy2

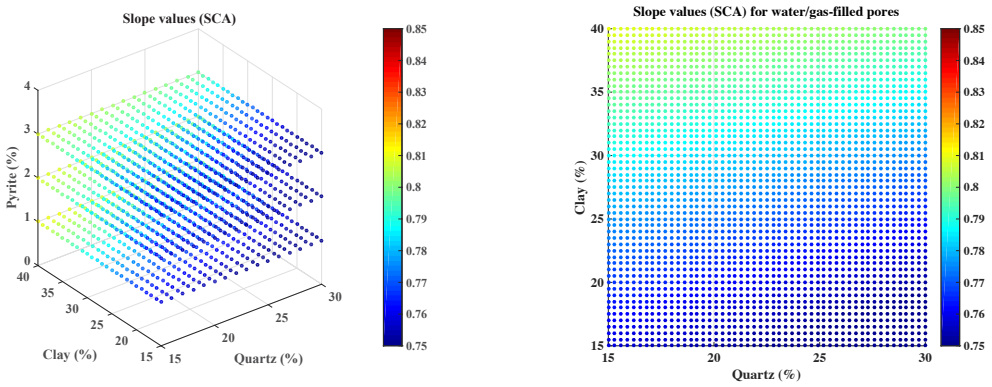

(a) (b)

Figure 3.6: (a) Results of self-consistent modeling for shale composition in equation 3.3 for water/gas-filled pores without ODF correction. The effect from small variations of pyrite and kerogen appears to be negligible and in (b) they are fixed at 2%, and 13%, respectively. The slope values before correction have the maximum of approximately 0.8 that increases after the correction (Figure 3.7). mdshales/. scawet,scawetpy2

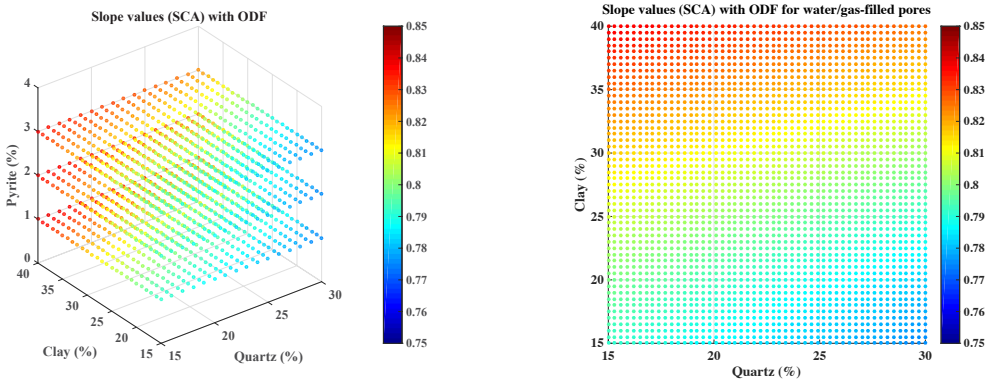

(a) (b)

Figure 3.7: (a) Results of self-consistent modeling for shale composition in equation 3.3 for water/gas-filled pores with ODF correction. The effect from small variations of pyrite and kerogen appears to be negligible and in (b) they are fixed at 2%, and 13%, respectively. The slope values after correction have the maximum of approximately 0.85, which is greater than the dry pores case . mdshales/. scawetODF,scawetODFpy2

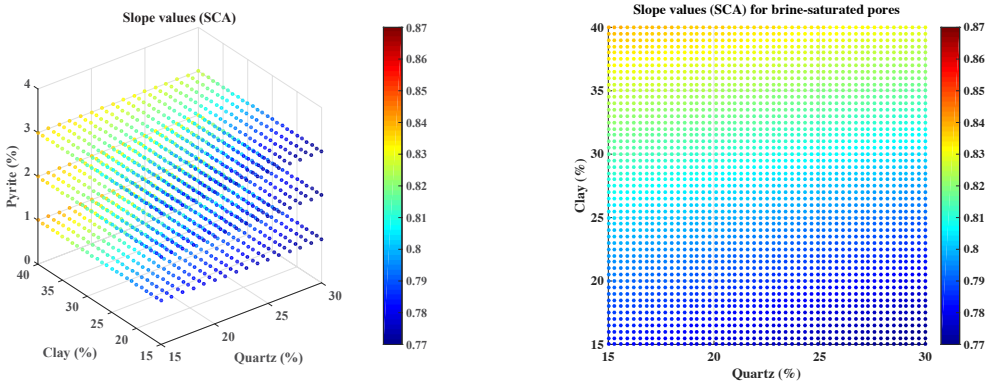

(a) (b)

Figure 3.8: (a) Results of self-consistent modeling for shale composition in equation 3.3 for brine-saturated pores without ODF correction. The effect from small variations of pyrite and kerogen appears to be negligible and in (b) they are fixed at 2%, and 13%, respectively. The slope values before correction have the maximum of 0.84 that increases after the correction (Figure 3.9). mdshales/. scabrine,scabrinepy2

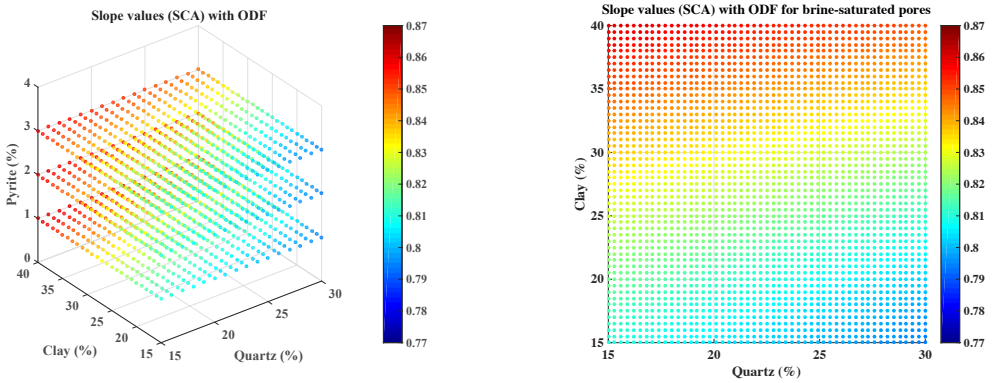

(a) (b)

Figure 3.9: (a) Results of self-consistent modeling for shale composition in equation 3.3 for brine-saturated pores with ODF correction. The effect from small variations of pyrite and kerogen appears to be negligible and in (b) they are fixed at 2%, and 13%, respectively. The slope values after correction have the maximum of > 0.85, which is the greatest among the three cases due to stiffer pores. mdshales/. scabrineODF,scabrineODFpy2

BACKUS AVERAGING

To further investigate this linear dependence, I apply Backus averaging to generate long-wavelength effective stiffnesses of the mineral framework of the synthetic shale used in the SCA as given in equation 3.3. Backus (1962) showed that, in the long-wavelength limit, an effective medium composed of layers of transversely isotropic materials has stiffness coefficients given by the following averaging formulas on constituent stiffnesses:

$$c_{11}^* = \langle c_{11} - c_{13}^2 c_{33}^{-1} \rangle + \langle c_{33}^{-1} \rangle^{-1} \langle c_{13} c_{33}^{-1} \rangle^2 \ , \tag{3.4}$$

$$c_{12}^* = \langle c_{12} - c_{13}^2 c_{33}^{-1} \rangle + \langle c_{33}^{-1} \rangle^{-1} \langle c_{13} c_{33}^{-1} \rangle^2 \ , \tag{3.5}$$

$$c_{33}^* = \langle c_{33}^{-1} \rangle^{-1} \ , \tag{3.6}$$

$$c_{13}^* = \langle c_{33}^{-1} \rangle^{-1} \langle c_{13} c_{33}^{-1} \rangle \ , \tag{3.7}$$

$$c_{55}^* = \langle c_{55}^{-1} \rangle^{-1} \ , \tag{3.8}$$

$$c_{66}^* = \langle c_{66} \rangle \ , \tag{3.9}$$

where the asterisk denotes effective value and the brackets $\langle \cdot \rangle$ indicate weighted average based on volumetric fractions. Assuming that the long-wavelength assumption is satisfied in the laboratory setting for ultrasonic measurements due to the miniature size of each mineral grain, I can use the range of mineral compositions from equation 3.3 and apply the Backus average (equations 3.4-3.9) to compute effective stiffnesses. The results for the mineral framework alone without fluid infills at a specific proportion of pyrite at 2% and kerogen at 13% are shown in Figure 3.10. The observed slope values fall in slightly lower range of values compared to those obtained in the previous section but have a similar trend of slope variation with respect to mineral proportion. The difference can be due to the effects of the orientation distribution of inclusions that are not taken into account in this method. Additionally, due

to the nature of Backus averaging being constructed from simple arithmetic and geometric averages, the introduction of much smaller stiffnesses of water, gas, and dry (vanishing) components will considerably distort the final results. Therefore, they are excluded when generating Figure 3.10(a). However, the similar trend between the result of Backus averaging and the SCA supports the reality of the empirical linear relationship (Figure 2.1).

DISCUSSION

Other possible methods for accurately modeling shale's elastic behavior include the Differential Effective Medium (DEM) (Nishizawa, 1982), the combination of SCA and DEM (Hornby et al., 1994; Bandyopadhyay, 2009), and the general T-matrix approach (Jakobsen et al., 2003). However, it has been shown by Jakobsen et al. (2003) that the SCA approach generally provides a reasonable first estimate of stiffnesses without the questionable physical basis of the DEM and the complexity of the T-matrix approach. It is also important to emphasize that the two methods for shale modeling used in this study — SCA and Backus averaging, are fundamentally different. Even though both methods provide a characterization of the effective medium in the long-wavelength limit, the former takes into account the effects of the statistical orientation distribution and shapes of different inclusions, whereas the latter does not. Because shapes and orientations are considered to be the most important causes of seismic anisotropy (Johansen et al., 2004; Sayers, 2005), failure to take them into consideration may lead to an error in the final estimate of effective stiffnesses. Nevertheless, the results in this paper provide some qualitative arguments that support the empirically observed linear relationship between parameters q_1 and q_3.

As mentioned in Chapter 2, possible extensions to the applicability of the

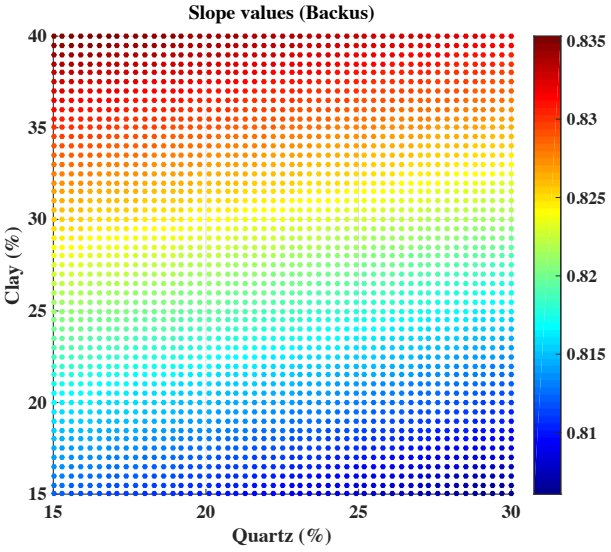

(a)

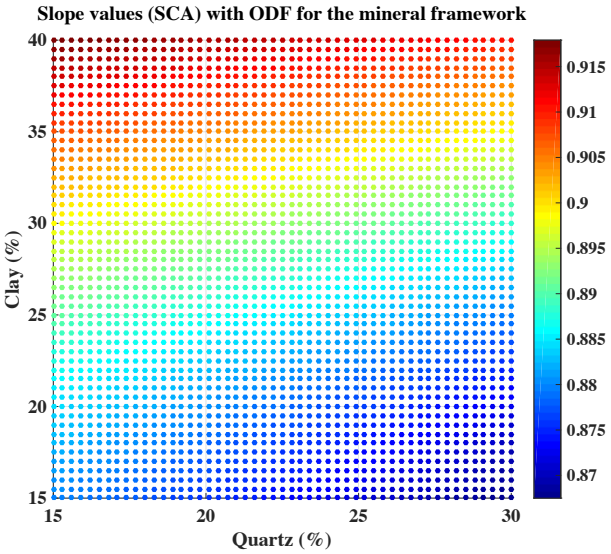

(b)

Figure 3.10: Comparison between resultant slope values computed from (a) Backus average (equations 3.4-3.9) and (b) from self-consistent modeling based on the mineral composition rules specified in equation 3.3 with pyrite and kerogen fixed at 2% and 13%, respectively. I can observe the same general trend in the change of slope values with the changes in mineral proportions. mdshales/. backusfwpy2,scafwODFpy2

empirical linear relationship to 3D orthorhombic anisotropy, require reliable lab measurements based on orthorhombic assumption rather than transverse isotropy. Moreover, they also require accurate rock physics modeling methods in 3D, which can be very challenging. However, the latest development of Backus averaging for general anisotropic media (Bos et al., 2016) may help pave the way to accomplish such task.

Using the linear slope may aid in obtaining additional information such as the subsurface lithology as pointed out the Chapter 2. Moreover, given the knowledge of shale lithology, one may use the linear slope as an indicator of the type of pore fluids. However, it should be cautioned that any conclusions drawn from this process are based on the degree of variation of anisotropy as captured by the linear slope value and should be use in supplement to other more deterministic processes.

In this chapter, I emphasize that there is an agreement between the the empirical relationship from lab measurements and the results from SCA modeling (Figures 3.4–3.9). I later point out a similarity between the SCA results and those from Backus averaging. However, I have not shown a link between the empirical relationship with the results from Backus averaging directly.

CONCLUSIONS

I investigate the empirical linear relationship between two anelliptic parameter q_1 and q_3 on the ground of self-consistent rock physics modeling and Backus averaging. Apart from serving as a basis for parameter reduction and an indicator of the degree of anisotropy, the emipirical linear relationship may also provide additional insights to subsurface lithology and pore fluids. The results from numerical experiments suggest that the general range of the slope values in shale samples is largely dictated

by the type of the fluid infills, with the case of brine-saturated pores leading to the highest slope values, whereas the lowest values correspond to the case of dry pores. Despite the significant changes in mineral proportion in the shale models, much smaller variations in the slope values are observed.

ACKNOWLEDGMENTS

I would like to thank M. Jakobsen and Q. Ren for helpful comments and suggestions on rock physics modeling methods. I thank the sponsors of the Texas Consortium for Computational Seismology (TCCS), the Exploration and Development Geophysics Education and Research Forum (EDGER), and the Rock Seismic Research project (ROSE) for financial support. I also acknowledges the additional support from the Statoil Fellows Program at the University of Texas at Austin.

Chapter 4

Sensitivity analysis with respect to qP kinematics

Properly chosen anisotropic parameters have clear physical meaning and allow complex formulas for seismic-wave attributes to be concisely expressed with the complexity hidden inside the notation. In application to parameter estimation, a desirable feature of good parameterization is orthogonality when both full and reduced sets are considered. I compare four parameterization schemes for qP waves in TI and orthorhombic anisotropy and analyze the sensitivity of the phase velocity, group velocity, and traveltime to different anisotropic parameterizations. To quantify parameter sensitivity, I use an approximate Hessian matrix for linearized velocity inversion when both the full parameterization and pseudoacoustic approximation are considered. Our results indicate that the Chapman-Miller-Fowler and Muir-Dellinger parameterizations may represent preferable schemes to characterize qP-wave kinematics for parameter estimation.

INTRODUCTION

Seismic anisotropy, defined as the dependence of velocity upon the propagation direction, has been widely recognized as one of the primary challenges in seismic pro-

Parts of this chapter were first published in Sripanich, Y., S. Fomel, and P. Fowler, 2016, A comparison of anisotropic parameterizations for TI and orthorhombic media and their sensitivity with respect to qP velocities: 86th Annual Meeting, *SEG Expanded Abstracts*, 479-484. This work was done under the supervision of Dr. Sergey Fomel.

cessing, imaging, and inversion (Tsvankin et al., 2010; Thomsen, 2014). To describe the effects of anisotropy on seismic data, previous researchers introduced several combinations of the stiffness coefficients that can be more meaningful than the stiffness coefficients themselves. These combinations, in the form of *anisotropic parameters*, provide intuitive understanding of seismic wave behavior and allow for constructive approximations with high level of accuracy.

The transversely isotropic (TI) model is the best studied and requires five stiffness coefficients to describe full elastic wave behavior (Tsvankin, 2012). *Thomsen parameters* (Thomsen, 1986) are commonly used in conventional analyses of anisotropic signatures in such model. Several other alternative parameterization schemes have been proposed: *Alkhalifah parameters* (Alkhalifah, 1998, 2000a), *Weak Anisotropy (WA) parameters* (Mensch and Rasolofosaon, 1997; Pšenčík and Gajewski, 1998), *Chapman-Miller-Fowler parameters* (Chapman and Miller, 1996; Schoenberg and de Hoop, 2000; Fowler, 2015), and *Muir-Dellinger parameters* (Muir and Dellinger, 1985; Dellinger et al., 1993; Fomel, 2004). All these parameterizations were derived based on different concepts and can be successfully applied in various problems concerning seismic anisotropy.

A TI model is often insufficient for fully characterizing the subsurface and orthorhombic models are more appropriate in cases where the effects of layering and orthogonal fracture sets are both present (Tsvankin and Grechka, 2011; Thomsen, 2014). In such a model, nine stiffnesses are required to describe full elastic wave behavior and there are three planes of symmetry where the waves behave similarly as in the TI media (Schoenberg and Helbig, 1997; Tsvankin, 2012). Extensions of aforementioned TI parameterization schemes have also been proposed (Tsvankin, 1997; Alkhalifah, 2003; Fowler, 2015; Sripanich and Fomel, 2015). A summary table of dif-

ferent TI parameterizations and their extensions to orthorhombic symmetry is shown in Table 1.1 and I refer the readers to Chapter 1 for the review of various anisotropic parameters.

I primarily focus on the four strictly defined parameterizations and exclude the dynamically defined WA parameters from consideration because they involve an additional degree of freedom requiring a choice of the reference velocity. I use the following criteria for comparison among anisotropic parameterization schemes:

1. Anisotropic parameters should have clear physical meanings.

2. TI parameterizations should have a natural extension to corresponding orthorhombic parameterizations.

3. A chosen parameterization should lead to pseudoacoustic simplifications for qP waves where the number of dependent anisotropic parameters for qP-wave analysis reduces from four to three in TI media and from nine to six in orthorhombic media.

4. Different parameters should possess orthogonal sensitivity to allow for a well-behaved parameter inversion problem.

The first three criteria have been addressed in Chapter 2 and 3 for MD parameters and in Chapter 1 for other schemes. In this chapter, to address the last criterion, I conduct a study on the sensitivity of qP-wave phase and group velocities in both TI and orthorhombic media comparing different choices of parameterizations when both the full set and the reduced set from the pseudoacoustic approximation are considered. My method of measuring sensitivity follows the approximate Hessian

approach of Sripanich and Fomel (2015). I show that the sensitivity of group velocity to different choices of anisotropic parameters agrees also with the sensitivity of travel-time and therefore, indicates the overall sensitivity of qP-wave kinematics to different choices of anisotropic parameters. I provide a summary table for the relative merit of each parameterization according to different criteria at the end of this chapter.

SENSITIVITY ANALYSIS

To compare sensitivities of different parameterizations, I adopt the following general formula of an approximate Hessian matrix (Sripanich and Fomel, 2015):

$$R_{ij} = \int_0^{\pi/2} \int_0^{\pi/2} \frac{\partial V^2}{\partial m_i} \frac{\partial V^2}{\partial m_j} \sin\theta d\theta d\phi \ , \tag{4.1}$$

where V is the exact qP phase (or group)-velocity expression, m_i and m_j are two of the four (nine) possible parameters present in each TI (orthorhombic) parameterization, θ is the phase angle measured from the vertical x_3, and ϕ is azimuthal angle measured from x_1. The matrix R_{ij} is an approximation of the Hessian of the linearized inversion of phase velocity squared, with respect to different parameterizations and therefore, an approximation of the inverse covariance matrix for these parameters (Appendix C). The term $\sin\theta$ is included to account for the determinant of Jacobian for the change of variables. In the case of 2D TI media, this term is absent because there is only an integration with respect to θ (Sripanich and Fomel, 2015). I normalize every velocity-like anisotropic parameter by the average velocity defined as $v_{av}^2 = 4/\pi \int_0^{\pi/2} \int_0^{\pi/2} V^2 \sin\theta d\theta d\phi$ to make them dimensionless.

Investigation on diagonal dominance

In the ideal scenario, R_{ij} is equal to an identity matrix, which suggests that different basis parameters are truly orthogonal to one another and are equally important (similar value of the diagonal elements in the identity matrix). However, in practice, this is not the case and one should seek a parameterization scheme such that R_{ij} is the most diagonally dominant. Assuming no summation convention of repeated indices, a $N \times N$ matrix R_{ij} is said to be diagonally dominant if

$$|R_{ii}| \geq \sum_{j \neq i} |R_{ij}| \quad \text{for all } i = 1, 2, \ldots, N-1, N \ , \tag{4.2}$$

which implies that for each row i-th of the matrix R_{ij}, the magnitude of the diagonal entry must be greater than or equal to the sum of the magnitudes of all non-diagonal entries. To quantify the degree of diagonal dominance for the R_{ij} from different anisotropic parameterizations, I propose to use the following *Diagonally Dominant Index* (DDI) given by

$$DDI = \frac{1}{N} \sum_{i=1}^{N} \frac{\sum_{j \neq i} |R_{ij}|}{|R_{ii}|} \ , \tag{4.3}$$

which goes to zero when the off-diagonal entries in every row becomes zero. Therefore, the smaller the DDI is, the more diagonally dominant the matrix becomes. I emphasize that the DDI only measures the relative magnitude of the off-diagonal entries with respect to that of the diagonal entries. Thus, it indicates orthogonality among the basis parameters. However, it doesn't indicate the balance in the contribution (magnitude of the diagonal entries) from different parameters.

For a benchmark test, I use Greenhorn shale parameters (Jones and Wang, 1981) that have stiffnesses specified as $c_{11} = 14.47$, $c_{33} = 9.57$, $c_{13} = 4.51$, and $c_{55} = 2.28$ (km^2/s^2) for a TI model and use the standard model of Schoenberg and

Helbig (1997) specified as $c_{11} = 9$, $c_{22} = 9.84$, $c_{33} = 5.9375$, $c_{13} = 2.25$, $c_{23} = 2.4$, $c_{12} = 3.6$, $c_{44} = 2$, $c_{55} = 1.6$, and $c_{66} = 2.182$ (km^2/s^2) for an orthorhombic model. Figures 4.1 and 4.2 show the symmetric matrix R_{ij} when considering four parameters for qP phase and group velocities in the Greenhorn shale TI model. I observe that the Muir-Dellinger (MD) parameters represents the most orthogonal parameterization with the smallest DDI and the high correlations concentrated along the diagonal. Figures 4.3 and 4.4 show similar plots when only three parameters are considered under pseudoacoustic approximation. One can observe that the Chapman-Miller-Fowler parameters are the most orthogonal but the Alkhalifah and Muir-Dellinger parameters are not far behind.

Figures 4.5–4.8 show similar plots of the approximate Hessians with DDI for the orthorhombic model for both qP phase and group velocities with nine and six parameters. Similar observations can be made as in the TI case. Muir-Dellinger parameters perform best when the full set of nine parameters is considered, while the Chapman-Miller-Fowler parameters are the most orthogonal when six parameters are considered under pseudoacoustic approximation.

Condition number analysis

For a more quantitative comparison with an additional consideration of the diagonal magnitudes, I propose to consider the condition number (κ) of the approximate Hessian (R_{ij}) as the indicator of a well-behaved parameterization. Its definition corresponds to the ratio of largest and smallest eigenvalues ($\lambda_{max}/\lambda_{min}$). The smaller the condition number is, the more uniform is the sensitivity to different parameters, and the more efficient the inversion becomes.

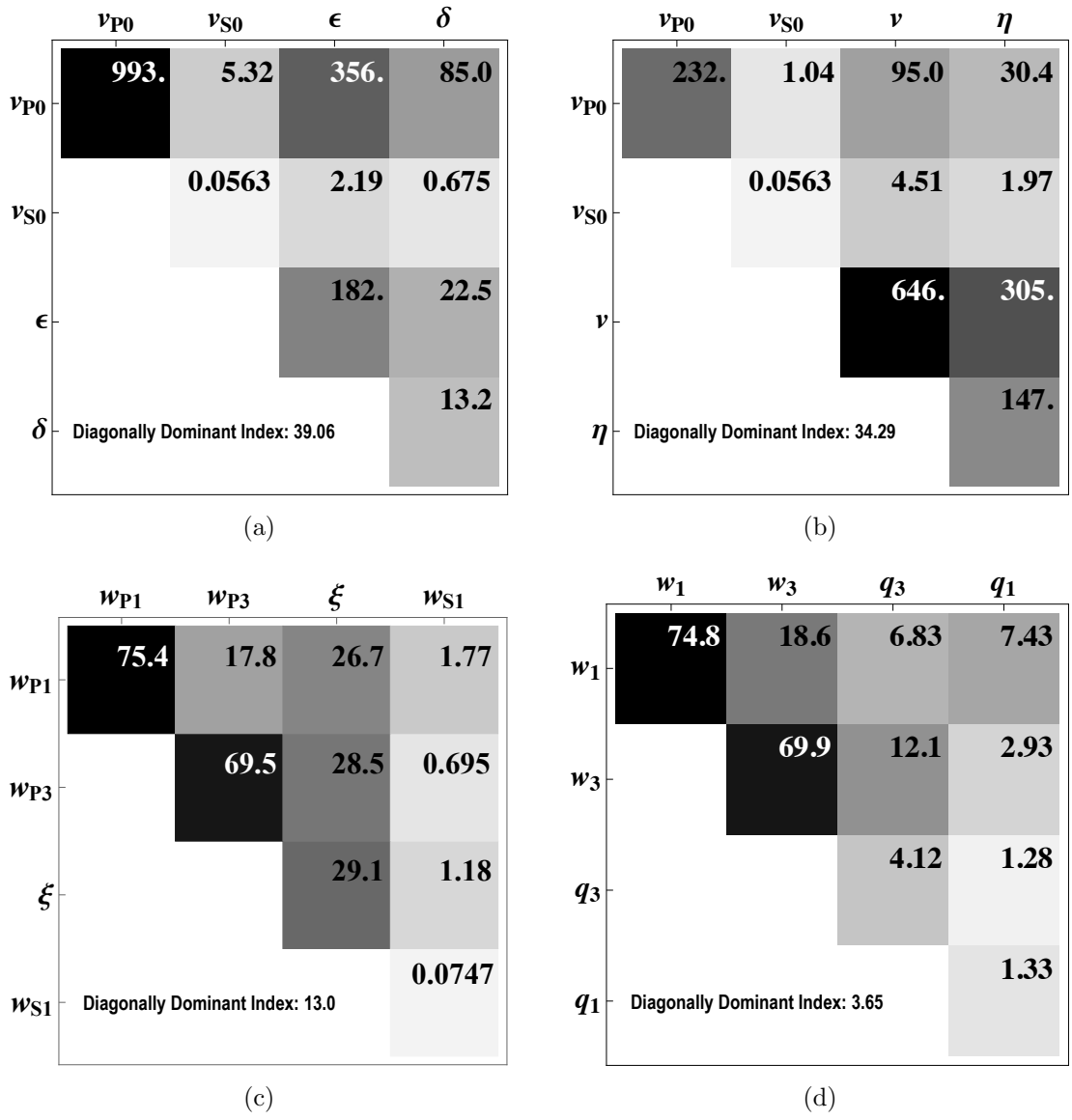

Figure 4.1: Plot of R_{ij} in the TI model when considering four parameters for qP phase velocity with (a) Thomsen (b) Alkhalifah (c) Chapman-Miller-Fowler and (d) Muir-Dellinger parameters. The smallest DDI can be observed in (d) suggesting the most diagonally dominant matrix. sensitivity/. TI-thomsen,TI-alka,TI-chapman,TI-zone

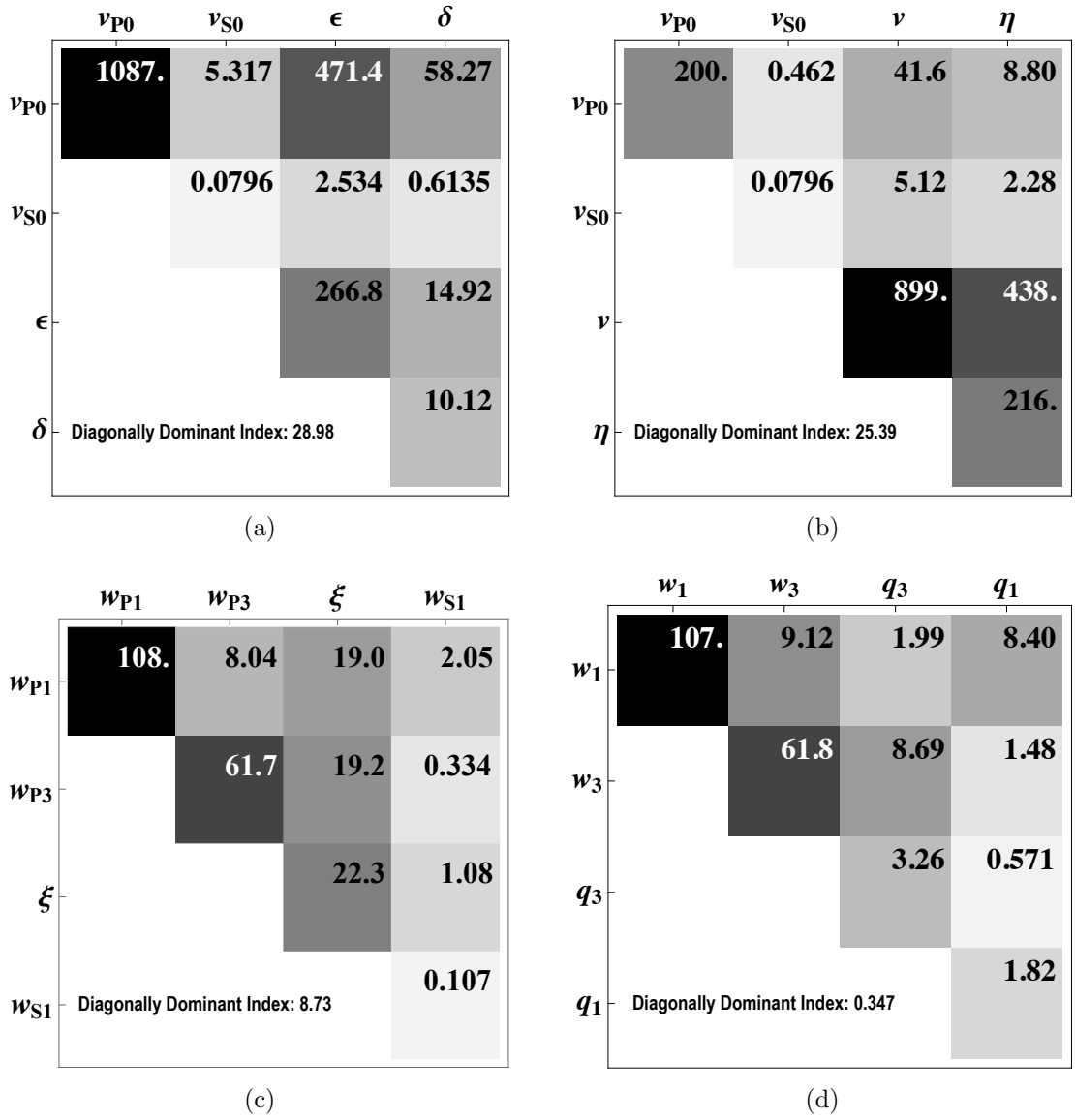

Figure 4.2: Plot of R_{ij} in the TI model when considering four parameters for qP group velocity with (a) Thomsen (b) Alkhalifah (c) Chapman-Miller-Fowler and (d) Muir-Dellinger parameters. The smallest DDI can be observed in (d) suggesting the most diagonally dominant matrix. sensitivity/. TI-thomsengroup,TI-alkagroup,TI-chapmangroup,TI-zonegroup

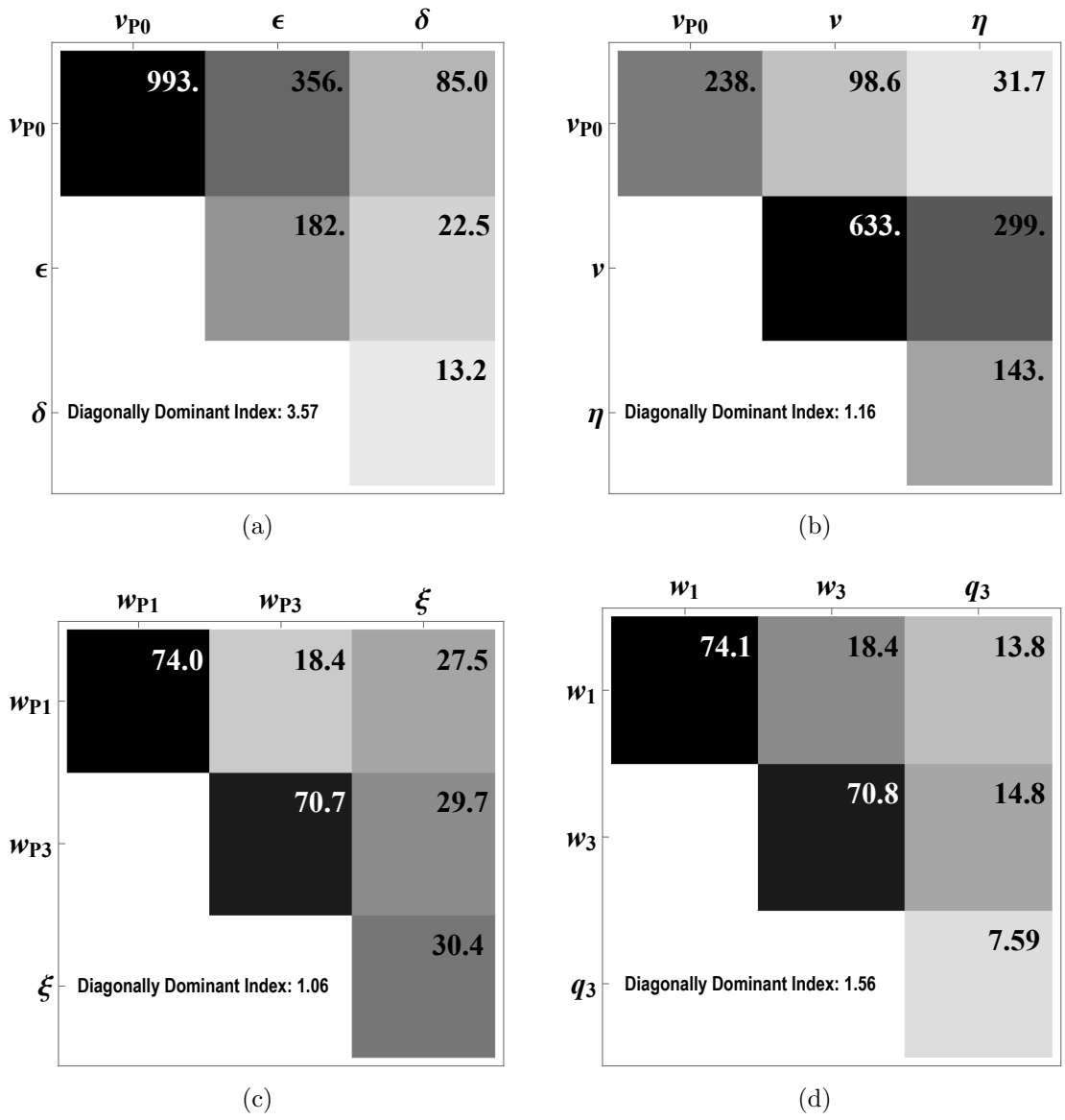

Figure 4.3: Plot of R_{ij} in the TI model when considering three parameters for qP phase velocity under pseudoacoustic approximation with (a) Thomsen (b) Alkhalifah (c) Chapman-Miller-Fowler and (d) Muir-Dellinger parameters. The smallest DDI can be observed in (c) suggesting the most diagonally dominant matrix. sensitivity/. TI-threethomsen,TI-threealka,TI-threechapman,TI-threezone

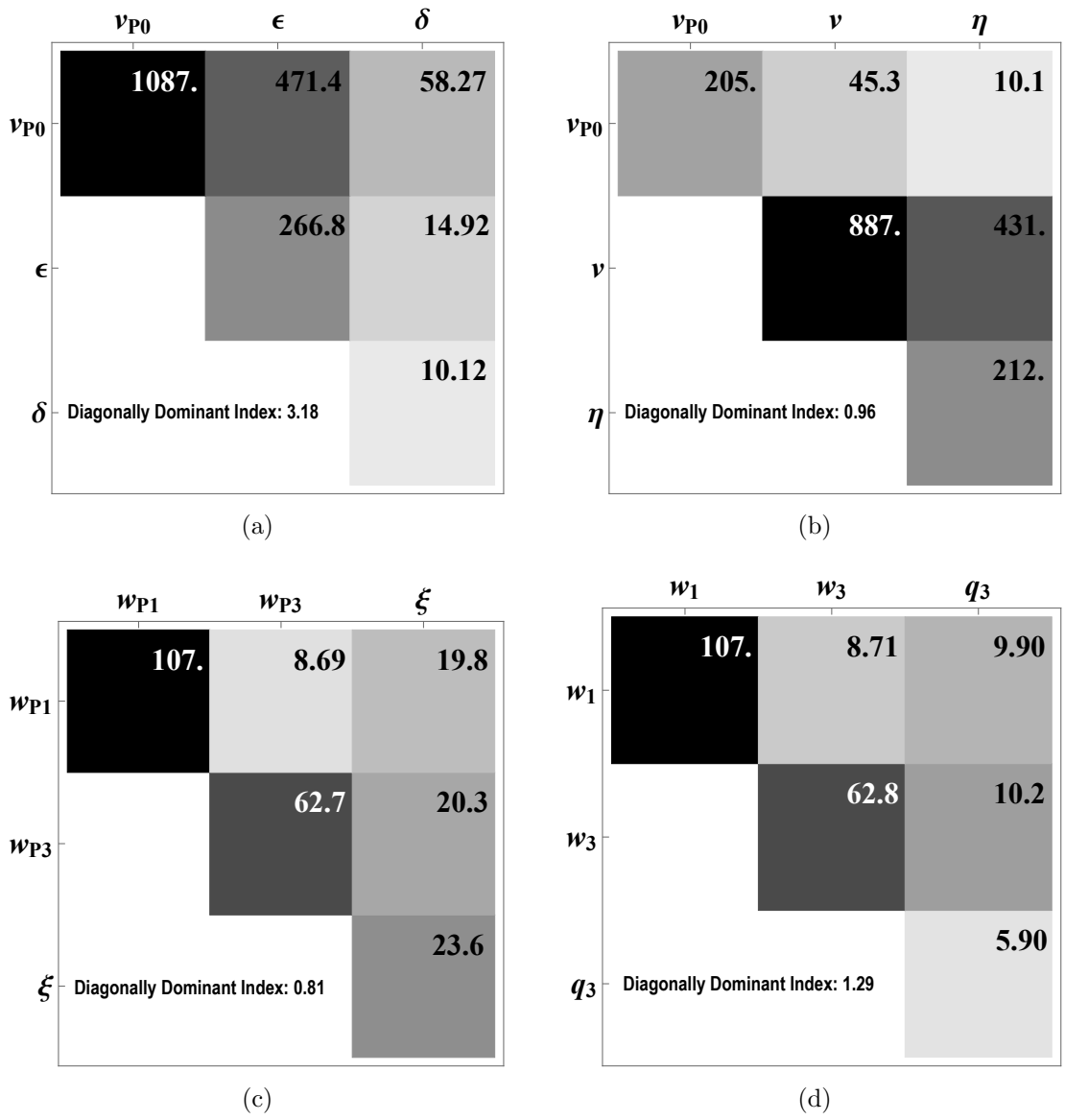

Figure 4.4: Plot of R_{ij} in the TI model when considering three parameters under pseudoacoustic approximation for qP group velocity with (a) Thomsen (b) Alkhalifah (c) Chapman-Miller-Fowler and (d) Muir-Dellinger parameters. The smallest DDI can be observed in (c) suggesting the most diagonally dominant matrix. sensitivity/. TI-threegthomsen,TI-threegalka,TI-threegchapman,TI-threegzone

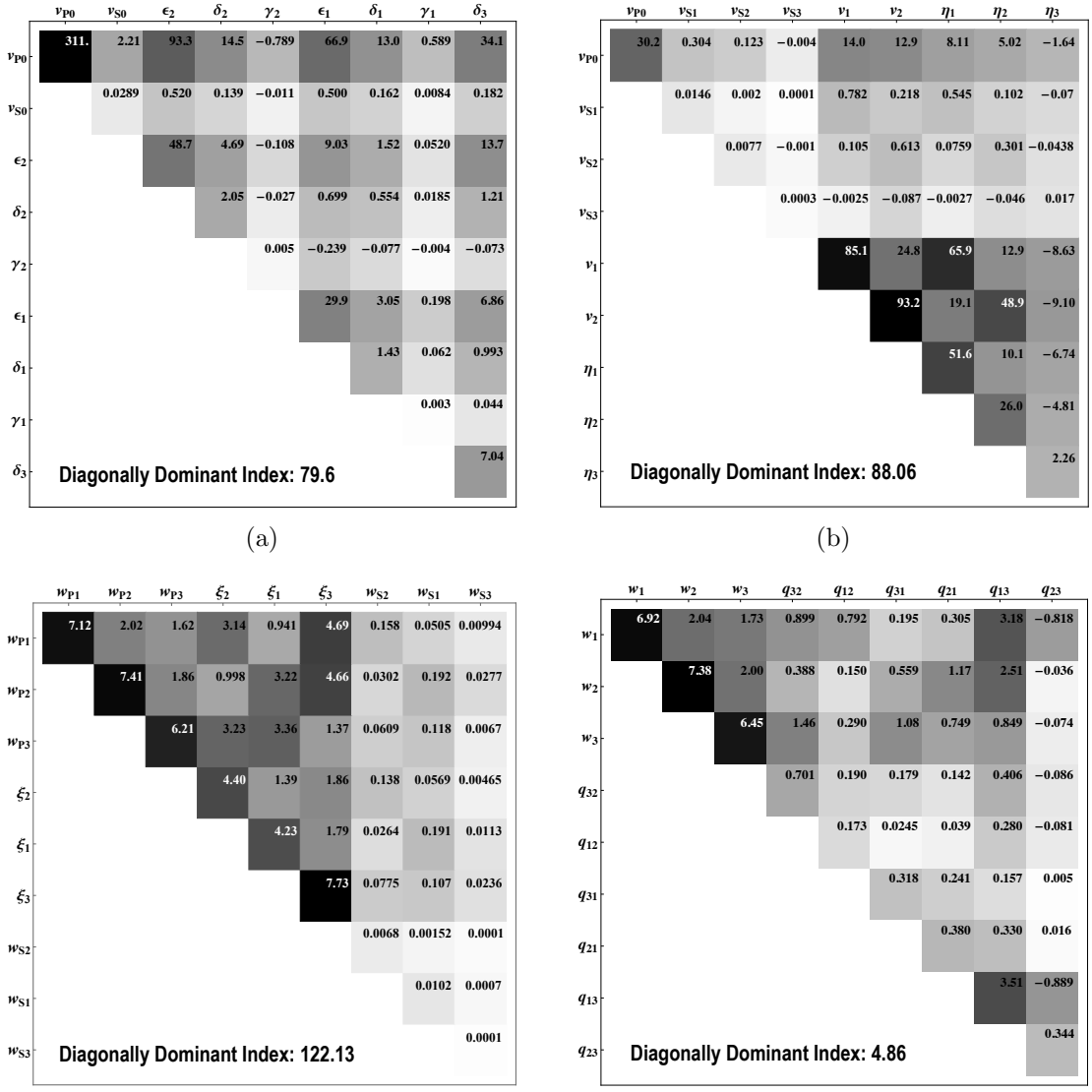

(a) (b)

(c) (d)

Figure 4.5: Plot of R_{ij} in the orthorhombic model when considering nine parameters for qP phase velocity with (a) Tsvankin (b) Alkhalifah (c) Chapman-Miller-Fowler and (d) Muir-Dellinger parameters. The smallest DDI can be observed in (d) suggesting the most diagonally dominant matrix. sensitivity/. ortho-thomsen,ortho-alka,ortho-chapman,ortho-zone

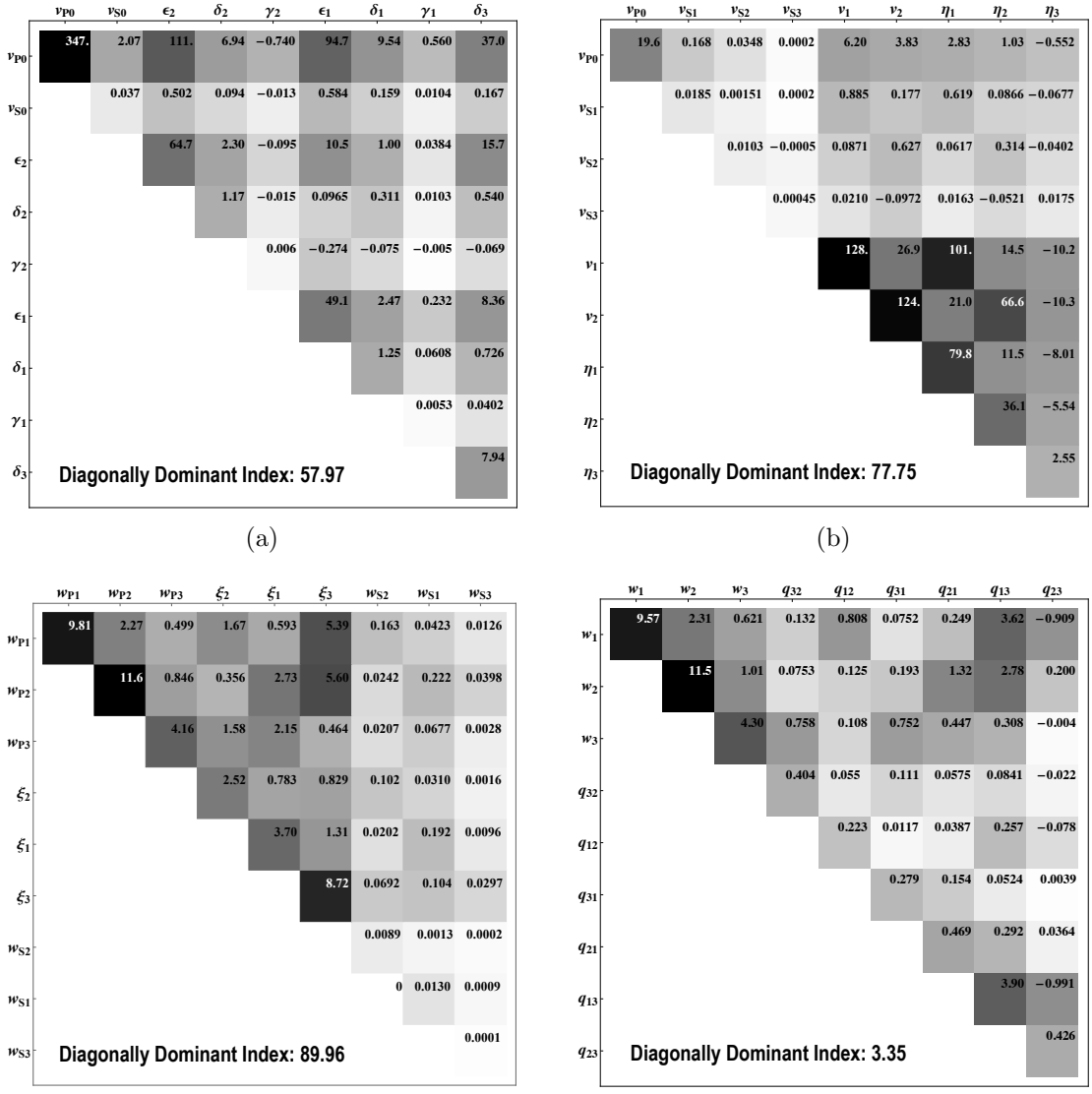

(a) (b) (c) (d)

Figure 4.6: Plot of R_{ij} in the orthorhombic model when considering nine parameters for qP group velocity with (a) Tsvankin (b) Alkhalifah (c) Chapman-Miller-Fowler and (d) Muir-Dellinger parameters. The smallest DDI can be observed in (d) suggesting the most diagonally dominant matrix. sensitivity/. ortho-thomseng,ortho-alkag,ortho-chapmang,ortho-zoneg

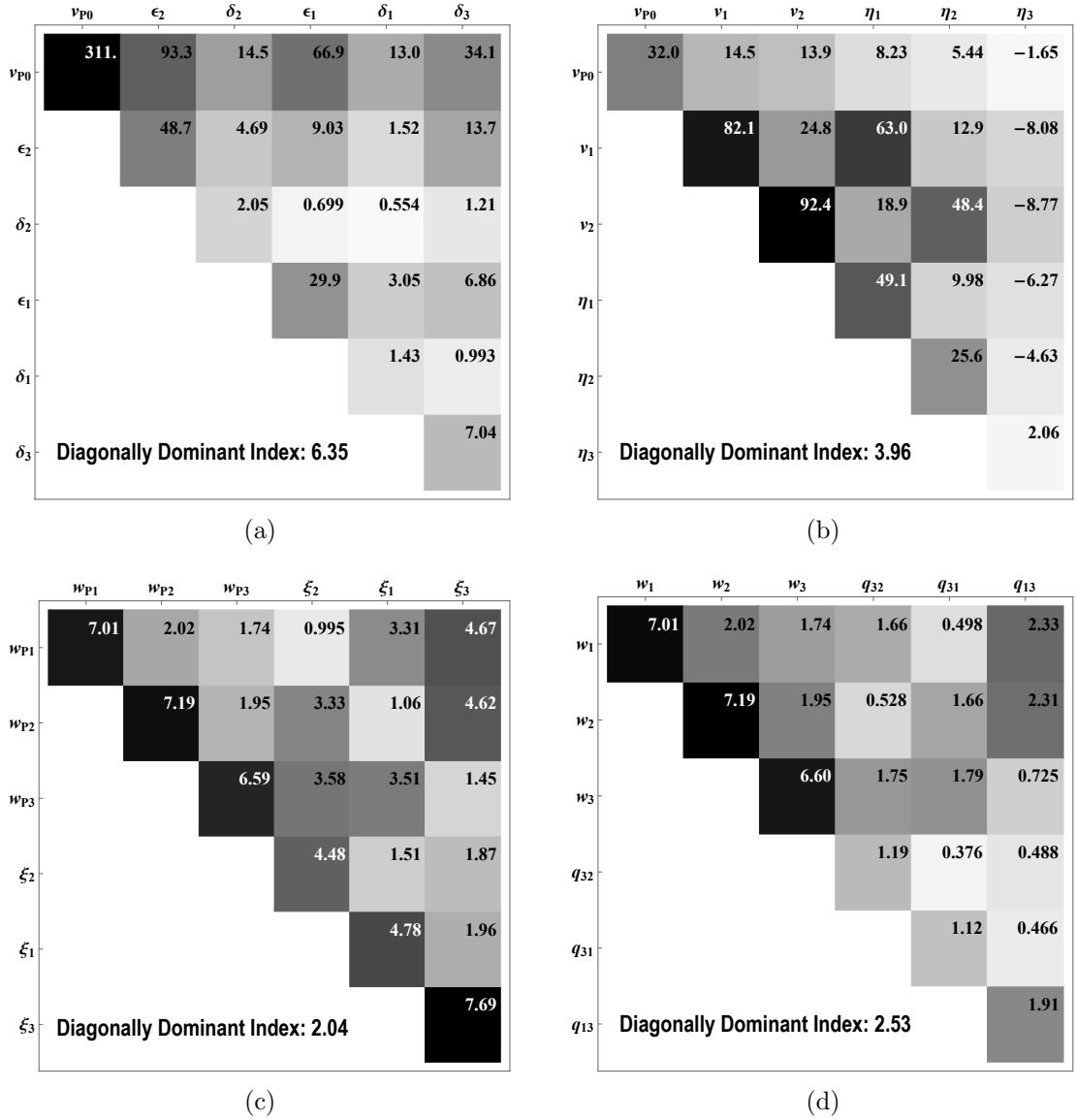

Figure 4.7: Plot of R_{ij} in the orthorhombic model when considering six parameters under pseudoacoustic approximation for qP phase velocity with (a) Tsvankin (b) Alkhalifah (c) Chapman-Miller-Fowler and (d) Muir-Dellinger parameters. The smallest DDI can be observed in (c) suggesting the most diagonally dominant matrix. sensitivity/. ortho-sixthomsen,ortho-sixalka,ortho-sixchapman,ortho-sixzone

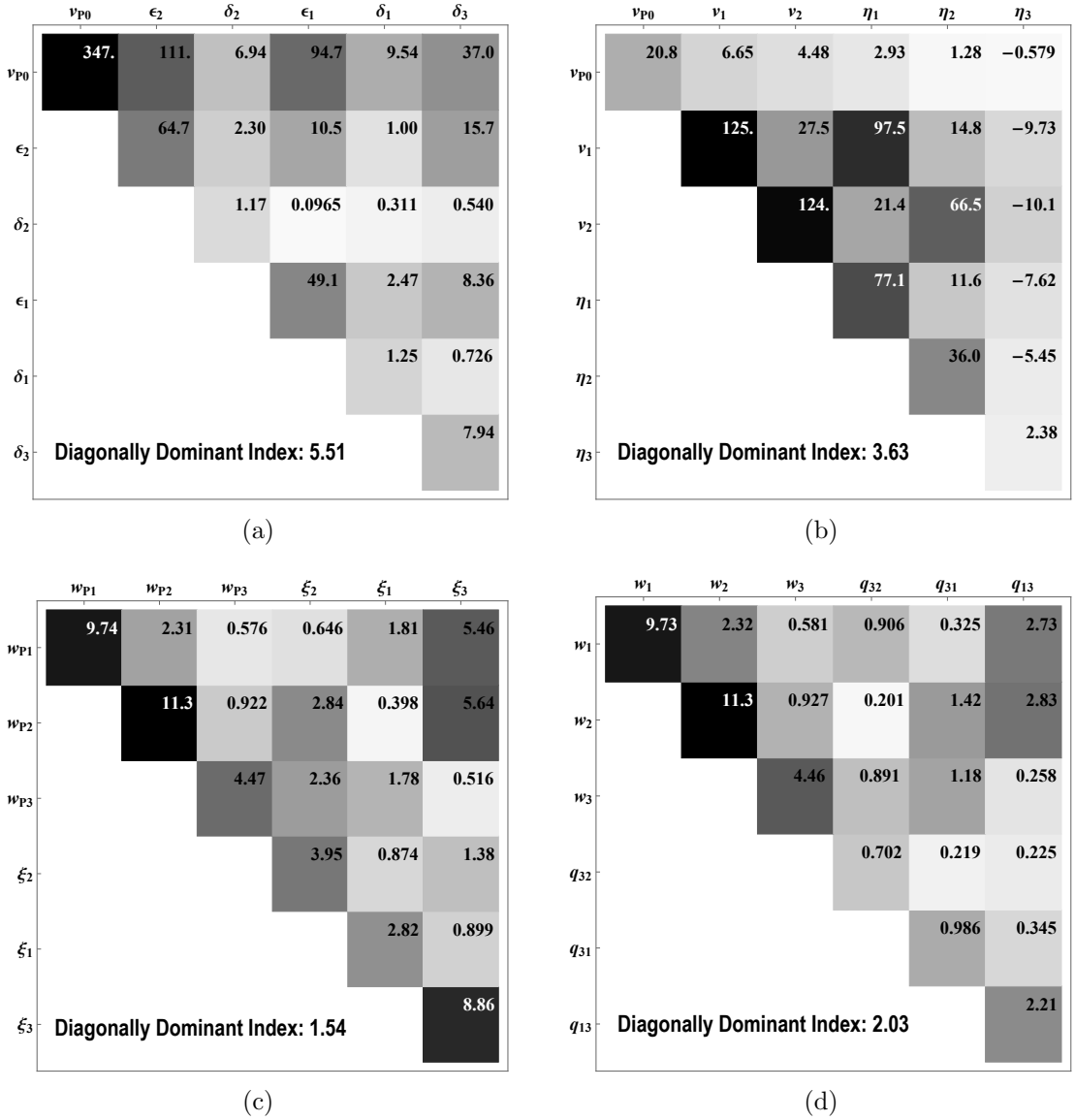

Figure 4.8: Plot of R_{ij} in the orthorhombic model when considering six parameters under pseudoacoustic approximation for qP group velocity with (a) Tsvankin (b) Alkhalifah (c) Chapman-Miller-Fowler and (d) Muir-Dellinger parameters. The smallest DDI can be observed in (c) suggesting the most diagonally dominant matrix.
sensitivity/. ortho-sixgthomsen,ortho-sixgalka,ortho-sixgchapman,ortho-sixgzone

Figures 4.9 and 4.10 display the plots of the logarithm of the eigenvalues for different parameterization schemes. Each plot point denotes one eigenvalue of the Hessian with respect to the specified parameterization scheme and the connecting line corresponds to the size of the condition number. Therefore, I seek a parameterization that gives the shortest line in each plot. The exact values of the logarithm of condition numbers are also shown. In consideration of the full set of parameters (four in TI and nine in orthorhombic), the Muir-Dellinger parameters lead to the smallest condition numbers as shown in Figures 4.9(a), 4.9(c), 4.10(a), and 4.10(c). This is not particularly surprising due to the fact that the qP-wave velocities are almost insensitive to the vertical qS-wave velocity in other schemes (Alkhalifah, 1998; Fowler, 2003) and this fact can also been seen from the small values corresponding to the vertical qS-wave velocity in the R_{ij} (Figures 4.1–4.8).

For a fairer comparison on similar ground, I reduce the number of dependent parameters from four to three in TI and nine to six in orthorhombic models according to the pseudoacoustic approximation (Figures 4.9(b), 4.9(d), 4.10(b), and 4.10(d)). Among the four parameterizations the optimal parameterization associated with the smallest condition number in both the cases of three (TI) and six (orthorhombic) parameters is the Chapman-Miller-Fowler scheme. However, the Muir-Dellinger parameters are not far behind. Rather than pseudoacoustic approximation, using an empirical linear relationship between q_1 and q_3 (Chapter 2) can serve as an alternative and better way to reduce the number of parameters.

Analysis with one-hundred sampled models

To mitigate the model-dependent nature of our results, I further analyze the sensitivity of one-hundred randomly sampled TI models generated under the following

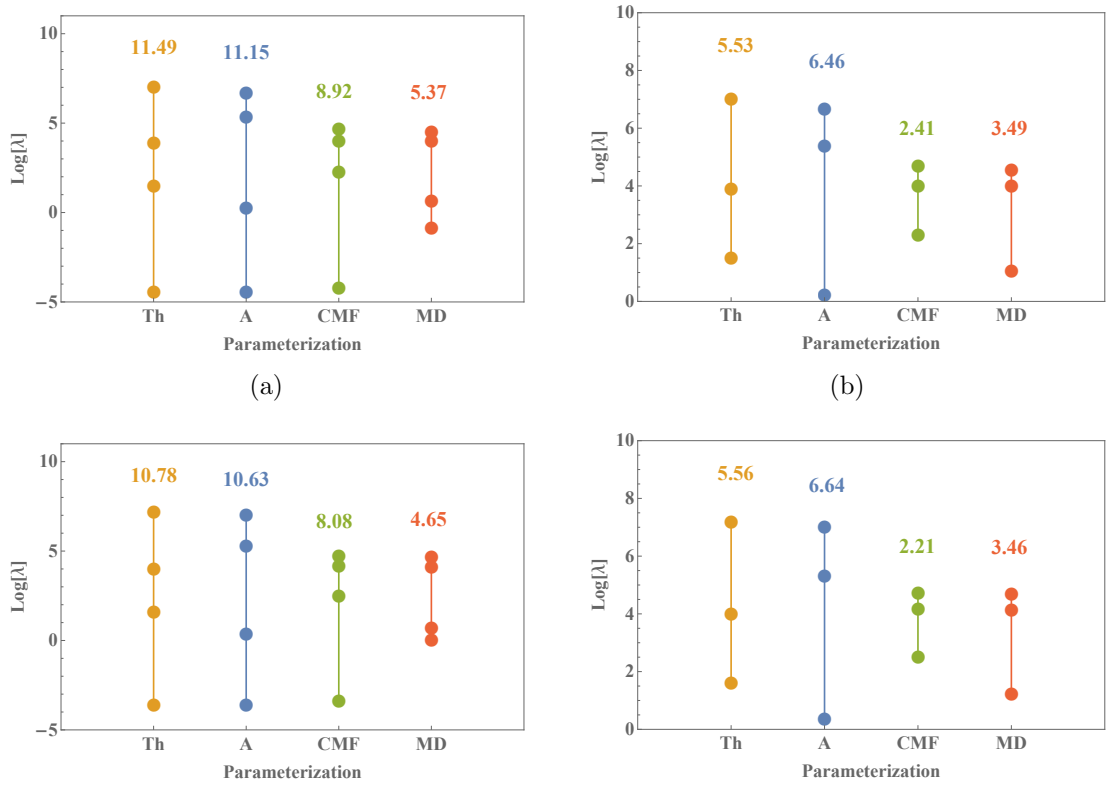

Figure 4.9: Distribution of eigenvalues of the sensitivity matrix in the TI model when considering (a) four and (b) three parameters for qP phase velocity and (c) four and (d) three parameters for qP group velocity. The acronyms Th, A, CMF, and MD stand for Thomsen, Alkhalifah, Chapman-Miller-Fowler, and Muir-Dellinger parameters and the corresponding condition numbers are listed. The plots indicate that MD has the lowest condition number when the full set is consider, but perform slightly worse than CMF with three parameters. sensitivity/. fourtrans,threetrans,fourgrouptrans,threegrouptrans

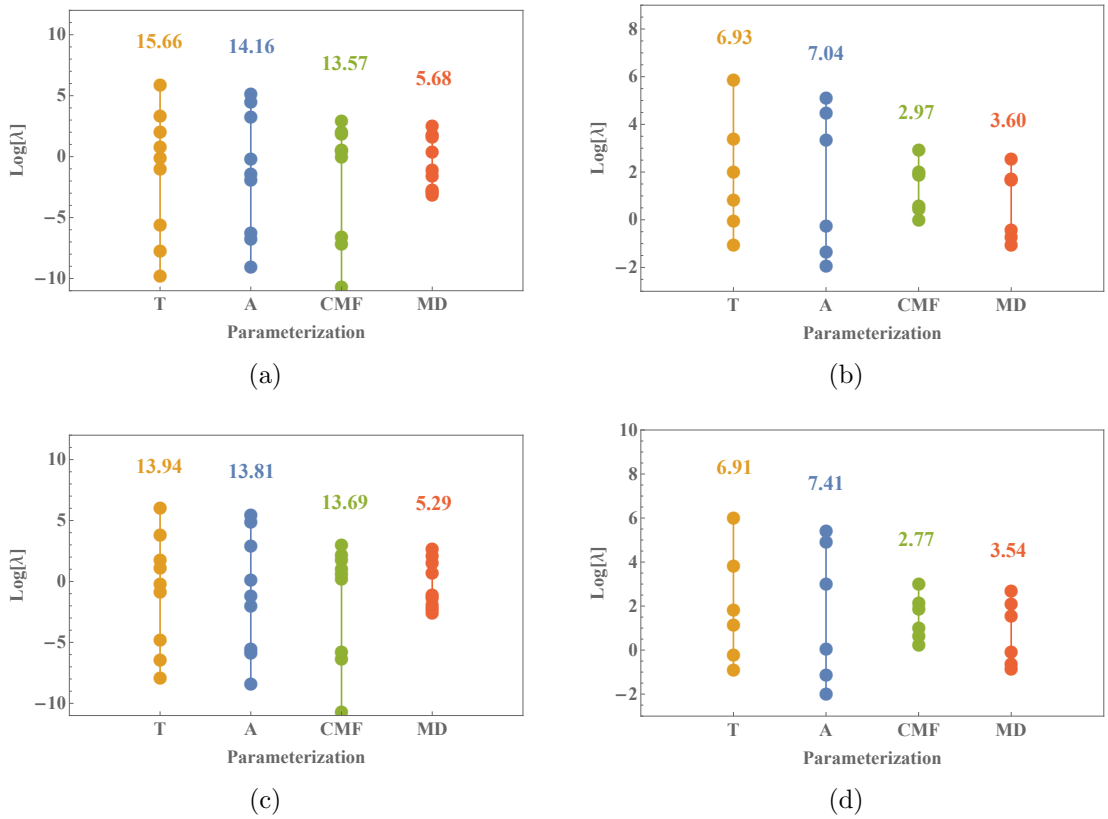

Figure 4.10: Similar to Figure 4.9 but for the orthorhombic model when considering (a) nine and (b) six parameters for qP phase velocity and (c) nine and (d) six parameters for qP group velocity. The acronyms T, A, CMF, and MD stand for Tsvankin, Alkhalifah, Chapman-Miller-Fowler, and Muir-Dellinger parameters. Similar conclusion as that from Figure 4.9 can be drawn. sensitivity/. ninetrans,sixtrans,ninegrouptrans,sixgrouptrans

constraints:

$$\begin{aligned} 2.5 \text{ km/s} < \quad & v_{P0} \quad < 4 \text{ km/s} , \\ 1 \text{ km/s} < \quad & v_{S0} \quad < 2 \text{ km/s} , \\ 0 < \quad & \epsilon \quad < 0.3 , \\ -0.1 < \quad & \delta \quad < 0.1 . \end{aligned} \tag{4.4}$$

Each realization is subjected to the energy constraints to ensure its viability. These constraints are given in equation 1.53. For generated orthorhombic models, the energy constraints are given in equation 1.56 and the model constraints include:

$$\begin{aligned} 2.5 \text{ km/s} < \quad & v_{P0} \quad < 4 \text{ km/s} , \\ 1 \text{ km/s} < \quad & v_{S0} \quad < 2 \text{ km/s} , \\ 0 < \quad & \epsilon_i \quad < 0.3 , \\ 0 < \quad & \gamma_i \quad < 0.2 , \\ -0.1 < \quad & \delta_j \quad < 0.1 , \end{aligned} \tag{4.5}$$

where $i \in \{1, 2\}$ and $j \in \{1, 2, 3\}$. Different seeds for random number generator are used to decrease the chance of anisotropic parameters of the same range to have similar value. Figures 4.11 and 4.12 show resultant histograms for the distribution of condition numbers in one-hundred generated TI models. The horizontal axes in all subplots are kept at the same scale to help demonstrate the spread length of possible condition numbers with respect to different parameterizations. I observe that Muir-Dellinger parameters behave best when the full set of four parameters are considered in the TI case agreeing with the observation made from Figures 4.9(a) and 4.9(c). The Chapman-Miller-Fowler parameters lead to lowest condition numbers while the Muir-Dellinger parameters are not far apart when only three parameters

under pseudoacoustic approximations as shown in Figure 4.12. Analogous plots for orthorhombic case are shown in Figures 4.13 and 4.14 and similar conclusions can be drawn.

Limited aperture experiments

In practice, the angular coverage of seismic experiments is limited and never becomes ideally complete as studied in the previous section. I repeat the same exercises using a limited range of angles in this section to demonstrate the efficiency of different parameterization schemes in these scenarios.

Figure 4.15 shows the condition number results in one-hundred TI models when only 0-30° aperture around the vertical axis is considered. This setting corresponds to the maximum ratio between offset and reflector depth of $1/\sqrt{3} \approx 0.577$. Thomsen parameters provide the smallest condition numbers in this setting due to the fact that an emphasis of the vertical direction is used in their definitions. However, the condition numbers, regardless of the choice of anisotropic parameterizations, are generally high because it might not be sufficiently accurate to estimate the effects of anisotropy on qP-wave kinematics with only limited aperture from 0-30° in the first place.

For a larger aperture range of 0-60° corresponding to the maximum ratio between offset and reflector depth of $\sqrt{3} \approx 1.732$ commonly present in wide-offset data (Figure 4.16), the Chapman-Miller-Fowler and Muir-Dellinger parameters behave the best. The general range of condition numbers for different schemes are also much smaller than before suggesting a better-posed estimation problem.

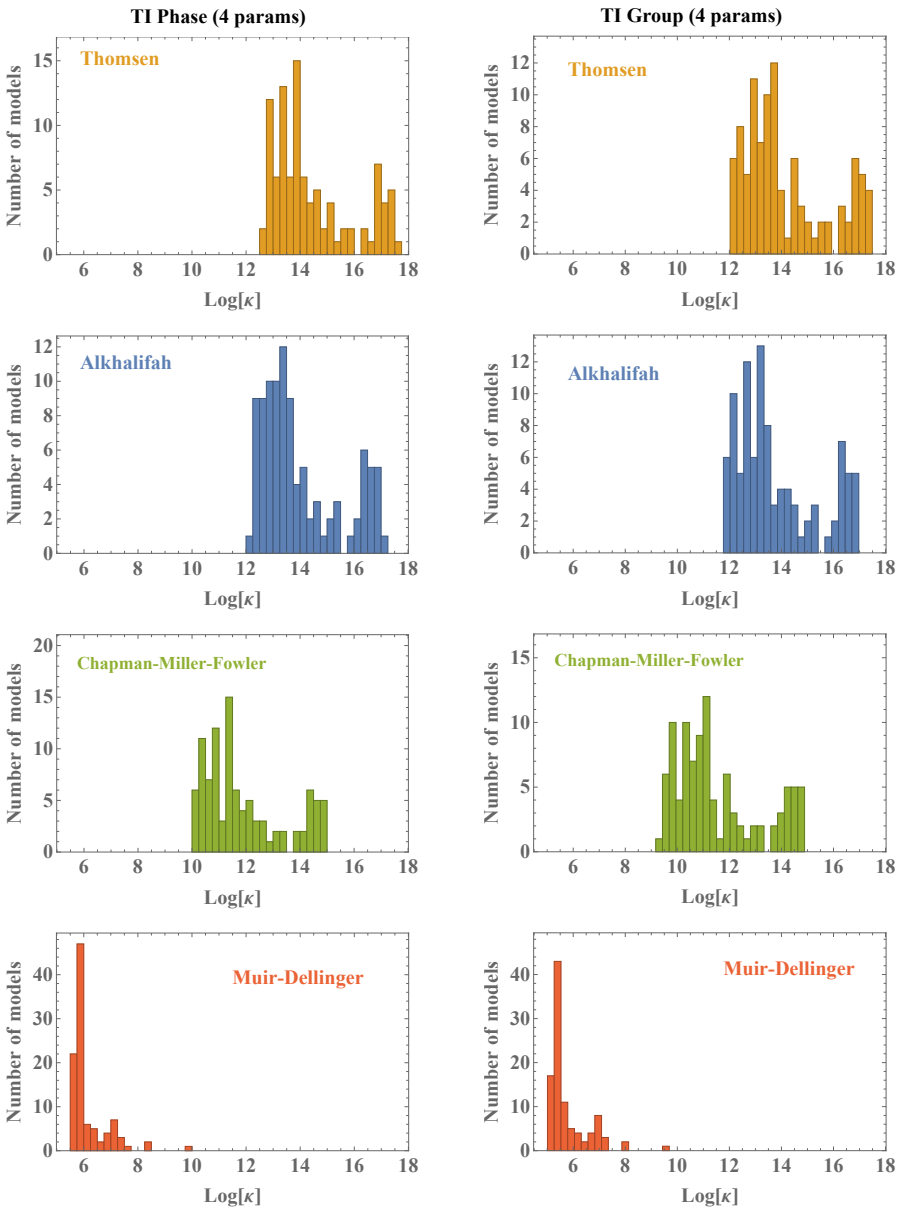

(a) (b)

Figure 4.11: Distribution of condition numbers (κ) of the sensitivity matrix in 100 TI models (equation 4.4) when considering four parameters for (a) qP phase velocity and (b) qP group velocity. Among these models, MD generally has the lowest condition numbers in this case agreeing with the results in Figures 4.9(a) and 4.9(c). sensitivity/. fourrange,fourgrouprange

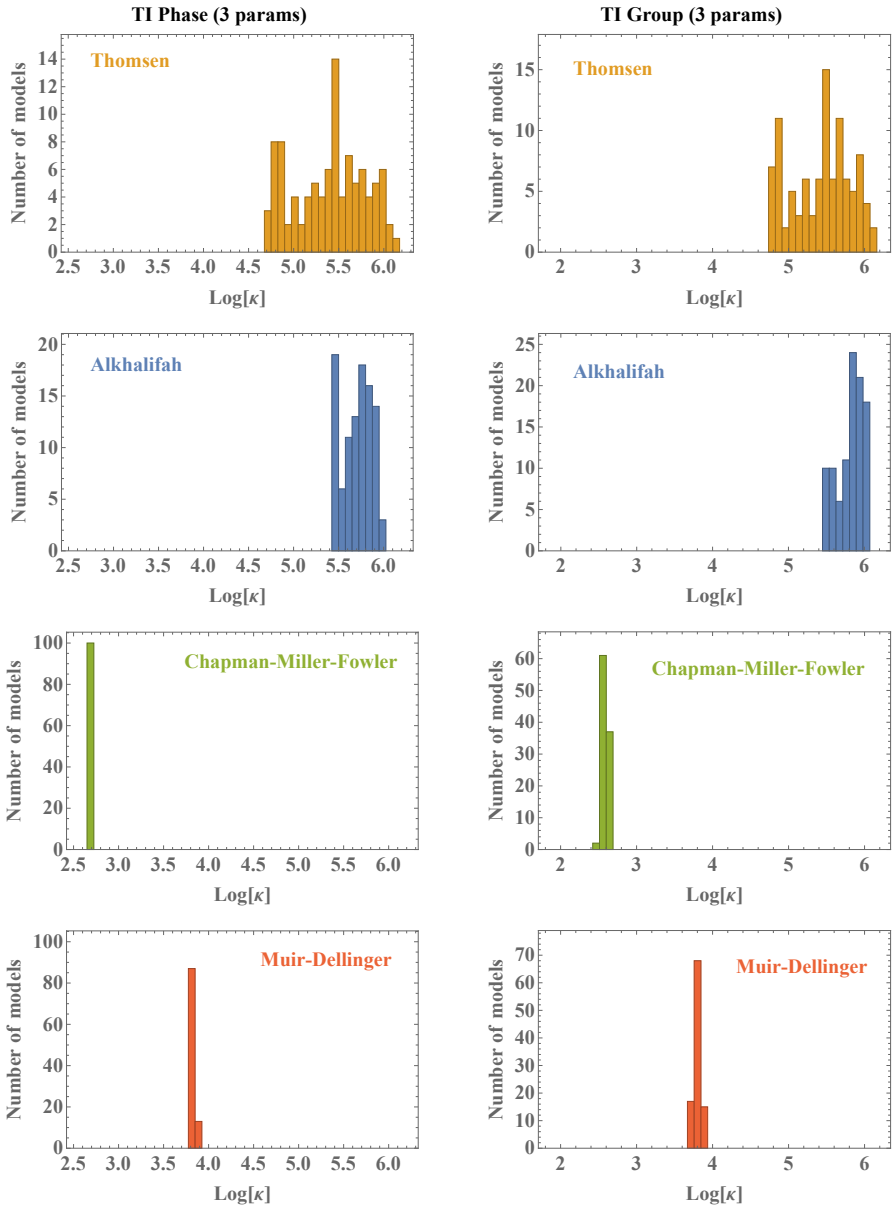

(a) (b)

Figure 4.12: Distribution of condition (κ) numbers of the sensitivity matrix in 100 TI models (equation 4.4) when considering three parameters under pseudoacoustic approximation for (a) qP phase velocity and (b) qP group velocity. Among these models, CMF and MD give the lowest condition numbers agreeing with previous observations made from Figures 4.9(b) and 4.9(d). sensitivity/. threerange,threegrouprange

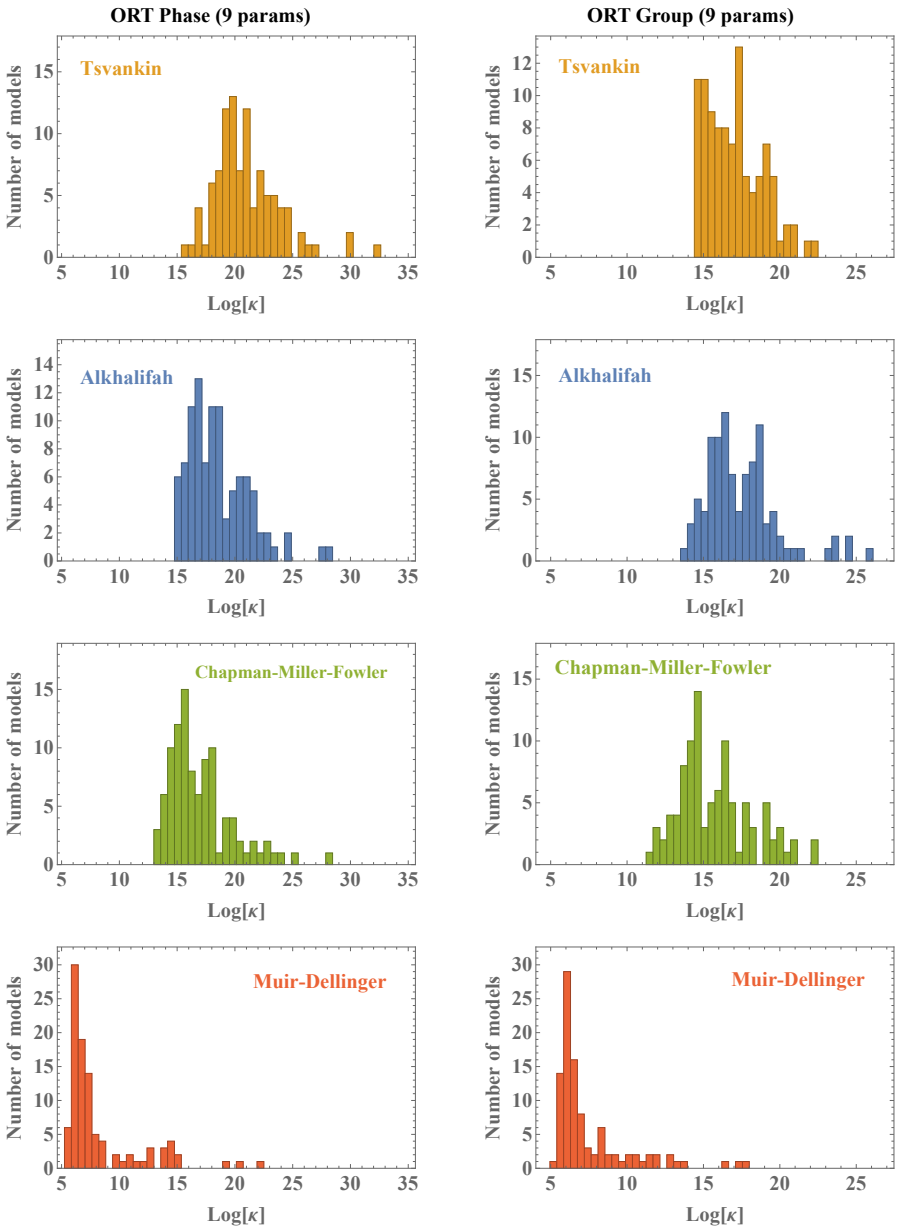

(a) (b)

Figure 4.13: Distribution of condition numbers (κ) of the sensitivity matrix in 100 orthorhombic models (equation 4.5) when considering nine parameters for (a) qP phase velocity and (b) qP group velocity. Among these models, MD generally has the lowest condition numbers in this case agreeing with the results in Figures 4.10(a) and 4.10(c). sensitivity/. ninerange,ninegrouprange

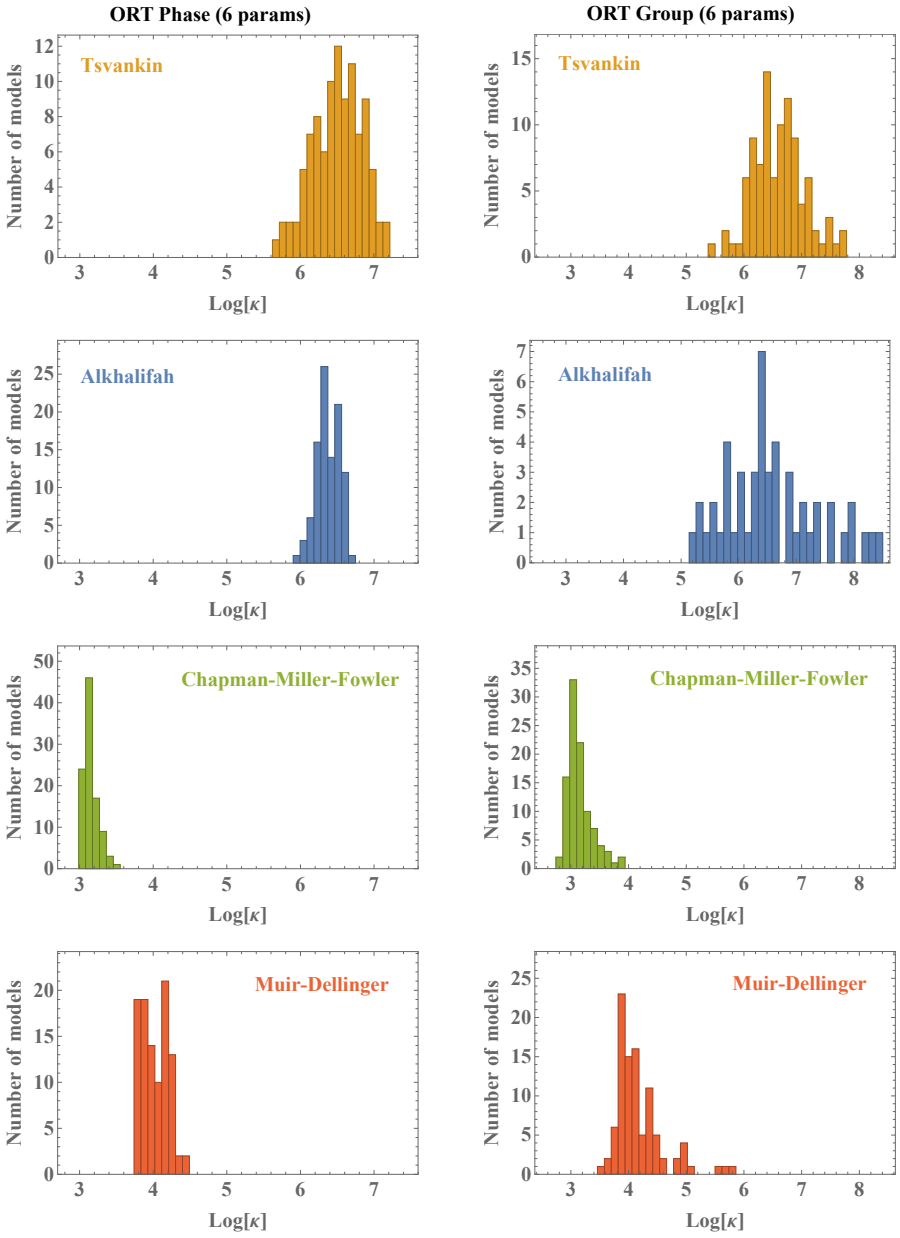

Figure 4.14: Distribution of condition numbers (κ) of the sensitivity matrix in 100 orthorhombic models (equation 4.5) when considering six parameters under pseudoacoustic approximation for (a) qP phase velocity and (b) qP group velocity. Among these models, CMF and MD give the lowest condition numbers agreeing with previous observations made from Figures 4.10(b) and 4.10(d). sensitivity/. sixrange,sixgrouprange

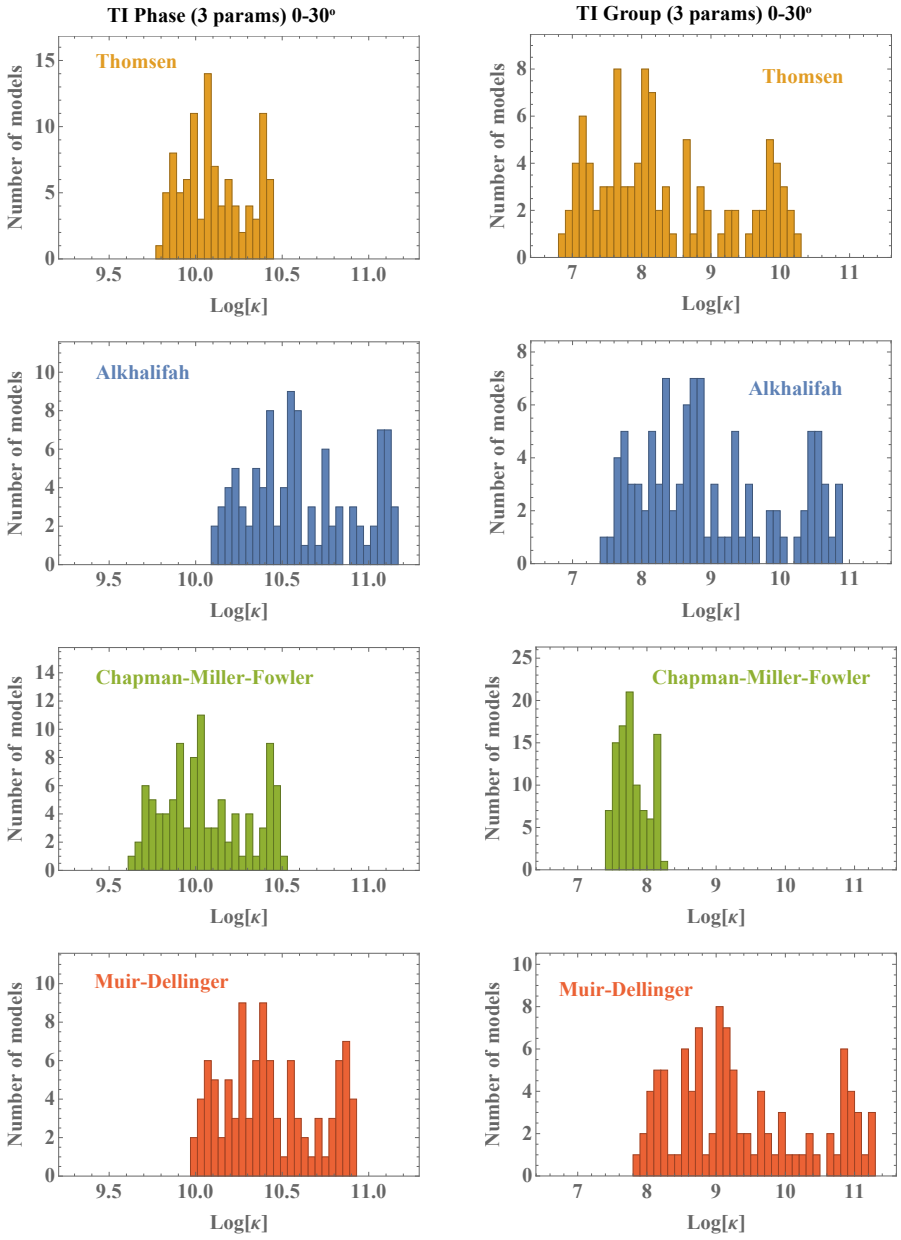

(a) (b)

Figure 4.15: Distribution of condition numbers (κ) of the sensitivity matrix in 100 TI models (equation 4.4) when considering three parameters under pseudoacoustic approximation for (a) qP phase velocity and (b) qP group velocity with 0-30° aperture. Thomsen parameters has the generally lowest condition number in both cases because the considered data range lies in the small aperture around the vertical axis. sensitivity/. threerange030,threegrouprange030

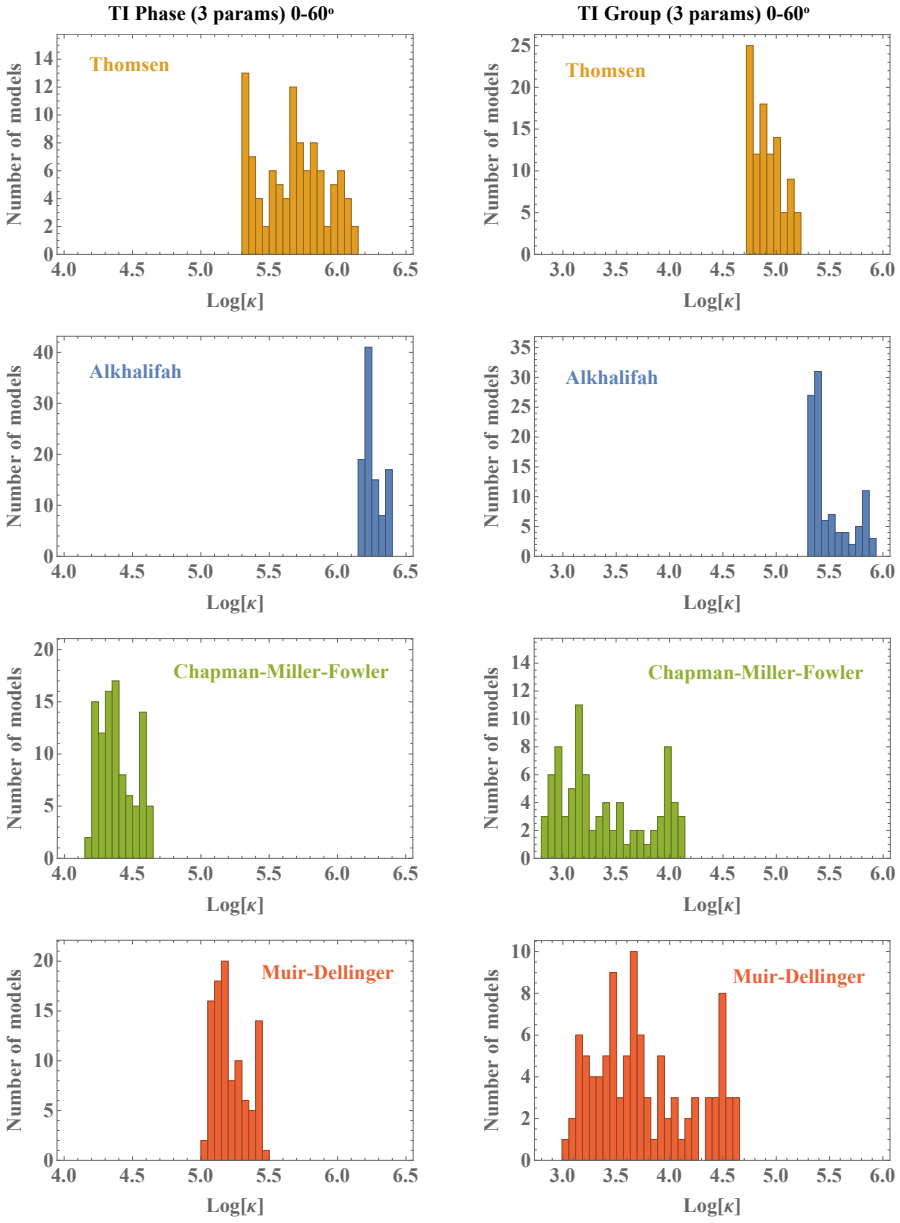

Figure 4.16: Distribution of condition numbers (κ) of the sensitivity matrix in 100 TI models (equation 4.4) when considering three parameters under pseudoacoustic approximation for (a) qP phase velocity and (b) qP group velocity with 0-60° aperture. CMF and MD parameters lead to the lowest condition numbers in both cases and become a better-behaved parameterization as a wider aperture is considered. sensitivity/. threerange060,threegrouprange060

Alternative sensitivity analysis on traveltime

Even though velocity plays an important role in governing the kinematics of seismic waves in general, one may choose to look at the sensitivity of traveltime, which is measured in seismic experiments, instead of velocity. A simple relation between group velocity and traveltime can be written as follows,

$$T = \frac{z v_{group}}{\cos\Theta} \ , \tag{4.6}$$

where T denotes one-way traveltime from the subsurface at depth z to the recording surface at zero depth and v_{group} denotes the traveling group velocity corresponding to the group angle Θ. The corresponding formula for the approximate Hessian matrix in 2D becomes

$$R_{ij} = \int_0^{\pi/2} \frac{\partial T^2}{\partial m_i} \frac{\partial T^2}{\partial m_j} d\Theta \ . \tag{4.7}$$

Due to the factor $\cos\Theta$ in the denominator of equation 4.7, I cannot obtain the sensitivity of traveltime with full aperture ($\Theta = 0$–$90°$). Figure 4.17 shows the result from the one-hundred generated TI models when three parameters are considered under pseudoacoustic approximation and with limited aperture from 0-60°. I can observe a general agreement with the results from the sensitivity of velocities that the Chapman-Miller-Fowler and Muir-Dellinger parameters lead to the lowest condition number in a good amount of models. Similar to what is observed from Figure 4.16(b), Thomsen parameters also lead to comparable performance in multiple models as well.

DISCUSSION

As mentioned in Chapter 1, despite stemming from the same concept, WA parameters and CMF parameters are defined differently; the former is defined based on

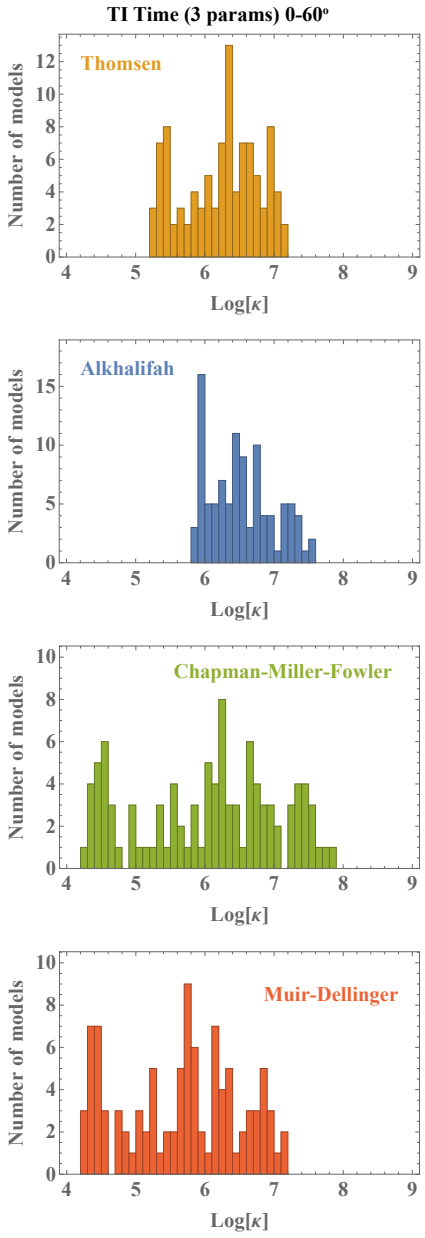

Figure 4.17: Distribution of condition numbers (κ) of the traveltime sensitivity matrix (equation 4.7) in 100 TI models when considering three parameters under pseudoacoustic approximation with 0-60° aperture. CMF and MD parameters lead to the lowest condition numbers but Thomsen parameters also show comparable performance in multiple models. sensitivity/. threetime060

the relative change of phase velocity squared, whereas the latter is defined based on the approximate velocity squared itself. Based on the sensitivity results from our numerical experiments, where I compare the results from Thomsen-Tsvankin (specifications of WA parameters) and CMF schemes, it is apparent that defining the parameters from approximate velocity squared leads to more preferable results. In light of this observation, it appears to be plausible to extend the CMF parameters to lower-symmetry media for well-behaved sensitivity as mentioned in the text.

CONCLUSIONS

I compare several previously proposed TI and orthorhombic parameterizations. A summary table for the relative merit of each parameterization according to different criteria is shown in Table 4.1. The results from sensitivity analysis using example models indicate that the Chapman-Miller-Fowler and Muir-Dellinger parameters are the most orthogonal among the four parameterizations considered and therefore, may lead to better-conditioned frameworks for inversion of qP-wave kinematics. Based on the results from velocity sensitivity, Thomsen parameters behave well in comparison with other parameterizations only when a small limited aperture coverage around the vertical axis is considered but degrade with larger coverage. Similar behavior of Thomsen parameters, although less distinct, can also be observed from traveltime sensitivity. As wide-offset and -azimuth data become more available in practice, the results of this study warrant further investigations of Chapman-Miller-Fowler and Muir-Dellinger parameters in application to seismic processing and inversion.

Considered aspects	Th-T	A	CMF	MD
Clear physical meaning	+	+	+	+
Easy extension to orthorhombic media without orientation aliases	-	-	+	+
Easy pseudoacoustic approximation	+	+	+	+
Orthogonal sensitivity	-	-	+	+

Table 4.1: Summary of parameterization schemes for qP-wave anisotropic parameters with respect to different aspects. "+", and "-" denote the degree of performance.

ACKNOWLEDGMENTS

I thank Z. Koren and I. Pšenčík for useful comments and suggestions. I thank the sponsors of the Texas Consortium for Computational Seismology (TCCS) for financial support.The first author acknowledges Statoil for the additional support by the Statoil Fellows Program at the University of Texas at Austin.

Chapter 5

Anelliptic approximations for qP velocities

Anelliptic approximations for phase and group velocities of qP waves in transversely isotropic (TI) media have been widely applied in various seismic data processing and imaging tasks. I revisit previously proposed approximations and suggest two improvements. The first improvement involves finding an empirical connection between anelliptic parameters along different fitting axes based on laboratory measurements of anisotropy of rock samples of different types (Chapter 2). The relationship between anelliptic parameters observed is strongly linear suggesting a novel set of anisotropic parameters suitable for the study of qP-wave signatures. The second improvement involves suggesting a new functional form for the anelliptic parameter term to achieve better fitting along the horizontal axis. These modifications lead to improved three-parameter and four-parameter approximations for phase and group velocities of qP waves in TI media. In a number of model comparisons, the new three-parameter approximations appear to be more accurate than previous approximations with the same number of parameters. These modifications also serve as a foundation for an extension to orthorhombic media where qP velocities involve nine indepen-

Parts of this chapter were first published in Sripanich, Y. and S. Fomel, 2014, Modified anelliptic approximations for qP velocities in transversely isotropic media: 84th Annual Meeting, *SEG Expanded Abstracts*, 409-414 and Sripanich, Y. and S. Fomel, 2014, Anelliptic approximations for qP velocities in orthorhombic media: 84th Annual Meeting, *SEG Expanded Abstracts*, 453-457. The peer-reviewed journal version appears as Sripanich, Y. and S. Fomel, 2015, On anelliptic approximations for qP velocities in TI and orthorhombic media: *Geophysics*, 80(5), C89-C105. This work was done under the supervision of Dr. Sergey Fomel.

dent elastic parameters. As shown by previous researchers, qP wave propagation in orthorhombic media can be adequately approximated using just six combinations of those nine parameters. I propose novel six-parameter approximations for phase and group velocities for qP waves in orthorhombic media. The proposed orthorhombic phase-velocity approximation provides a more accurate alternative to previously known approximations and can find applications in full-wave modeling, imaging, and inversion. The proposed group-velocity approximation is also highly accurate and can find applications in ray tracing and velocity analysis.

INTRODUCTION

Anellipticity is a well-known characteristic of elastic wave propagation in anisotropic media. The simplest, yet practically important case of anellipticity, occurs in transversely isotropic media (Grechka, 2009; Tsvankin, 2012; Thomsen, 2014). In recent years, it has been recognized that transverse isotropy may not be sufficient to characterize the actual media encountered in many regions of the world and as a result, orthorhombic anisotropy has become a significant topic of interest (e.g. Tsvankin, 1997, 2012; Bakulin et al., 2000; Xu et al., 2005; Vasconcelos and Tsvankin, 2006; Grechka, 2009; Fowler and Lapilli, 2012; Thomsen, 2014). One important example of an orthorhombic medium is a sedimentary basin exhibiting parallel vertical cracks embedded in a background medium with vertical transverse isotropy (Schoenberg and Helbig, 1997; Tsvankin, 1997, 2012; Grechka, 2009). In such media, three-dimensional anellipticity remains an important characteristic of elastic wave propagation. Tsvankin (1997, 2012) pointed out that the elastic wave propagation in TI media resembles the elastic wave propagation in the symmetry plane of orthorhombic media. This observation enables an accurate description of orthorhombic anelliptic-

ity using only a limited number of parameters by extending the approach used to approximate anellipticity in TI media.

The exact expressions for qP phase and group velocities in TI media involve four independent parameters (equation 1.58). Only three combinations of those four parameters are sufficient to describe qP wave propagation with high accuracy as discussed in Chapter 1. Although the exact expression of phase velocity in terms of phase angle is known, the exact expression for group velocity in terms of group angle appears too complicated for practical use. Therefore, accurate approximations involving a small number of independent parameters are needed. In orthorhombic media, the exact expression for qP phase velocity can be derived as a solution of a cubic equation and involves nine parameters. However, only six combinations of those nine parameters are sufficient to accurately describe qP wave propagation (Tsvankin, 1997, 2012). The exact expression of qP group velocity in orthorhombic media can be derived from phase velocity expressions, but this expression is again cumbersome and can only be expressed in terms of the phase angle instead of group angle. Therefore, this expression is not always convenient for practical applications such as ray tracing and moveout correction, where the expression in terms of the group angle (seismic ray direction) is often preferred.

Many approximations have been proposed previously for both phase and group velocities in TI media (e.g. Dellinger et al., 1993; Alkhalifah and Tsvankin, 1995; Tsvankin, 1996; Alkhalifah, 1998, 2000a,b; Schoenberg and de Hoop, 2000; Stopin, 2001; Zhang and Uren, 2001; Daley et al., 2004; Fomel, 2004; Ursin and Stovas, 2006; Fomel and Stovas, 2010; Stovas, 2010; Farra and Pšenčík, 2013). Fowler (2003) presented a comprehensive comparative review of many of these approximations. Accuracy comparison of several group-velocity approximations (in terms of moveout

approximations) was also presented by Aleixo and Schleicher (2010) and Golikov and Stovas (2012). Among these different approaches, Fomel (2004) proposed an extension of the Muir-Dellinger approach (Muir and Dellinger, 1985; Dellinger et al., 1993) using the shifted-hyperbola functional form. The resultant three-parameter approximation for phase velocity is identical to the acoustic approximation of Alkhalifah (1998, 2000a) and the empirical approximation of Stopin (2001). The corresponding three-parameter approximation for group velocity was new at the time and proved to be exceptionally accurate in comparison with other known approximations.

In the first part of this study, I revisit the anelliptic approximations by Fomel (2004) and further improve their accuracy by using an empirical relationship between the vertical and horizontal anelliptic parameters extracted from many laboratory measurements of stiffness tensor coefficients (Chapter 2). I also modify the functional form of the approximations to improve their behavior at large angles.

Many studies of elastic wave propagation and velocity approximations in orthorhombic media have been reported in the literature, and several alternative six-parameter approximations for qP phase velocity have been proposed (Tsvankin, 1997; Alkhalifah, 2003; Grechka, 2009; Song and Alkhalifah, 2013; Hao and Stovas, 2014). Several group-velocity approximations for orthorhombic media have been proposed in the form of moveout approximations (Xu et al., 2005; Vasconcelos and Tsvankin, 2006). Using the fact that the elastic wave propagation in each of the three symmetry planes of orthorhombic media is controlled by the same Christoffel equation as in the case of TI media (Tsvankin, 1997, 2012), I develop novel approximations for orthorhombic qP velocities by starting from my approximations in TI media. I extend my anelliptic TI approximations to a 3D form suitable for approximation of phase and group velocities of qP waves in orthorhombic media.

Using a set of test models, I check the accuracy of the proposed approximations and verify that they provide more accurate alternatives to the previously known approximations. In some of the models, the improvement in accuracy is dramatic and reaches an order of magnitude. The proposed approximations can readily be used in seismic data processing and imaging applications. I show examples of applying the proposed phase-velocity approximations for TI and orthorhombic media in wave extrapolation experiments.

TRANSVERSELY ISOTROPIC MEDIA

Muir and Dellinger approximations

The phase velocity of qP waves in TI media has the well-known explicit expression given in equation 1.58. Group velocity can be determined from phase velocity using the general expression 1.42. Similar to the derivations by Fomel (2004), the Muir-Dellinger approximations (Muir and Dellinger, 1985; Dellinger et al., 1993) serve as the starting point of my derivation. The Muir-Dellinger phase-velocity approximation is of the following form:

$$v^2_{phase}(n_1,n_3) \approx e(n_1,n_3) + \frac{(q-1)w_1w_3n_1^2n_3^2}{e(n_1,n_3)} \ , \tag{5.1}$$

where q is the anelliptic parameter ($q = 1$ in case of elliptical anisotropy), $w_1 = c_{11}$ denotes the horizontal (n_1) velocity squared, $w_3 = c_{33}$ denotes the vertical (n_3) velocity squared, and $e(n_1,n_3)$ describes the elliptical part of the velocity and is defined by

$$e(n_1,n_3) = w_1n_1^2 + w_3n_3^2 \ . \tag{5.2}$$

The group-velocity approximation takes a similar form, but with symmetric changes in the coefficients and variables due to the reciprocity between phase velocity

and group slowness (Chapter 1):

$$\frac{1}{v^2_{group}(N_1, N_3)} \approx E(N_1, N_3) + \frac{(Q-1)W_1 W_3 N_1^2 N_3^2}{E(N_1, N_3)} \ , \tag{5.3}$$

where $N_1 = \sin\Theta$, $N_3 = \cos\Theta$, Θ is group angle (from vertical), $W_1 = 1/w_1$ denotes the horizontal slowness squared, $W_3 = 1/w_3$ denotes the vertical slowness squared, $Q = 1/q$, and $E(N_1, N_3)$ describes the elliptical part of the slowness and is defined by

$$E(N_1, N_3) = W_1 N_1^2 + W_3 N_3^2 \ . \tag{5.4}$$

As suggested by Muir and Dellinger (1985), the q parameter can be found by fitting the curvature of phase velocity around either the vertical axis ($\theta = 0$) or the horizontal axis ($\theta = \pi/2$). The explicit expressions of q fitting in those two cases are given in equations 2.1 and 2.2. If I define Q in equation 5.3 by fitting the group slowness around either $\Theta = 0$ or $\Theta = \pi/2$, I find that

$$Q_i = 1/q_i \ . \tag{5.5}$$

which is noted in Chapter 2. Extending this idea, Muir (1990) and Dellinger et al. (1993) proposed four-parameter approximations for phase and group velocities using both q_1 and q_3.

Previous approximations

To obtain more accurate approximations, Fomel (2004) suggested applying the shifted-hyperbola functional form, which introduces shift parameters s (for phase velocity) and S (for group velocity) into the approximations using the following functional form:

$$v^2_{phase} \approx e(n_1, n_3)(1-s) + s\sqrt{e^2(n_1, n_3) + \frac{2(q-1)w_1 w_3 n_1^2 n_3^2}{s}} \ , \tag{5.6}$$

$$\frac{1}{v_{group}^2} \approx E(N_1, N_3)(1-S) + S\sqrt{E^2(N_1, N_3) + \frac{2(Q-1)W_1W_3N_1^2N_3^2}{S}} \ . \qquad (5.7)$$

Parameters s and S can be found by fitting the fourth derivatives $d^4v_{phase}/d\theta^4$ and $d^4v_{group}/d\Theta^4$ to the exact phase and group velocities, respectively. The results derived by Fomel (2004) for the vertical fitting ($\theta = 0$ or $\Theta = 0$) are

$$s = \frac{(w_1 - w_3)(q_3 - 1)(q_1 - 1)}{2[w_1(1 - q_1 - q_3(1 - q_3)) - w_3((q_1 - 1)^2 + q_1(q_3 - q_1))]} \ , \qquad (5.8)$$

$$S = \frac{(W_3 - W_1)(Q_3 - 1)(Q_1 - 1)}{2[W_1(Q_1 - Q_3^3 + Q_3^2 - 1) + W_3(Q_1(Q_3^2 - Q_3 - 1) + 1)]} \ . \qquad (5.9)$$

The introduction of parameters s and S leads to an increase in the number of parameters from three to four. To reduce this number back to three, Fomel (2004) suggested setting $q_1 = q_3$, or equivalently, $Q_1 = Q_3$, which results in $s = 1/2$ and $S = 1/2(1 + Q_3)$. Note that if I use equation 2.2 and set $q_1 = q_3$, this substitution will transform approximations 5.6 and 5.7 to the following form:

$$v_{phase}^2(\theta) \approx \frac{1}{2}e(\theta) + \frac{1}{2}\sqrt{e^2(\theta) + 4(q_3 - 1)w_1w_3 \sin^2\theta\cos^2\theta} \ , \qquad (5.10)$$

and

$$\frac{1}{v_{group}^2(\Theta)} \approx \frac{1 + 2Q_3}{2(1 + Q_3)}E(\Theta) + \frac{1}{2(1 + Q_3)}\sqrt{E^2(\Theta) + 4(Q_3^2 - 1)W_1W_3 \sin^2\Theta\cos^2\Theta} \ , \qquad (5.11)$$

The phase-velocity approximation in equation 5.10 is equivalent to the acoustic approximation of Alkhalifah (1998, 2000a) and the empirical approximation of Stopin (2001), which were derived in a different way. As discussed in Chapter 2, making an acoustic approximation by taking $q_1 = q_3$, or, equivalently, $Q_1 = Q_3$, is not necessarily the optimal choice, because the values of these two parameters may

depend on the material properties of the media of interest. The actual empirical relationship between q_1 and q_3 can be extracted from laboratory or in situ measurements of the stiffness tensor elements in various media (Figures 2.1-2.3). Furthermore, equations 5.10 and 5.11 are derived by fitting the derivatives up to fourth-order at either the vertical or horizontal axis, whereas fitting at the other axis is only first-order. This low-order fitting may lead to a loss of accuracy at larger angles (θ or Θ).

Proposed Approximations

To derive a more symmetric form, I return to the four-parameter expressions (equations 5.6 and 5.7) and propose to modify them as follows:

$$v^2_{phase} \approx e(n_1, n_3)(1 - \hat{s}) + \hat{s}\sqrt{e^2(n_1, n_3) + \frac{2(\hat{q} - 1)w_1 w_3 n_1^2 n_3^2}{\hat{s}}} \ , \tag{5.12}$$

and

$$\frac{1}{v^2_{group}} \approx E(N_1, N_3)(1 - \hat{S}) + \hat{S}\sqrt{E^2(N_1, N_3) + \frac{2(\hat{Q} - 1)W_1 W_3 N_1^2 N_3^2}{\hat{S}}} \ , \tag{5.13}$$

where

$$\hat{q} = \tfrac{q_1 w_1 n_1^2 + q_3 w_3 n_3^2}{w_1 n_1^2 + w_3 n_3^2}, \ \hat{Q} = \frac{Q_1 W_1 N_1^2 + Q_3 W_3 N_3^2}{W_1 N_1^2 + W_3 N_3^2} \ , \tag{5.14}$$

$$\hat{s} = \tfrac{s_1 w_1 n_1^2 + s_3 w_3 n_3^2}{w_1 n_1^2 + w_3 n_3^2}, \ \hat{S} = \frac{S_1 W_1 N_1^2 + S_3 W_3 N_3^2}{W_1 N_1^2 + W_3 N_3^2} \ . \tag{5.15}$$

The modifications in equation 5.14 are equivalent to the second anelliptic approximations by Dellinger et al. (1993) first proposed by Muir (1990). Again, parameters q_3 and q_1 can be found by fitting the velocity profile curvatures at the vertical ($\theta = 0$) and horizontal ($\theta = \pi/2$) axis, respectively and are defined in equations 2.1 and 2.2. Analogously, s_3 and s_1 can be found by fitting the fourth-order derivative ($d^4 v_{phase}/d\theta^4$) at the same angle. A similar strategy applies to fitting parameters

for the group-velocity approximation. Following this approach, I derive the following expressions for s_1, s_3, S_1, and S_3:

$$\begin{aligned} s_1 &= a_1/b_1 \ , \\ a_1 &= (w_3 - w_1)(q_1 - 1)^2(q_3 - 1) \ , \\ b_1 &= 2[w_3(q_1(q_1(q_1 - 2) + 3) - 2q_1q_3 + q_3^2 - 1) \\ &\quad -w_1(q_3(q_1(q_1 - 4) + q_3 + 1) + 2q_1 - 1)] \ , \end{aligned} \tag{5.16}$$

$$\begin{aligned} s_3 &= a_3/b_3 \ , \\ a_3 &= (w_1 - w_3)(q_1 - 1)(q_3 - 1)^2 \ , \\ b_3 &= 2[w_1(q_3(q_3(q_3 - 2) + 3) - 2q_1q_3 + q_1^2 - 1) \\ &\quad -w_3(q_1(q_3(q_3 - 4) + q_1 + 1) + 2q_3 - 1)] \ , \end{aligned} \tag{5.17}$$

$$\begin{aligned} S_1 &= A_1/B_1 \ , \\ A_1 &= (W_1 - W_3)(Q_1 - 1)^2(Q_3 - 1) \ , \\ B_1 &= 2[W_1(Q_3^2 + 2Q_1 + Q_1Q_3(Q_1(Q_1 - 2) - 1) - 1) \\ &\quad -W_3(Q_3^2 - 2Q_1Q_3 + Q_1(Q_1(Q_1 - 1)^2 + 2) - 1)] \ , \end{aligned} \tag{5.18}$$

$$\begin{aligned} S_3 &= A_3/B_3 \ , \\ A_3 &= (W_3 - W_1)(Q_1 - 1)(Q_3 - 1)^2 \ , \\ B_3 &= 2[W_3(Q_1^2 + 2Q_3 + Q_1Q_3(Q_3(Q_3 - 2) - 1) - 1) \\ &\quad -W_1(Q_1^2 - 2Q_1Q_3 + Q_3(Q_3(Q_3 - 1)^2 + 2) - 1)] \ . \end{aligned} \tag{5.19}$$

Note that expressions for s_3 and S_3 are different from equations 5.8 and 5.9 and that equations 5.12 and 5.13 introduce three more parameters generating six parameters in total, namely w_1, w_3, q_1, q_3, s_1, and s_3 for equation 5.12 or W_1, W_3, Q_1, Q_3, S_1, and S_3 for equation 5.13. However, expressing s_i and S_i in terms of q_i and Q_i in equations 5.16-5.19, I effectively reduce the dependency to four parameters. This reduction leads to four-parameter anelliptic approximations, which fit up to the fourth-order accuracy along both axes. The exact phase- and group-velocity expressions also require the total of four independent parameters. However, the advantage of the proposed approximations lies in the existence of the group-velocity expression (equation 5.13) with analogous functional form as the phase-velocity expression (equation 5.12). To reduce the number of parameters to three, I utilize the linear relationships between q_1 and q_3 given in Figures 2.1-2.3. The required Q_1 and Q_3 parameters for the group-velocity approximations can be found from the reciprocals of q_1 and q_3 for phase-velocity approximations, as mentioned above. Therefore, both phase- and group-velocity approximations derived on the basis of this approach require the same number of parameters.

Moveout approximation

The group-velocity approximation in equation 5.13 can be easily converted into the corresponding moveout equation using the relationship between offset (x), vertical distance (z), and total reflection traveltime (t) given by

$$t(x) = \frac{2\sqrt{(x/2)^2 + z^2}}{v_{group}(\arctan(x/2z))} \ , \tag{5.20}$$

where $z = t_0 v_{group}(0)/2$ is the depth of the reflector, t_0 is the vertical two-way reflection traveltime, and $v_{group}(\Theta)$ is the approximated group velocity. The moveout

equation corresponding to equation 5.13 is thus,

$$t^2(x) = H(x)(1-\hat{S}) + \hat{S}\sqrt{H^2(x) + \frac{2(\hat{Q}-1)t_0^2x^2}{\hat{S}Q_3v^2}}\ , \tag{5.21}$$

where

$$\hat{Q} = \frac{\frac{Q_1}{Q_3v^2}x^2 + Q_3t_0^2}{\frac{1}{Q_3v^2}x^2 + t_0^2}, \quad \hat{S} = \frac{\frac{S_1}{Q_3v^2}x^2 + S_3t_0^2}{\frac{1}{Q_3v^2}x^2 + t_0^2}\ ,$$

v denotes the NMO-velocity (Alkhalifah and Tsvankin, 1995) and is given by (equation 1.64)

$$v^2 = \frac{1}{W_1Q_3} = w_1q_3 = v_{P0}^2\frac{1+2\epsilon}{1+2\eta} = v_{P0}^2(1+2\delta)\ . \tag{5.22}$$

$H(x)$ denotes the hyperbolic part of the reflection traveltime squared and is given by

$$H(x) = t_0^2 + \frac{x^2}{Q_3v^2}\ . \tag{5.23}$$

Assuming a particular media type and using a linear relationship between q_1 and q_3, I reduce the number of independent moveout parameters in the similar manner. However, note that S_1 (equations 5.18) and S_3 (equation 5.19) also depend on W_1 and W_3. Therefore, to effectively reduce the number of parameters in the moveout approximation (equation 5.21) to three, I suggest, as an approximation, to adopt $Q_1 = Q_3$ only for equations 5.18 and 5.19, which lead to

$$S_1 = S_3 = \frac{1}{2(1+Q_3)}\ . \tag{5.24}$$

As a result, the moveout approximation depends on t_0, v, and Q_3. For small offsets, the Taylor expansion of equation 5.21 is

$$t^2(x) \approx t_0^2 + \frac{x^2}{v^2} - \frac{1-2S_3(Q_1+1)+Q_3(4S_3+Q_3-2)}{2S_3Q_3^2t_0^2v^4}x^4\ , \tag{5.25}$$

which reduces to the expression given by Fomel (2004) by setting $Q_1 = Q_3$. The slope of the asymptote of this expression for unbounded offset x is given by

$$\frac{1}{Q_3v^2} = \frac{1}{w_1}\ , \tag{5.26}$$

which is the horizontal velocity squared.

In the Muir-Dellinger notation, another nonhyperbolic moveout approximation, the generalized nonhyperbolic moveout approximation (Fomel and Stovas, 2010; Stovas, 2010) can be expressed as

$$
\begin{aligned}
t^2(x) &\approx t_0^2 + \frac{x^2}{v^2} + \frac{Ax^4}{v^4\left(t_0^2 + B\frac{x^2}{v^2} + \sqrt{t_0^4 + 2Bt_0^2\frac{x^2}{v^2} + C\frac{x^4}{v^4}}\right)}\ , \qquad (5.27)\\
A &= \frac{(Q_3-1)^2(Q_1W_3 - Q_3W_1)}{Q_3(Q_1-1)(W_1-W_3)}\ ,\\
B &= \frac{(Q_3-1)\left[(2Q_3^2-1)W_1 + W_3 - 2Q_1Q_3W_3\right]}{Q_3(Q_1-1)(W_1-W_3)}\ ,\\
C &= \frac{(Q_3-1)^2}{(Q_1-1)^2Q_3^2}\ .
\end{aligned}
$$

If the empirical assumption of $Q_1 = Q_3$, or equivalently acoustic approximation is used, equation 5.27 reduces to the moveout approximation of Fomel (2004).

Examples

To investigate the accuracy of the proposed approximations, I make the relative error comparison with both plots and tables using several anisotropy models based on values from laboratory measurements on rock samples. The plots in Figure 5.1 are generated using the stiffness tensor measurements of Greenhorn shales (Jones and Wang, 1981), which have been applied for various approximation comparisons in the past (e.g. Dellinger, 1991; Fomel, 2004; Stovas, 2010; Farra and Pšenčík, 2013). Additionally, Tables 5.1 and 5.2 show the RMS relative error results of the new approximations, in comparison with results from some of the previously suggested approximations using the normalized stiffness tensor measurements given in Table 5.3.

The RMS error computation is based on

$$\text{RMS error} = \sqrt{\sum_{\psi=0}^{90}(v_{exact}(\psi) - v_{approx}(\psi))^2} \ , \tag{5.28}$$

where ψ denotes phase or group angle as appropriate. In all comparisons, I apply the relationships shown in Figures 2.1-2.3 to reduce the number of parameters from four to three. For each model, the best-performing approximation is denoted in red and bold. The proposed approximations appear to be the most accurate in nearly all of the cases.

Sample	Thomsen (1986)	Alkhalifah (1998)	Proposed
1	0.6789	0.1422	**0.0978**
2	0.6482	0.2254	**0.0503**
3	0.4564	0.1399	**0.0273**
4	0.2978	**0.0485**	0.0506
5	0.1244	0.0541	**0.0201**
6	0.5710	0.1631	**0.0149**

Table 5.1: RMS relative error (%) from 0-90° of phase-velocity approximations by Thomsen (1986), Alkhalifah (1998) (similar to Fomel (2004)), and of the proposed three-parameter approximation for transversely-isotropic elastic models from Table 5.3. Bold red highlight indicates the best-performing approximation. In all the cases, except sample 4, the proposed approximation appears to be the most accurate.

ORTHORHOMBIC MEDIA

Extended Muir-Dellinger Approximations

Considering the Muir-Dellinger approximations for qP velocities in TI media (equations 5.1 and 5.3) and the subscript convention introduce in the first section, I can naturally extend them to orthorhombic media as follows:

$$v^2_{phase}(n_1, n_2, n_3) \approx e(n_1, n_2, n_3) + \sum_{j=1}^{3} \frac{(q_{ij} - 1)w_i w_k n_i^2 n_k^2}{e(n_1, n_2, n_3)} \ , \tag{5.29}$$

Sample	Alkhalifah and Tsvankin (1995)	Fomel (2004)	Farra and Pšenčík (2013)	Proposed
1	1.0149	0.1210	0.2530	**0.0801**
2	0.3306	0.2179	0.1351	**0.0564**
3	0.4602	0.1311	0.0977	**0.0194**
4	0.1369	**0.0467**	0.0983	0.0492
5	**0.0188**	0.0540	0.0194	0.0202
6	0.4258	0.1541	0.1412	**0.0084**

Table 5.2: RMS relative error (%) from 0-90° of group-velocity approximations by Alkhalifah and Tsvankin (1995), Fomel (2004), Farra and Pšenčík (2013) (second-order) and of the proposed three-parameter approximation for transversely-isotropic elastic models from Table 5.3. Bold red highlight indicates the best-performing approximation. In all the cases, except samples 4 and 5, the proposed approximation appears to be the most accurate.

Shales sample	c_{11}	c_{33}	c_{13}	c_{55}	v_{P0}	v_{S0}	ϵ	δ
1. Greenhorn	14.47	9.57	4.51	2.28	3.094	1.510	0.256	-0.0505
2. Hard (brine)	20.89	13.89	3.048	5.655	3.727	2.378	0.252	0.0347
3. North Sea (brine)	7.292	5.248	1.578	1.798	2.291	1.341	0.195	-0.0139
4. Dog Creek	5.098	3.5163	2.4832	0.6823	1.875	0.826	0.225	0.0998
5. Mesaverde	17.653	14.055	1.3391	6.87	3.749	2.621	0.128	0.0781
6. North Sea (dry)	22.051	14.90	5.336	4.928	3.860	2.220	0.240	0.0199

Table 5.3: Normalized stiffness tensor coefficients (in km^2/s^2) from different TI samples: 1 is from Jones and Wang (1981), 2 and 3 are from Wang (2002), 4 and 5 are from Thomsen (1986), and 6 is from Vernik and Liu (1997).

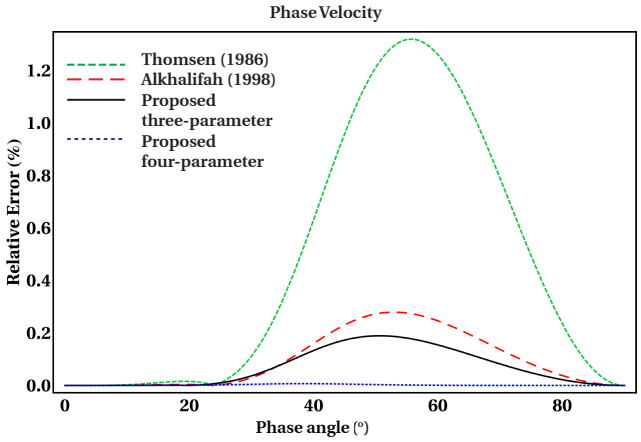

(a)

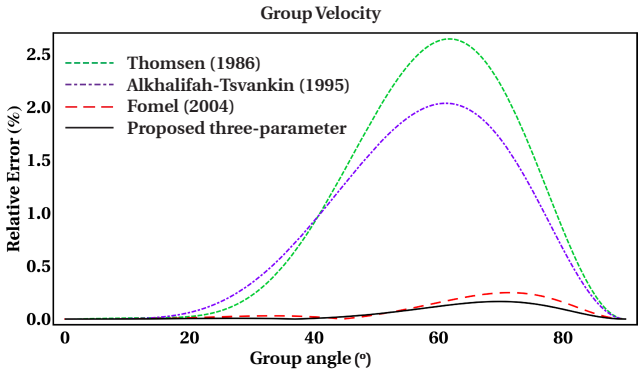

(b)

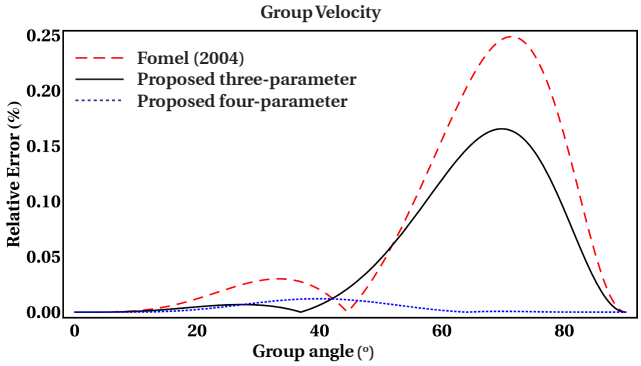

(c)

Figure 5.1: Relative error plots using Greenhorn Shale measurements. (a) Phase velocity. (b) Group velocity. (c) Group velocity (finer scale). orthorhombic/. vtiphaseplotlegnew,vtigroupplotleg1new,vtigroupplotleg2new

where q_{ij} are the anelliptic parameters ($q_{ij} = 1$ in case of elliptical anisotropy), $w_i = c_{ii}$ denotes velocity squared along the n_i axis, and $e(n_1, n_2, n_3)$ describes the ellipsoidal part of the velocity and is defined by

$$e(n_1, n_2, n_3) = w_1 n_1^2 + w_2 n_2^2 + w_3 n_3^2 \ . \tag{5.30}$$

For subscript convention in 3D, I adopt the notation that, for each combination of i, j, and k, the first digit indicates the index of the fitting axis and the second digit indicates the index of the axis defining the symmetry plane. Therefore, in this notation, i, j, and k are integers between 1 and 3 and in each expression, they must be different from one another.

Extension 5.29 is based on the consideration of an ellipsoid in 3D as opposed to an ellipse in 2D and the additional two anelliptic terms involving q_{ij} parameters from considering a total of three symmetry planes in orthorhombic media. It is also valid to consider q_{kj} instead of q_{ij} because in consistent with the original Muir-Dellinger approximation (equation 5.1), only one anelliptic parameter is needed in each symmetry plane. According to the Muir-Dellinger approach, I can also derive the group-velocity approximation, which takes a similar form, with symmetric changes in the coefficients and variables as shown below:

$$\frac{1}{v_{group}^2(N_1, N_2, N_3)} \approx E(N_1, N_2, N_3) + \sum_{j=1}^{3} \frac{(Q_{ij} - 1) W_i W_k N_i^2 N_k^2}{E(N_1, N_2, N_3)} \ , \tag{5.31}$$

where $N_1 = \sin\Theta\cos\Phi$, $N_2 = \sin\Theta\sin\Phi$, $N_3 = \cos\Theta$, Θ is zenith group angle (from vertical), Φ is azimuthal group angle (from n_1), $Q_{ij} = 1/q_{ij}$, $W_i = 1/w_i$ denotes slowness squared along the N_i axis, and $E(N_1, N_2, N_3)$ describes the elliptical part of the slowness, defined by

$$E(N_1, N_2, N_3) = W_1 N_1^2 + W_2 N_2^2 + W_3 N_3^2 \ . \tag{5.32}$$

This simple extension from 2D to 3D stems from the observation that elastic wave propagation in each symmetry plane of orthorhombic media is controlled by the same Christoffel equation as in the case of TI media (Tsvankin, 1997, 2012). Therefore, if any n_i or N_i is zero, the extended expressions will simply reduce to the 2D Muir-Dellinger approximations for TI media in equations 5.1 and 5.3. Note that the expression in equation 5.29 is equivalent to the two leading terms of the phase-velocity pseudo-acoustic approximation derived by Fowler and Lapilli (2012) and Fowler et al. (2014).

Proposed Approximations

In the preceding section, I suggest an improvement to the anelliptic approximations for transversely isotropic media with vertical symmetry axis (VTI) media previously proposed by Fomel (2004). Applying a similar modification to the extended Muir and Dellinger approximations (equations 5.29 and 5.31), I can write the resultant approximations in a new form suitable for approximation of velocities in orthorhombic media, as follows:

$$v_{phase}^2 \approx e(n_1,n_2,n_3)(1-\hat{s}) + \hat{s}\sqrt{e^2(n_1,n_2,n_3) + \frac{2\sum_{j=1}^{3}(\hat{q}_j-1)w_i w_k n_i^2 n_k^2}{\hat{s}}}\ , \tag{5.33}$$

where

$$\hat{s} = \frac{\hat{s}_1 w_1 n_1^2 + \hat{s}_2 w_2 n_2^2 + \hat{s}_3 w_3 n_3^2}{w_1 n_1^2 + w_2 n_2^2 + w_3 n_3^2}\ , \tag{5.34}$$

and

$$\frac{1}{v_{group}^2} \approx E(N_1,N_2,N_3)(1-\hat{S}) + \hat{S}\sqrt{E^2(N_1,N_2,N_3) + \frac{2\sum_{j=1}^{3}(\hat{Q}_j-1)W_i W_k N_i^2 N_k^2}{\hat{S}}}\ , \tag{5.35}$$

where

$$\hat{S} = \frac{\hat{S}_1 W_1 N_1^2 + \hat{S}_2 W_2 N_2^2 + \hat{S}_3 W_3 N_3^2}{W_1 N_1^2 + W_2 N_2^2 + W_3 N_3^2} \ , \tag{5.36}$$

$$\hat{q}_j = \frac{q_{ij} w_i n_i^2 + q_{kj} w_k n_k^2}{w_i n_i^2 + w_k n_k^2}, \ \hat{Q}_j = \frac{Q_{ij} W_i N_i^2 + Q_{kj} W_k N_k^2}{W_i N_i^2 + W_k N_k^2} \ , \tag{5.37}$$

$$\hat{s}_j = \frac{s_{jk} w_i n_i^2 + s_{ji} w_k n_k^2}{w_i n_i^2 + w_k n_k^2}, \ \hat{S}_j = \frac{S_{jk} W_i N_i^2 + S_{ji} W_k N_k^2}{W_i N_i^2 + W_k N_k^2} \ . \tag{5.38}$$

Figure 2.6 shows the locations of the fitting indices in each symmetry plane and Figure 5.2 shows the working coordinate in 3D. Note that the subscript rule explained earlier still applies, and the relationship $Q_{ij} = 1/q_{ij}$ still holds. In my notation, $\hat{q}$ and $\hat{Q}$ represent weighted averages of anelliptic parameters (q and Q) in a plane whereas $\hat{s}$ and $\hat{S}$ represent weighted averages at an axis.

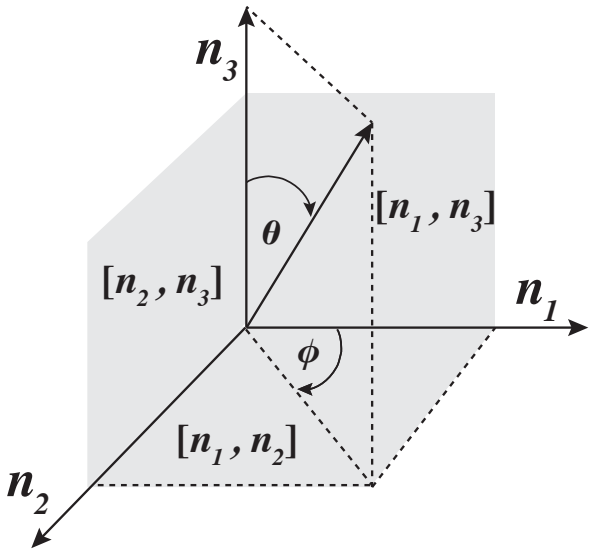

Figure 5.2: Parametization rule for working coordinates. orthorhombic/. coordinate

Similar to the derivation in the TI case, q_{ij} and Q_{ij} can be found by fitting the curvatures to the exact velocities along orthogonal directions in each of the three planes. Likewise, s_{ij} and S_{ij} can be found by fitting the fourth-order derivative ($d^4 v_{phase}/d\theta^4$ and $d^4 v_{group}/d\Theta^4$) at the same positions. Note that the expressions of

q_{i2}, Q_{i2}, s_{i2}, and S_{i2} are similar to those in the TI case for q_i, Q_i, s_i, and S_i for $i = 1, 3$. As a result, I need to specify parameter expressions only for the other two planes. Fitting both phase- and group-velocity expressions along both axes in each symmetry plane leads to six different expressions for each of the fitting parameters. This is different for the case of extended Muir-Dellinger approximations (equations 5.29 and 5.31) where only three expressions are allowed.

Since the Christoffel equation in the three symmetry planes is similar to that in TI media, the functional forms of every parameter expression remain the same. Therefore, I can compute parameters needed by equations 5.33 and 5.35 using the formulas derived in [n_1,n_3] plane for the TI case. Thus, I obtain:

$$q_{ij} = \frac{(c_{ik} + c_{pp})^2 + c_{pp}(c_{ii} - c_{pp})}{c_{kk}(c_{ii} - c_{pp})} , \tag{5.39}$$

$$\begin{aligned} s_{ij} &= a_{ij}/b_{ij} , \\ a_{ij} &= (w_k - w_i)(q_{ij} - 1)^2(q_{kj} - 1) , \\ b_{ij} &= 2[w_k(q_{ij}(q_{ij}(q_{ij} - 2) + 3) - 2q_{ij}q_{kj} + q_{kj}^2 - 1) \\ &\quad -w_i(q_{kj}(q_{ij}(q_{ij} - 4) + q_{kj} + 1) + 2q_{ij} - 1)] , \end{aligned} \tag{5.40}$$

$$\begin{aligned} S_{ij} &= A_{ij}/B_{ij} , \\ A_{ij} &= (W_i - W_k)(Q_{ij} - 1)^2(Q_{kj} - 1) , \\ B_{ij} &= 2[W_i(Q_{kj}^2 + 2Q_{ij} + Q_{ij}Q_{kj}(Q_{ij}(Q_{ij} - 2) - 1) - 1) \\ &\quad -W_k(Q_{kj}^2 - 2Q_{ij}Q_{kj} + Q_{ij}(Q_{ij}(Q_{ij} - 1)^2 + 2) - 1)] . \end{aligned} \tag{5.41}$$

where $p = j + 3$. Recall that the indices $ij \neq ji$ and therefore, there are six expressions corresponding to each formula from equations 5.39-5.41. Equations 5.33

and 5.35 amount to the nine-parameter approximations for both velocities where the required parameters include w_1, w_2, w_3, q_{21}, q_{31}, q_{12}, q_{32}, q_{13}, and q_{23} for equation 5.33 or their reciprocals, W_1, W_2, W_3, Q_{21}, Q_{31}, Q_{12}, Q_{32}, Q_{13}, and Q_{23} for equation 5.35. However, these nine parameters can be easily reduced to six using the linear relationships between q_{ij} and q_{kj} for different lithologies from the previous discussion on TI media (Figures 2.1-2.3). Similar conversion rules apply for anisotropic parameters in each symmetry plane and are summarized in Table 2.1. Note that the required independent parameters for the group-velocity approximations derived based on Muir-Dellinger approach can be found in a one-to-one relationship simply from the reciprocals of the required parameters for phase-velocity approximations as mentioned before. Therefore, phase- and group-velocity approximations derived on the basis of this approach require exactly the same number of parameters.

Moveout approximation

To convert the proposed group-velocity approximation (equation 5.35) to the corresponding moveout approximation, I apply again the general expression given in equation 5.20. Adopting the same notation rules, the moveout approximation takes the form:

$$\begin{aligned} t^2 &= H_{ortho}(x,y)(1-\hat{S}) + \hat{S}\sqrt{F}\ , \\ F &= H^2_{ortho}(x,y) + \frac{2}{\hat{S}}\left(\frac{(\hat{Q}_1-1)t_0^2y^2}{Q_{31}v_1^2} + \frac{(\hat{Q}_2-1)t_0^2x^2}{Q_{32}v_2^2} + \frac{(\hat{Q}_3-1)x^2y^2}{(Q_{31}v_1^2)(Q_{32}v_2^2)}\right)\ , \end{aligned} \tag{5.42}$$

where

$$\hat{S} = \frac{\frac{\hat{S}_1}{Q_{32}v_2^2}x^2 + \frac{\hat{S}_2}{Q_{31}v_1^2}y^2 + \hat{S}_3t_0^2}{\frac{1}{Q_{32}v_2^2}x^2 + \frac{1}{Q_{31}v_1^2}y^2 + t_0^2}\ , \tag{5.43}$$

$$\hat{Q}_1 = \frac{\frac{Q_{21}}{Q_{31}v_1^2}y^2 + Q_{31}t_0^2}{\frac{1}{Q_{31}v_1^2}y^2 + t_0^2}, \quad \hat{Q}_2 = \frac{\frac{Q_{12}}{Q_{32}v_2^2}x^2 + Q_{32}t_0^2}{\frac{1}{Q_{32}v_2^2}x^2 + t_0^2}, \quad \hat{Q}_3 = \frac{\frac{Q_{13}}{Q_{32}v_2^2}x^2 + \frac{Q_{23}}{Q_{31}v_1^2}y^2}{\frac{1}{Q_{32}v_2^2}x^2 + \frac{1}{Q_{31}v_1^2}y^2} \ , \quad (5.44)$$

$$\hat{S}_1 = \frac{\frac{S_{13}}{Q_{31}v_1^2}y^2 + S_{12}t_0^2}{\frac{1}{Q_{31}v_1^2}y^2 + t_0^2}, \quad \hat{S}_2 = \frac{\frac{S_{23}}{Q_{32}v_2^2}x^2 + S_{21}t_0^2}{\frac{1}{Q_{32}v_2^2}x^2 + t_0^2}, \quad \hat{S}_3 = \frac{\frac{S_{32}}{Q_{32}v_2^2}x^2 + \frac{S_{31}}{Q_{31}v_1^2}y^2}{\frac{1}{Q_{32}v_2^2}x^2 + \frac{1}{Q_{31}v_1^2}y^2} \ , \quad (5.45)$$

x denotes the offset in N_1 direction, y denotes the offset in N_2 direction, $v_2 = \sqrt{1/W_1Q_{32}}$ denotes the NMO-velocity in N_1 direction, $v_1 = \sqrt{1/W_2Q_{31}}$ denotes the NMO-velocity in N_2 direction, and $H_{ortho}(x,y)$ denotes the hyperboloidal part of reflection traveltime squared given below,

$$H_{ortho}(x,y) = t_0^2 + \frac{x^2}{Q_{32}v_2^2} + \frac{y^2}{Q_{31}v_1^2} \ . \quad (5.46)$$

I apply the same strategy to reduce the number of parameters with an approximation on Q_{ij} for S_{ij} as in equation 5.24. For small offset, the Taylor expansion of equation 5.42 is

$$\begin{aligned} t^2(x) \approx t_0^2 + \frac{x^2}{v_2^2} + \frac{y^2}{v_1^2} - \quad (5.47)\\ \frac{1 - 2S_{32}(Q_{12}+1) + Q_{32}(4S_{32} + Q_{32} - 2)}{2S_{32}Q_{32}^2t_0^2v_2^4}x^4 - \\ \frac{1 - 2S_{31}(Q_{21}+1) + Q_{31}(4S_{31} + Q_{31} - 2)}{2S_{31}Q_{31}^2t_0^2v_1^4}y^4 + \\ \frac{S_{31}(Q_{32}-1)^2 - S_{32}(Q_{32}-1)(Q_{32}+2Q_{31}-3) - 2S_{32}^2(Q_{32}+Q_{31}-Q_{13}-1)}{2S_{32}^2Q_{31}Q_{32}t_0^2v_1^2v_2^2}x^2y^2 + ... \end{aligned}$$

The slope of the asymptote of this expression for unbounded offsets x and y is given by

$$\frac{1}{Q_{32}v_2^2} = \frac{1}{w_1} \quad \text{and} \quad \frac{1}{Q_{31}v_1^2} = \frac{1}{w_2} \ , \quad (5.48)$$

which denote the horizontal velocities squared along N_1 and N_2 directions respectively.

Examples

To evaluate the accuracy of the proposed approximations, I produce relative error plots and tables, using several sets of normalized stiffness tensor measurements summarized in Table 5.4, which can be converted to any parameterization scheme (Table 2.1). The error plots in Figures 5.3-5.9 are generated using the standard model (Schoenberg and Helbig, 1997) and are presented as both 3D surfaces and stereographic projections with θ (or Θ) changing radially and ϕ (or Φ) changing azimuthally. The standard model assumes a shale background with a set of parallel vertical cracks; therefore, I use the following relationship between anelliptic parameters in shales (Figure 2.1) to reduce the number of parameters in the vertical [n_1,n_3] and [n_2,n_3] planes. The anisotropy in the horizontal plane [n_1,n_2], on the other hand, corresponds to a different cause, which in this case is assumed to be vertical fractures. Because I do not know a proper relationship between anelliptic parameters for such feature, I resort to the previously used assumption of $q_{13} = q_{23}$. Tables 5.5 and 5.6 show RMS relative error results of my approximations in comparison with results from some of the previously suggested approximations, which are computed based on

$$\text{RMS error} = \sqrt{\sum_{\psi_1=0}^{90}\sum_{\psi_2=0}^{90}(v_{exact}(\psi_1,\psi_2) - v_{approx}(\psi_1,\psi_2))^2}\ , \tag{5.49}$$

where ψ_1 and ψ_2 denote the zenith and azimuthal phase or group angles as appropriate. The best-performing approximation is denoted in red and bold. In all examples, the proposed approximations appear to be significantly more accurate than the other known approximations.

Sample	c_{11}	c_{22}	c_{33}	c_{44}	c_{55}	c_{66}	c_{12}	c_{23}	c_{13}
1. Standard model	9	9.84	5.938	2	1.6	2.182	3.6	2.4	2.25
2. Tsvankin 1	11.7	13.5	9	1.728	1.44	2.246	8.824	5.981	5.159
3. Tsvankin 2	17.1	13.5	9	1.728	1.44	2.246	9.772	4.580	7.745
4. Alkhalifah 1	1.452	2.016	1	0.25	0.25	0.25	1.089	0.695	0.599
5. Alkhalifah 2	1.452	2.016	1	0.49	0.36	0.49	0.608	0.206	0.378

Table 5.4: Normalized stiffness tensor coefficients (in km^2/s^2) from different orthorhombic samples: 1 is from Schoenberg and Helbig (1997), 2 and 3 are from Tsvankin (1997), and 4 and 5 are from Alkhalifah (2003).

Sample	Tsvankin (1997)	Alkhalifah (2003)	Proposed
1	0.5787	0.1742	**0.1029**
2	0.5918	0.0645	**0.0275**
3	0 .7104	0.0952	**0.0637**
4	0.8960	0.1382	**0.0293**
5	1.0736	0.3274	**0.2084**

Table 5.5: RMS relative error (%) from 0-90 ° (both θ and ϕ) of orthorhombic phase-velocity approximations by Tsvankin (1997), Alkhalifah (2003), and of proposed six-parameter approximation. Bold red highlight indicates the best-performing approximation. In all cases, the proposed approximation appears to be the most accurate.

Sample	Xu-Vasconcelos	Proposed
1	0.8985	**0.1446**
2	0.6066	**0.1354**
3	0.7966	**0.0311**
4	0.4907	**0.0387**
5	0.4588	**0.1729**

Table 5.6: RMS relative error (%) from 0-90 ° (both Θ and Φ) of orthorhombic group-velocity approximations by Xu et al. (2005) and Vasconcelos and Tsvankin (2006), and of proposed six-parameter approximation. Bold red highlight indicates the best-performing approximation. In all cases, the proposed approximation appears to be more accurate.

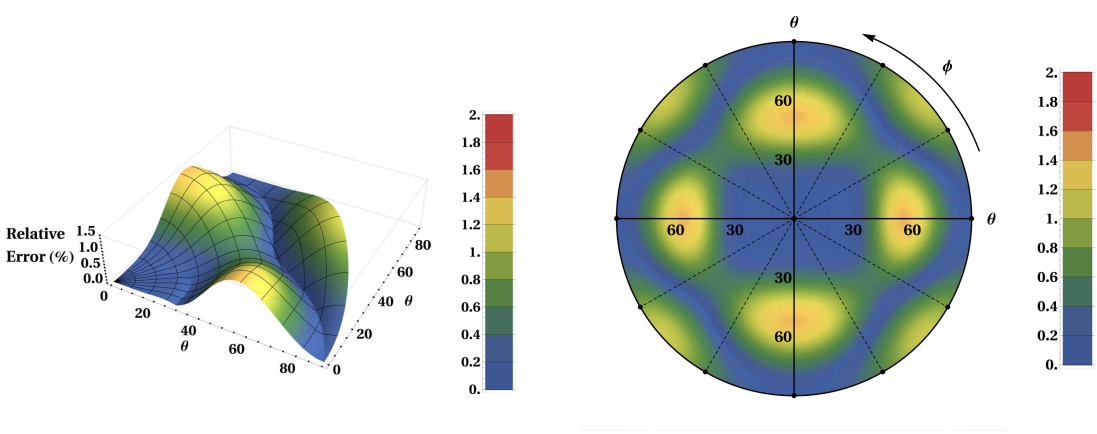

(a) (b)

Figure 5.3: Relative error of phase-velocity approximation by Tsvankin (1997). (a) from azimuth 0 to 90°. (b) from azimuth 0 to 360°. orthorhombic/. phaseweak90leglow,phaseweakleglow

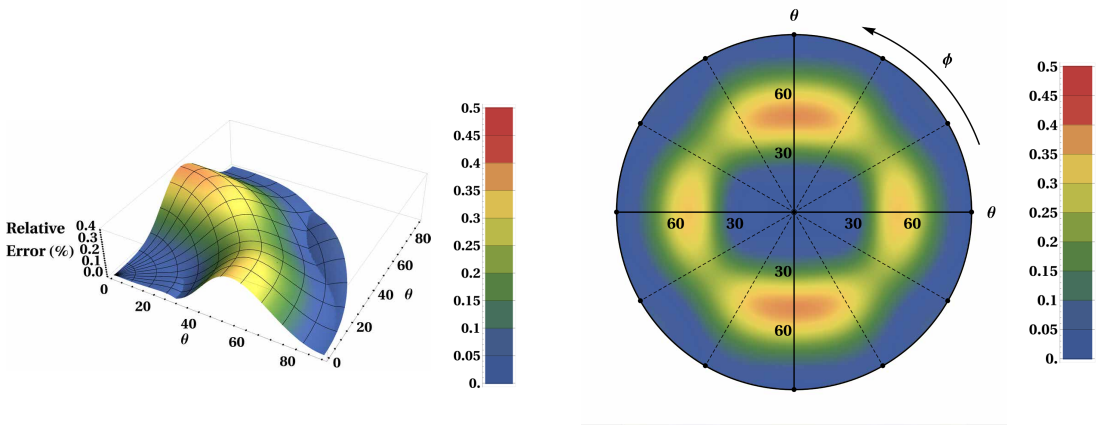

(a) (b)

Figure 5.4: Relative error of phase-velocity approximation by Alkhalifah (2003). (a) from azimuth 0 to 90°. (b) from azimuth 0 to 360°. orthorhombic/. phaseacoustic90leglow,phaseacousticleglow

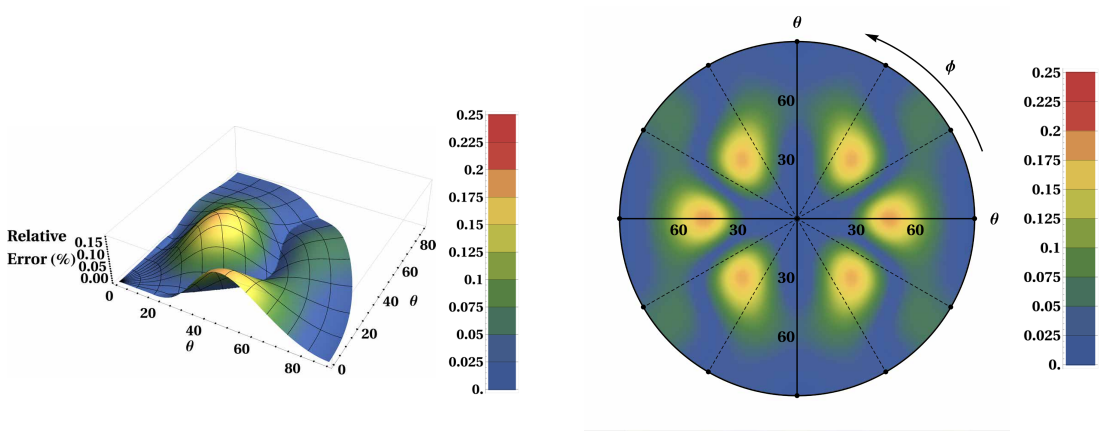

(a) (b)

Figure 5.5: Relative error of proposed six-parameter phase-velocity approximation. (a) from azimuth 0 to 90°. (b) from azimuth 0 to 360°. orthorhombic/. phasemshappq90leglownew,phasemshappqleglownew

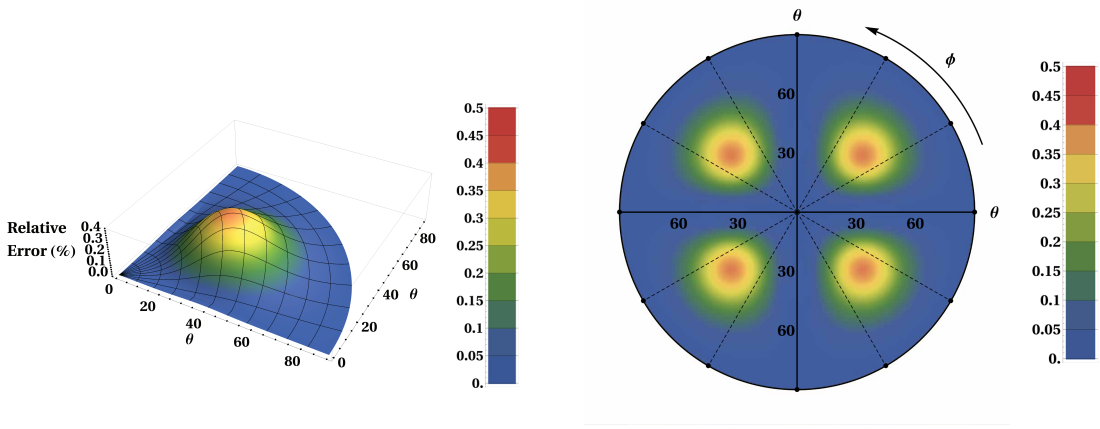

(a) (b)

Figure 5.6: Relative error of proposed nine-parameter phase-velocity approximation. (a) from azimuth 0 to 90°. (b) from azimuth 0 to 360°. orthorhombic/. phasemshtrueq90leglow,phasemshtrueqleglow

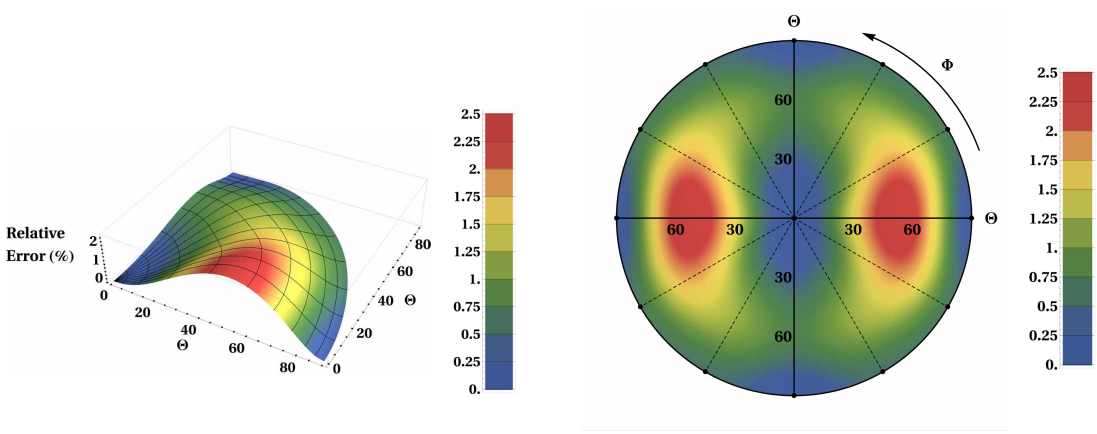

(a) (b)

Figure 5.7: Relative error of group-velocity approximation by Xu et al. (2005) and Vasconcelos and Tsvankin (2006). (a) from azimuth 0 to 90 °. (b) from azimuth 0 to 360 °. orthorhombic/. groupxu90leglow,groupxuleglow

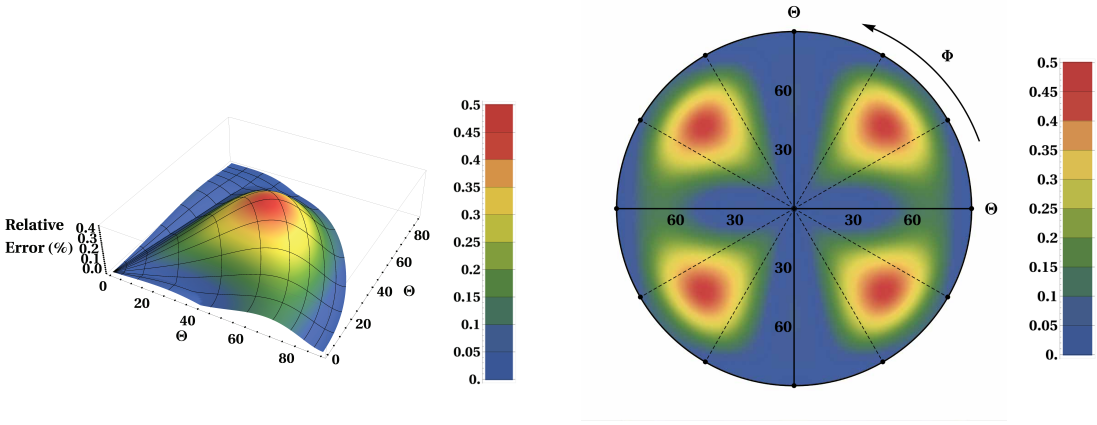

(a) (b)

Figure 5.8: Relative error of the proposed six-parameter group-velocity approximation. (a) from azimuth 0 to 90 °. (b) from azimuth 0 to 360 °. orthorhombic/. groupmshappq90leglownew,groupmshappqleglownew

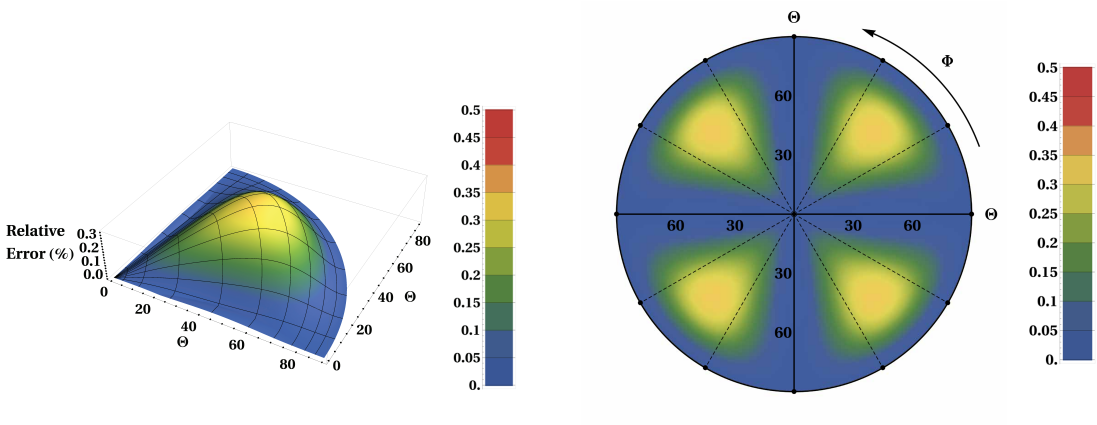

(a) (b)

Figure 5.9: Relative error of the proposed nine-parameter group-velocity approximation. (a) from azimuth 0 to 90°. (b) from azimuth 0 to 360°. orthorhombic/. groupmshtrueq90leglow,groupmshtrueqleglow

APPLICATION TO WAVE EXTRAPOLATION

One possible application of the proposed phase-velocity approximations (equations 5.12 and 5.33) is seismic wave extrapolation based on the anisotropic wave equation. Fomel et al. (2013) and Sun and Fomel (2015) presented a lowrank approximation method to accomplish this task. The proposed phase-velocity approximations (both in TI and orthorhombic media) are converted to their corresponding dispersion relations involving frequency and wavenumber and incorporated into the wave extrapolator formulated in the Fourier domain. An example of wave extrapolation in the complex BP 2007 TTI model (Figure 5.10) is shown in Figure 5.11. The same portion of the model was investigated by Fomel et al. (2013) and Sun and Fomel (2015). For simplicity, I take the shear-wave velocity ($v_{S0} = \sqrt{c_{55}}$) to be $v_{P0}/2$. The results are shown in Figure 5.11 and demonstrate noticeably smaller phase errors obtained from the proposed approximation.

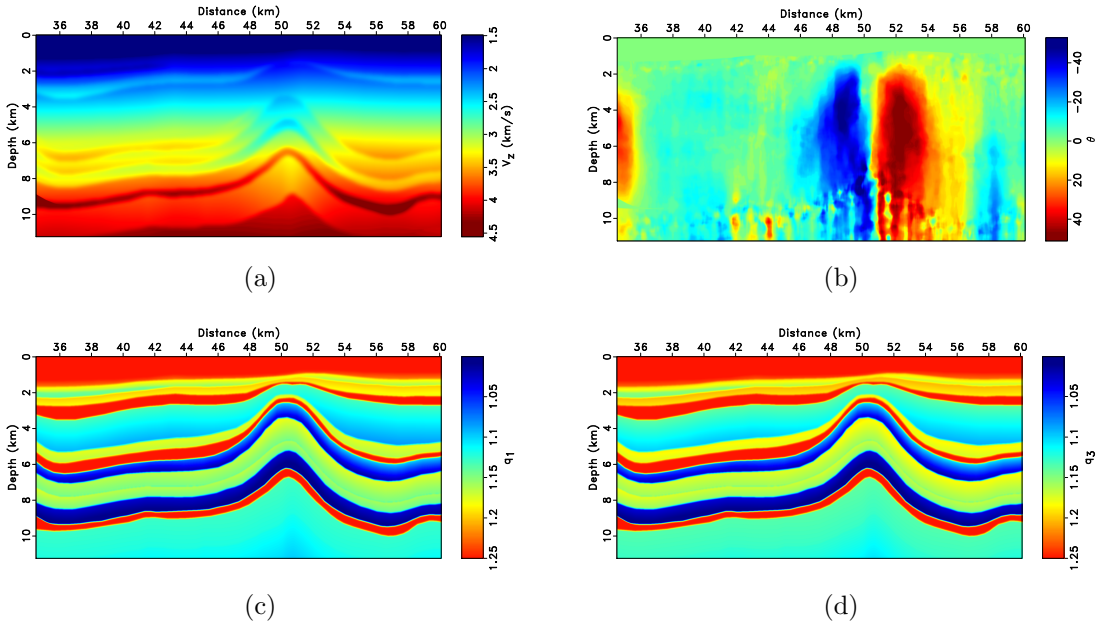

Figure 5.10: Portion of BP-2007 anisotropic benchmark model. (a) Velocity along the axis of symmetry. (b) Tilt of the symmetry axis. (c) Anellipticity parameter along the axis perpendicular to the axis of symmetry (q_1). (d) Anellipticity parameter along the axis of symmetry (q_3). orthorhombic/bptti vpend2,thetaend2,q1,q3

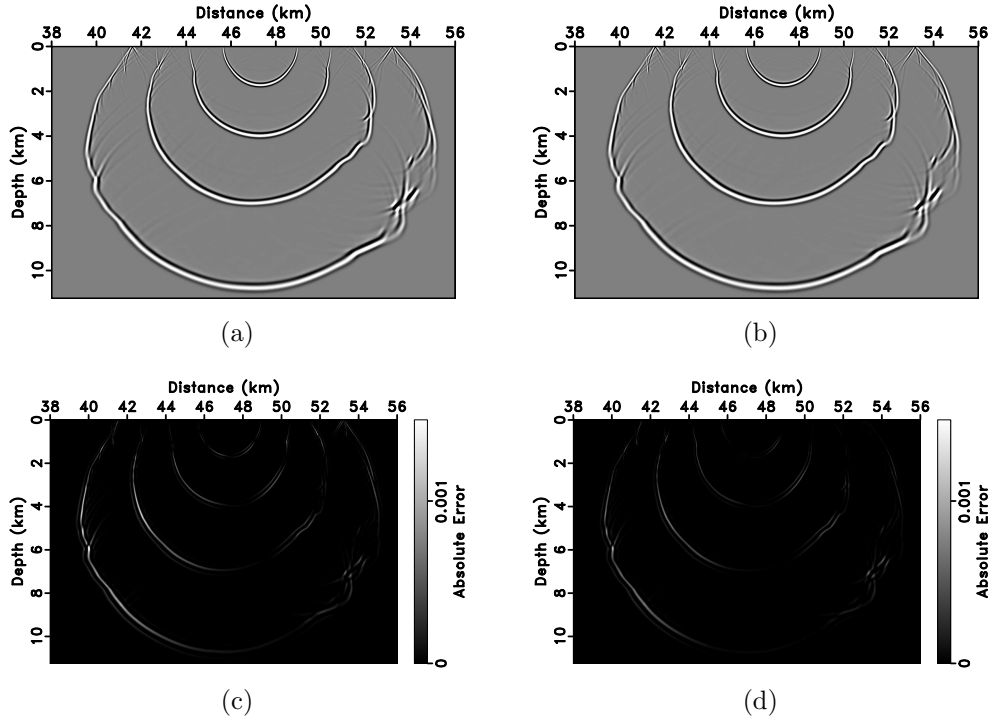

Figure 5.11: Multiple snapshots and errors of the wavefield extrapolation results for the BP TTI 2007 model. (a) Wavefield extrapolation using exact phase velocity. (b) Wavefield extrapolation using proposed phase-velocity approximation (5.12). (c) Absolute error in n_1-n_3 plane of the acoustic approximation. (d) Absolute error in n_1-n_3 plane of the proposed approximation (six-parameter). orthorhombic/bptti snaptssum-0,snaptssum-1,errortssum-2,errortssum-1

An example in a heterogeneous tilted orthorhombic medium is shown in Figures 5.12 and 5.13 using the parameters of the tilted orthorhombic model from Song and Alkhalifah (2013). In this model, the anisotropic parameters in the notation of Alkhalifah (2003) (equation 1.65)are specified in the range, $v_1 = 1500 : 3686$ m/s, $v_2 = 1500 : 3088$ m/s, $v_{P0} = 1500 : 3474$ m/s, $\eta_1 = 0.1$, $\eta_2 = 0.3$, and $\gamma = 1.03$. The exact formulas for v_1, v_2, and v_{P0} are

$$v_1 = 1500 + 60x^2 + 40(y-1.5)^2 + 40(z-1)^2 \ , \tag{5.50}$$

$$v_2 = 1500 + 40x^2 + 30(y-1.5)^2 + 30(z-1)^2, \tag{5.51}$$

$$v_{P0} = 1500 + 50x^2 + 35(y-1.5)^2 + 40(z-1)^2 \ , \tag{5.52}$$

where x, y, and z are components in the model. These values of parameters correspond to $q_{21} = 0.857 : 0.879$, $q_{31} = 0.833$, $q_{12} = 0.670 : 0.727$, $q_{32} = 0.625$, $q_{13} = 0.993 : 1.414$, and $q_{23} = 0.993 : 1.442$. The model, according to the right-hand rule is rotated 45° counterclockwise around the n_3 axis and subsequently 45° counterclockwise around the n_1 axis. I perform wave extrapolation using the exact dispersion relation and compare it with the results from the proposed approximation (equation 5.33), as well as the weak-anisotropy approximation (Tsvankin, 1997), and the acoustic approximation (Alkhalifah, 2003; Song and Alkhalifah, 2013). The error plots shown in Figure 5.13 demonstrate noticeably smaller phase errors from the proposed approximation.

DISCUSSION

My choice of Muir-Dellinger parametrization leads naturally to a four-parameter velocity approximation in TI media and a nine-parameter approximation in orthorhombic media. The approximations are improved by shifted-hyperboloid functional form.

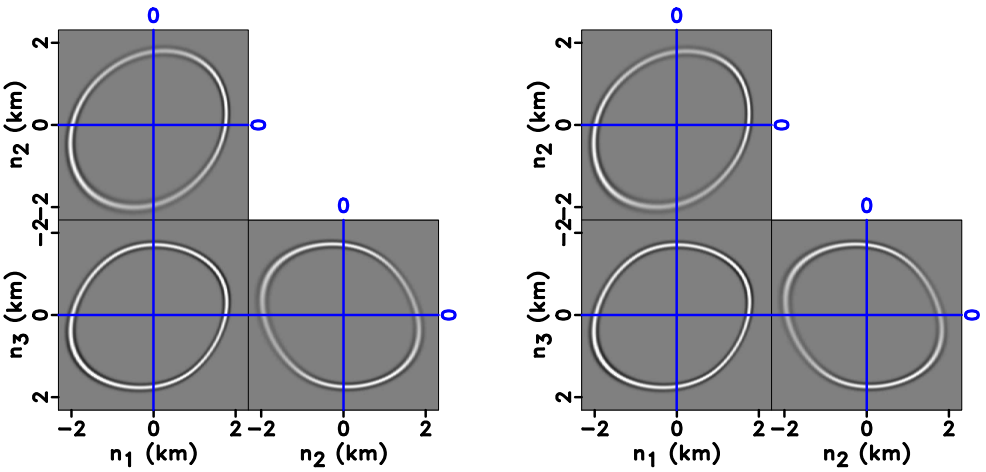

Figure 5.12: Wavefield extrapolation results in an example of the tilted orthorhombic model. (a) Wavefield extrapolation using the exact phase velocity. (b) Wavefield extrapolation using the proposed phase-velocity approximation (equation 5.33). The wavefields are virtually identical. orthorhombic/tiltorthocompare wave0,wave1

Although highly accurate, these approximations require the same number of parameters as the exact expressions. The benefits of their introduction may not be apparent in the case of phase velocity but are apparent in the consideration of group-velocity approximations because the exact expressions for group velocity in both types of media can be prohibitively complex and cannot be expressed easily in terms of group angle. As observed by previous researchers, the sufficient number of parameters to describe qP wave propagation in TI and orthorhombic media is smaller: three and six respectively. Therefore, I apply the novel relationships between anisotropic parameters summarized in Figures 2.1-2.3 to effectively reduce the number of parameters from the proposed four- and nine-parameter approximations to three- and six-parameter approximations respectively. An application to the proposed group-velocity approximation is in ray tracing as shown by Sripanich and Fomel (2014c).

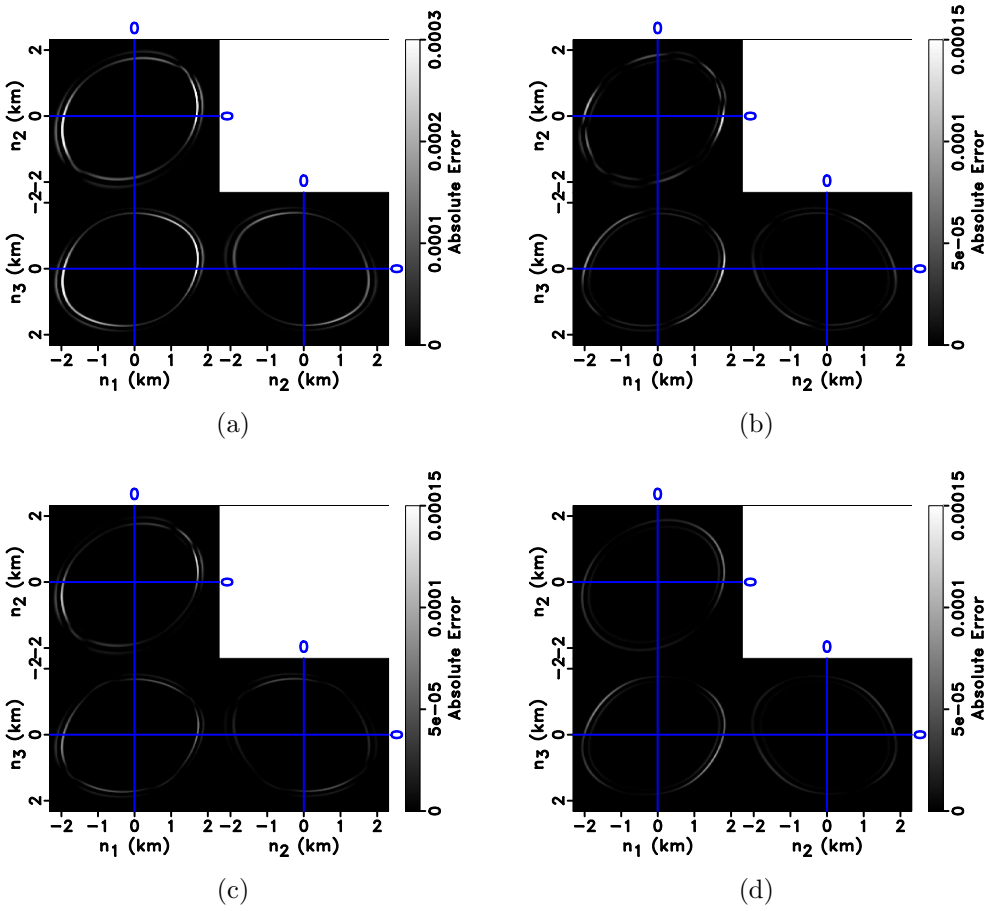

Figure 5.13: Errors in wavefield extrapolation results in an example of the tilted orthorhombic. (a) Absolute error of the weak-anisotropy phase-velocity approximation. (b) Absolute error of the acoustic phase-velocity approximation. (c) Absolute error of the proposed phase-velocity approximation (six-parameter). (d) Absolute error of the proposed phase-velocity approximation (nine-parameter). orthorhombic/tiltorthocompare error3,error2,error1,error4

Apart from the functional form proposed in this paper, many other forms of phase-velocity and group-velocity approximations, especially in TI media, have been extensively investigated in the past (e.g. Alkhalifah and Tsvankin, 1995; Tsvankin, 1996; Mensch and Rasolofosaon, 1997; Pšenčík and Gajewski, 1998; Alkhalifah, 1998, 2000a,b; Farra, 2001; Stopin, 2001; Zhang and Uren, 2001; Farra and Pšenčík, 2003; Daley et al., 2004; Ursin and Stovas, 2006; Fomel and Stovas, 2010; Stovas, 2010; Aleixo and Schleicher, 2010; Farra and Pšenčík, 2013; Hao and Stovas, 2014). While some of them are based on physical assumptions, others are derived purely from mathematical arguments. The proposed approximation is an alternative, which provides both accuracy and connection with the physical wave phenomena. They are based on the original Muir-Dellinger approximations (Muir and Dellinger, 1985; Dellinger et al., 1993), which were derived on the basis of perturbation from elliptical phase-velocity surfaces. The primary advantage of the Muir-Dellinger parameterization is the ease of conversion between the phase- and group-velocity approximations (e.g. equations 5.12 and 5.13), which provides practical convenience. Alternative highly accurate form for phase- and group-velocity approximations is the generalized moveout approximation (Fomel and Stovas, 2010), which was recently applied to anisotropic velocity approximations by Hao and Stovas (2014) and Sripanich et al. (2017).

The proposed approximations are readily applicable to approximate phase and group velocities in the case of transversely isotropic and orthorhombic media whose symmetry axis is aligned with the coordinate axis, e.g., VTI, HTI, and VOR. In the case of TTI (tilted transversely isotropic) and TOR (tilted orthorhombic), the coordinates simply need to be rotated via Bond transformation before applying the proposed approximations.

CONCLUSIONS

I have introduced novel forms of anelliptic approximations for qP velocities in TI and orthorhombic media. The first modification is an empirical connection between q_1 and q_3 parameters, which depends on the dominant lithology. The second modification is a new functional form of the phase- and group-velocity approximations, allowing up to fourth-order fitting along both symmetry and non-symmetry axes. As a result of these modifications, I arrive at highly accurate four-parameter approximations and new three-parameter approximations for TI media with better accuracy than previously suggested three-parameter approximations for both phase and group velocities. On the basis of the modified anelliptic approximations in TI media, I also propose anelliptic approximations for qP velocities in orthorhombic media, which can be implemented using either six or nine parameters. The proposed orthorhombic phase-velocity approximation maintains the algebraic symmetry and appears to be a more accurate alternative to previously proposed approximations. The group-velocity approximation has an analogous functional form and is also very accurate. The superior accuracy of the proposed phase-velocity approximations in TI and orthorhombic media is confirmed additionally using wave extrapolation experiments.

ACKNOWLEDGMENTS

I would like to thank M. van der Baan, I. Ravve, A. Stovas, and an anonymous reviewer for constructive comments and helpful suggestions. I also thank J. Dellinger, P. Fowler, Q. Hao, and J. Sun for useful discussions. I thank the sponsors of the Texas Consortium for Computational Seismology (TCCS) for financial support.

Chapter 6

Conclusion

Summary

In this dissertation, I propose a novel perspective to look at seismic anisotropy and its effects using the Muir-Dellinger parameters. In Chapter 2, I show that the qP-wave kinematics under MD parameterization are captured in such a way that two (q_1 and q_3) out of the four controlling parameters become approximately linearly dependent on each other, and one may use the newly discovered linear relationship to reduce the number of involving parameters in qP-wave analyses with high fidelity. This particular empirical linear relationship is confirmed by different rock physics measurements in the literature and can also provide more insights towards subsurface lithology and type of pore fluids directly from qP kinematics. I provide some supportive evidence for its reality from self-consistent rock physics modeling and Backus averaging in Chapter 3.

Apart from these intriguing rock physics implications, I found that the Muir-Dellinger parameters also lead to one of the most optimal frameworks for parameter estimation problem with qP waves. I conduct a detailed study on their sensitivity with respect to qP-wave kinematics in comparison with other previously proposed schemes in Chapter 4. The results from this study indicates that Muir-Dellinger parameters can lead to well-conditioned inverse problems in a large number of TI and orthorhombic models in comparison with other conventional parameterizations.

Finally, I use the Muir-Dellinger parameters as the basis for phase and group-velocity approximations in Chapter 5. The proposed approximations have similar functional form for phase velocity and group slowness but with reciprocal coefficients thanks to the use of MD parameters. This result leads to a practical convenience when considering both phase (wavefront) and group (ray) velocities. I show in a number of models that the proposed velocity approximations can perform with higher accuracy despite using the same number of dependent parameters as in other previously proposed velocity approximations.

In summary the main contributions of this research work include:

1. An alternative approach to characterize the effects of seismic anisotropy through the Muir-Dellinger parameters.

2. A novel empirical linear relationship under MD parameterization that can be used to infer rock physics properties such as lithology and the type of pore fluids directly from qP-wave kinematics.

3. A convenient basis for subsurface parameter estimation using MD parameters.

4. Practical analytical approximations with high accuracy for qP-wave phase and group velocities in transversely isotropic and orthorhombic media.

Discussion and possible future works

Despite the detailed discussion at the end of each chapter, I reemphasize several important points. Some of them may lead to future research opportunities with MD parameters.

I reemphasize that Muir-Dellinger parameters were specifically designed to work with qP waves and an attempt to use them to study qS waves may lead to complications as discussed at the end of Chapter 2. However, the discovery of the linear relationship may aid in understanding the connection between seismic anisotropy and rock physics of the subsurface. Alternatively, one may choose to convert the newly discovered linear relationship from MD to other anisotropic parameterizations of choice (Table 2.1) and use it to supplement in the current practice of anisotropic processing and analysis to readily obtain more information about the subsurface.

The novel empirical linear relationship was observed based on rock physics measurements with TI assumption, hence it must be used with care when considering an orthorhombic model as discussed in Chapter 2 and 3. Further proofs of its applicability in orthorhombic or even monoclinic models requires reliable rock physics measurements and effective elastic modeling in fractured rocks. The recently proposed generalization of Backus averaging (Bos et al., 2016) may help pave the way to accomplish such task. Additionally, the effects of pressure on the stiffness measurements were neglected in Figures 2.1–2.3 and there exists a research opportunity to investigate a plausible variation of the slope parameter with pressure.

The sensitivity results in Chapter 4 serve as a theoretical indicator of better-posed inverse problems when using MD parameters to study qP-wave kinematics. There are research opportunities to investigate the performance of Muir-Dellinger parameters in practice in the context of moveout analysis, tomography, and full-waveform inversion. An exact Dix-typed layer stripping method for estimating interval anisotropic parameters from quartic moveout coefficients recently proposed by Sripanich and Fomel (2016), together with accurate 3D moveout approximation (Sripanich et al., 2017), may represent a first step towards that goal.

So far, I have only considered Muir-Dellinger parameters with respect to the kinematic signatures of qP waves. Even though MD parameters may have limited applicability to study beyond qP kinematics, it is possible to extend the use of MD parameters to study the dynamic signatures such as amplitudes and reflection/transmission coefficients of qP waves. These results may lead to an alternative way to look at amplitude variation with offset (AVO) and further discoveries on the advantages of the empirical linear relationship.

Eventually, one may try to investigate the relationship between MD, its linear relationship, and fracture parameters. In combination with other findings, the MD parameters and its linear relationship may lead to useful conclusions when working with unconventional reservoirs.

Appendix

APPENDIX A: AN ANALYSIS ON THE INSENSITIVITY OF qP-WAVE PHASE VELOCITY TO THE SLOPE PARAMETER

Under MD parameterization, reducing the number of dependent parameters for qP-wave analysis involves fixing the slope value, which is different from weak-anisotropy approximation and from the pseudoacoustic approximation. In this Appendix, I propose to investigate this process by inspecting the derivative $\frac{\partial v_{qP}^2}{\partial s}$, which should be small if the qP-wave phase velocity is relatively insensitive to the change in slope.

Starting from the exact qP phase velocity under the MD parameterization in equation 2.15, I can substitute $q_1 = 1 + s(q_3 - 1)$ or $q_3 = 1 + (q_1 - 1)/s$, which leads to the dependence of the resulting v_{qP}^2 expression on w_1, w_3, q_1 or q_3, and s. It follows that $\frac{\partial v_{qP}^2}{\partial s} = 0$ when either of these two conditions is satisfied:

1. $w_1 = w_3$, which implies isotropic models or anelliptic models with similar velocity along the symmetry and its orthogonal.

2. $q_1 = 1$ or $q_3 = 1$, which implies elliptical anisotropic models.

Therefore, the first-order effects from the change of slope parameter on qP-wave phase velocity is negligible when considering an isotropic model, or an elliptical anisotropic model, or an anelliptic model with equal velocity along the symmetry axis and its orthogonal. For any other models close to those conditions, the derivative $\frac{\partial v_{qP}^2}{\partial s}$ can be expected to be small.

Let us consider the same example model as in Figure 2.8 whose model parameters under MD parameterization are fairly different from the above conditions and are given by $w_1 = 22.4\ km^2/s^2$, $w_3 = 16\ km^2/s^2$, $q_1 = 0.649$, $q_3 = 0.643$, and $s = 0.9813$.

I compare the derivative $\frac{\partial v_{qP}^2}{\partial s}$ with $\frac{\partial v_{qP}^2}{\partial v_{S0}^2}$ when the velocity is expressed under Thomsen parameterization. Figure A-1 shows the resultant plots of the magnitude of both derivatives while varying v_{S0} and the slope s. For a fair comparison on magnitude, I normalize the derivative $\frac{\partial v_{qP}^2}{\partial s}$ by the average velocity $v_{av}^2 = 2/\pi \int_0^{\pi/2} v_{qP}^2 d\theta$ to make it dimensionless. I can observe that the magnitude of the derivative $\frac{\partial v_{qP}^2}{\partial s}$ remains small despite a significant change in the slope value and is comparable to what is observed from $\frac{\partial v_{qP}^2}{\partial v_{S0}^2}$ when the velocity is expressed under Thomsen parameterization. Hence, parameter reduction by fixing the slope value in MD parameterization can be observed from both empirically based on rock physics measurements and from investigating the derivative $\frac{\partial v_{qP}^2}{\partial s}$.

APPENDIX B: CORRECTION FOR ORIENTATION DISTRIBUTION FUNCTION IN SELF-CONSISTENT MODELING

In our study, the results from self-consistent modeling in equations 3.1-3.2 are corrected for average orientation distribution following the method proposed by Johansen et al. (2004) given below,

$$\mathbf{C}^r = (\mathbf{T}_{000} + W_{200}^N \mathbf{T}_{200} + W_{400}^N \mathbf{T}_{400})\mathbf{C}^a \ , \tag{B-1}$$

where $\mathbf{C}^a = [c_{11}^*, c_{33}^*, c_{13}^*, c_{55}^*, c_{66}^*]$ and $\mathbf{C}^r = [c_{11}^{**}, c_{33}^{**}, c_{13}^{**}, c_{55}^{**}, c_{66}^{**}]$ denote vectors of effective stiffnesses before and after orientation distribution correction respectively. The former is obtained from equation 3.1. The normalized Legendre function coefficients W_{ijk}^N are defined as

$$W_{200}^N = 4\pi^2 \int_{-1}^{1} \frac{1}{2} W(\xi)(3\xi^2 - 1) d\xi \ , \tag{B-2}$$

$$W_{400}^N = 4\pi^2 \int_{-1}^{1} \frac{1}{8} W(\xi)(35\xi^4 - 30\xi^2 + 3) d\xi \ , \tag{B-3}$$

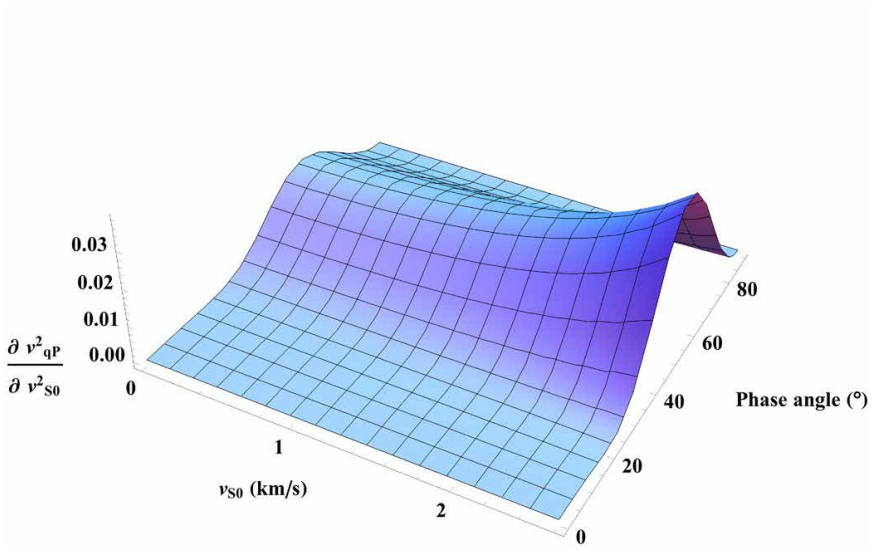

(a)

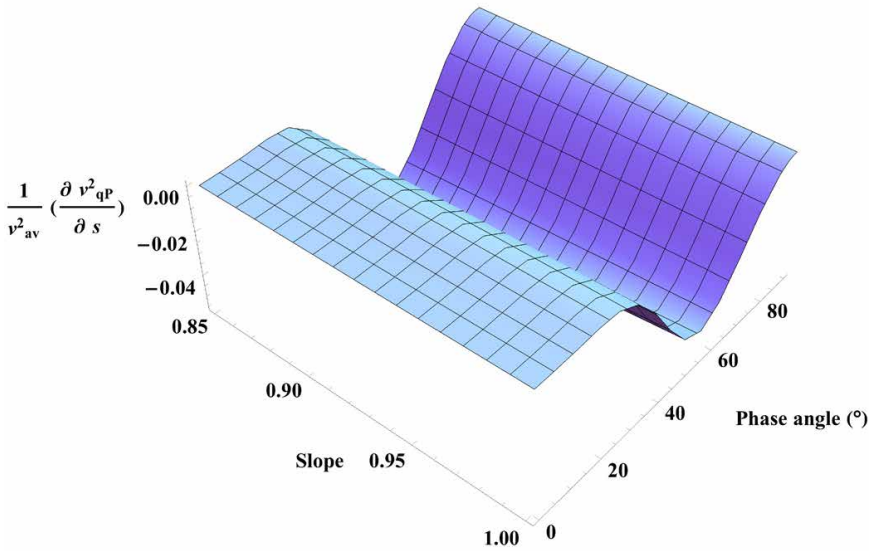

(b)

Figure A-1: The magnitude of derivative (a) $\frac{\partial v^2_{qP}}{\partial v^2_{S0}}$in TI media under Thomsen parameterization and (b) $\frac{1}{v^2_{av}}\left(\frac{\partial v^2_{qP}}{\partial s}\right)$ under MD parameterization. I can observe a comparable range of magnitude that indicate the relative insensitivity of qP-wave phase velocity to both parameters in different parameterizations. disser-conclusion/. dvs0,dslope

where ξ denotes the cosine of the angle difference between the vertical axis of the local and global coordinates Johansen et al. (2004). $W(\xi)$ represents the orientation distribution function (ODF) of choice that has to satisfies

$$\int_{-1}^{1} W(\xi) d\xi = \frac{1}{4\pi^2} \ . \tag{B-4}$$

In this study, we assume a Gaussian ODF, which is defined by

$$W(\xi) = k(\sigma) \exp\left[-\frac{1}{2}\left(\frac{\arccos\xi}{\sigma}\right)^2\right] \ , \tag{B-5}$$

$$k(\sigma) = \frac{\exp(\sigma^2/2)}{\sqrt{2}\pi^{5/2}\sigma\left[2\mathrm{erfi}\left(\frac{\sigma}{\sqrt{2}}\right) - \mathrm{erfi}\left(\frac{\sigma^2 - i\pi}{\sqrt{2}\sigma}\right) - \mathrm{erfi}\left(\frac{\sigma^2 + i\pi}{\sqrt{2}\sigma}\right)\right]} \ , \tag{B-6}$$

where σ is the standard deviation for the ODF. The remaining parameters are defined as follows:

$$\mathbf{T}_{000} = \frac{1}{15}\begin{bmatrix} 8 & 3 & 4 & 8 & 0 \\ 8 & 3 & 4 & 8 & 0 \\ 6 & 1 & 8 & -4 & -10 \\ 1 & 1 & -2 & 6 & 5 \\ 1 & 1 & -2 & 6 & 5 \end{bmatrix} \ , \tag{B-7}$$

$$\mathbf{T}_{200} = \frac{1}{21}\begin{bmatrix} 8 & -6 & -2 & -4 & 0 \\ -16 & 12 & 4 & 8 & 0 \\ -6 & 1 & 5 & -4 & 14 \\ 1 & 1 & -2 & 3 & -7 \\ -2 & -2 & 4 & -6 & 14 \end{bmatrix} \ , \tag{B-8}$$

$$\mathbf{T}_{400} = \frac{1}{35}\begin{bmatrix} 3 & 3 & -6 & -12 & 0 \\ 8 & 8 & -16 & -32 & 0 \\ -4 & -4 & 8 & 16 & 0 \\ -4 & -4 & 8 & 16 & 0 \\ 1 & 1 & -2 & -4 & 0 \end{bmatrix} \ . \tag{B-9}$$

APPENDIX C: DERIVATION OF THE APPROXIMATE HESSIAN

In this appendix, I provide a derivation of the approximate Hessian (equation 4.1) that I use to study the parameter sensitivity in Chapter 4. I begin with the definition

of data residual (misfit function) given by

$$\begin{aligned} R(m_i) &= \frac{1}{2}\int_0^{\pi/2}\int_0^{\pi/2}\left(V^2(m_i,\theta,\phi)-\hat{V}^2(\theta,\phi)\right)^2 \sin\theta d\theta d\phi \ , \\ &= \frac{1}{2}\int_0^{\pi/2}\int_0^{\pi/2}\left(\Delta V^2(m_i)\right)^2 \sin\theta d\theta d\phi \ , \end{aligned} \tag{B-10}$$

where V denotes the phase (or group) velocity that depends on different anisotropic parameters m_i and $\hat{V}$ denotes observed velocity. The factor $\sin\theta$ denotes the Jacobian for the change of variables for the double integration. Assuming the updated model m_i can be written as a sum of the starting model m_i^0 plus a perturbation model $\Delta m_i = m_i - m_i^0$, we can obtain the following Taylor expansion of the misfit function as:

$$R(m_i^0+\Delta m) \approx R(m_i^0) + \sum_i \frac{\partial R}{\partial m_i}\Big|_{m_i^0}\Delta m_i \tag{B-11}$$

$$+\frac{1}{2}\sum_i\sum_j \frac{\partial^2 R}{\partial m_i \partial m_j}\Big|_{m_i^0}\Delta m_i \Delta m_j \ , \tag{B-12}$$

where $\frac{\partial R}{\partial m_i}$ and $\frac{\partial^2 R}{\partial m_i \partial m_j}$ (Hessian) are given by

$$\frac{\partial R}{\partial m_i} = \int_0^{\pi/2}\int_0^{\pi/2}\left[\frac{\partial V^2}{\partial m_i}\Delta V^2\right]\sin\theta d\theta d\phi \ , \tag{B-13}$$

$$\frac{\partial^2 R}{\partial m_i \partial m_j} = \int_0^{\pi/2}\int_0^{\pi/2}\left[\frac{\partial V^2}{\partial m_i}\frac{\partial V^2}{\partial m_i} + \frac{\partial^2 V^2}{\partial m_i m_j}\Delta V^2\right]\sin\theta d\theta d\phi \ . \tag{B-14}$$

Under the assumption that the problem is approximately linear, the second derivative $\frac{\partial^2 V^2}{\partial m_i m_j} \approx 0$ and the approximate Hessian is given by

$$R_{ij} = \frac{\partial^2 R}{\partial m_i \partial m_j} = \int_0^{\pi/2}\int_0^{\pi/2}\frac{\partial V^2}{\partial m_i}\frac{\partial V^2}{\partial m_i}\sin\theta d\theta d\phi \ , \tag{B-15}$$

which is similar to equation 4.1 in Chapter 4.

Bibliography

Aki, K., and P. G. Richards, 2002, Quantitative Seismology, 2 ed.: University Science Books.

Aleixo, R., and J. Schleicher, 2010, Traveltime approximations for q-P waves in vertical transversely isotropy media: Geophysical Prospecting, **58**, 191–201.

Alkhalifah, T., 1998, Acoustic approximations for processing in transversely isotropic media: Geophysics, **63**, 623–631.

———, 2000a, An acoustic wave equation for anisotropic media: Geophysics, **65**, 1239–1250.

———, 2000b, The offset-midpoint traveltime pyramid in traversely isotropic media: Geophysics, **65**, 1316–1325.

———, 2003, An acoustic wave equation for orthorhombic anisotropy: Geophysics, **68**, 1169–1172.

Alkhalifah, T., and I. Tsvankin, 1995, Velocity analysis for transversely isotropic media: Geophysics, **60**, 1550–1566.

Anderson, D. L., 1989, Theory of the Earth: Blackwell Scientific Publications.

Auld, B. A., 1973, Acoustic Fields and Waves in Solids: Robert E. Krieger Publishing Company.

Backus, G., 1970, A geometrical picture of anisotropic elastic tensors: Reviews of Geophysics and Space Physics, **8**, no. 3, 633–671.

Backus, G. E., 1962, Long-wave elastic anisotropy produced by horizontal layering: Journal of Geophysical Research, **67**, 4427–4440.

Bakker, P. M., and E. Duveneck, 2011, Stability analysis for acoustic wave propa-

gation in tilted TI media by finite differences: Geophysical Journal International, **185**, 911–921.

Bakulin, A., V. Grechka, and I. Tsvankin, 2000, Estimation of fracture parameters from reflection seismic data–Part II: Fractured models with orthorhombic symmetry: Geophysics, **65**, no. 6, 1803–1817.

Bandyopadhyay, K., 2009, Seismic Anisotropy: Geological causes and its implications to Reservoir Geophysics: PhD thesis, Stanford University.

Berryman, J. G., 1979, Long-wave elastic anisotropy in trasversely isotropic media: Geophysics, **44**, 896–917.

———, 1980a, Long-wavelength propagation in composite elastic media I. Spherical inclusions: J. Acoust. Soc. Am., **68**, no. 6, 1809–1819.

———, 1980b, Long-wavelength propagation in composite elastic media II. Ellipsoidal inclusions: J. Acoust. Soc. Am., **68**, no. 6, 1820–1831.

Bos, L., D. R. Dalton, M. A. Slawinski, and T. Stanoev, 2016, On backus average for generally anisotropic layers: Journal of Elasticity, 1–18.

Brendow, K., 2003, Global oil shale issues and perspectives: Oil Shale, **20**, no. 1, 81–92.

Bube, K. P., T. Nemeth, J. P. Stefani, W. Liu, K. T. Nihei, R. Ergas, and L. Zhang, 2012a, First-order systems for elastic and acoustic variable-tilt TI media: Geophysics, **77**, no. 5, T157–T170.

———, 2012b, On the instability in second-oreder systems for acoustic VTI and TTI media: Geophysics, **77**, no. 5, T171–186.

Budiansky, B., 1965, On the elastic moduli of some heterogeneous materials: J. Mech. Phys. Solids, **13**, 223–227.

Carcione, J. M., 2001, Wave Fields in Real Media: Wave Propagation in Anisotropic, Anelastic and Porous Media: Pergamon.

Carrion, P., J. Costa, J. E. F. Pinheiro, and M. Schoenberg, 1992, Cross-borehole tomography in anisotropic media: Geophysics, **57**, no. 9, 1194–1198.

Červený, V., 2001, Seismic Ray Theory: Cambridge University Press.

Chapman, C., 2004, Fundamentals of Seismic Wave Propagation: Cambridge University Press.

Chapman, C., and D. Miller, 1996, Velocity sensitivity in transversely isotropic media: Geophysical Prospecting, **44**, no. 3, 525–549.

Chapman, C., and R. G. Pratt, 1992, Traveltime tomography in anisotropic media — I. Theory: Geophysical Journal International, **109**, no. 1, 1–19.

Cheng, J., and W. Kang, 2014, Simulating propagation of separated wave modes in general anisotropic media, Part I: qP-wave propagators: Geophysics, **79**, no. 1, C1–C18.

Claerbout, J., 1985, Imaging the Earth's Interior: Blackwell Scientific Publications.

Cowin, S. C., 1989, Properties of the anisotropic elasticity tensor: Quarterly Journal of Mechanics and Appllied Mathematics, **42**, 249–266.

Crampin, S., 1984, An introduction to wave propagation in anisotropic media: Geophysical Journal of the Royal Astronomical Society, **76**, 17–28.

———, 1991, Effects of point singularities on shear-wave propagation in sedimentary basins: Geophysical Journal International, **107**, 531–543.

Crampin, S., and M. Yedlin, 1981, Shear-wave singularities of wave propagation in anisotropic media: Journal of Geophysics, **49**, 43–46.

Daley, P. F., E. S. Krebes, and L. R. Lines, 2004, Phase velocity approximations in a transversely isotropic medium: Technical report, University of Calgary.

Dellinger, J., F. Muir, and M. Karrenbach, 1993, Anelliptic approximations for TI media: Journal of Seismic Exploration, **2**, 23–40.

Dellinger, J., D. J. Vasicek, and C. Sondergeld, 1998, Kelvin notation for stabilizing elastic-constant inversion: Oil and Gas Science and Technology, **53**, no. 5, 709–719.

Dellinger, J. A., 1991, Anisotropic Seismic Wave Propagation: PhD thesis, Stanford University.

Dewhurst, D. N., A. F. Siggins, J. Sarout, M. D. Raven, and H. M. Nordgård-Bolås, 2011, Geomechanical and ultrasonic characterization of a Norwegian Sea shale: Geophysics, **76**, no. 3, WA101–WA111.

Domnesteanu, P., C. McCann, and J. Sothcott, 2002, Velocity anisotropy and attenuation of shale in under- and overpressured conditions: Geophysical Prospecting, **50**, 487–503.

Du, X., P. Fowler, and R. Fletcher, 2014, Recursive integral time-extrapolation methods for waves: A comparative review: Geophysics, **79**, no. 1, T9–T26.

Farra, V., 2001, High-order perturbations of the phase velocity and polarization of qP and qS waves in anisotropic media: Geophysical Journal International, **147**, 93–104.

Farra, V., and I. Pšenčík, 2003, Properties of the zeroth-, first-, higher-order approximations of attributes of elastic waves in weakly anisotropic media: Journal of the Acoustical Society of America, **114**, no. 3, 1366–1378.

———, 2013, Moveout approximations for P- and SV-waves in VTI media: Geophysics, **78**, no. 5, WC81–WC92.

Farra, V., I. Pšenčík, and P. Jílek, 2016, Weak-anisotropy moveout approximations for P-waves in hormogeneous layers of monoclinic or higher anisotropy symmetries: Geophysics, **81**, no. 2, C17–C37.

Fedorov, F. I., 1968, Theory of Elastic Waves in Crystals: Springer.

Fletcher, R., X. Du, and P. Fowler, 2009, Reverse time migration in tilted transversely isotropic (TTI) media: Geophysics, **74**, no. 6, WCA179–WCA187.

Fomel, S., 2004, On anelliptic approximations for qP velocities in VTI media: Geophysical Prospecting, **52**, 247–259.

Fomel, S., and A. Stovas, 2010, Generalized nonhyperbolic moveout approximation: Geophysics, **75**, no. 2, U9–U18.

Fomel, S., L. Ying, and X. Song, 2013, Seismic wave extrapolation using lowrank symbol approximation: Geophysical Prospecting, **61**, 526–536.

Fowler, P., 2015, Some pitfalls in orthorhombic parameter estimation: 85th Annual International Meeting Expanded Abstracts, Society of Exploration Geophysicists, 493–497.

Fowler, P., X. Du, and R. P. Fletcher, 2010, Coupled equations for reverse time migration in transversely isotropic media: Geophysics, **75**, no. 1, S11–S22.

Fowler, P. J., 2003, Practical VTI approximations: A systematic anatomy: Journal of Applied Geophysics, 347–367.

Fowler, P. J., C. Chu, C. Lapilli, P. Anno, and B. Macy, 2014, Recursive integral time extrapolation of P-waves in orthorhombic media: Geophysics. (To be submitted).

Fowler, P. J., and C. Lapilli, 2012, Generalized pseudospectral methods for orthorhombic modeling and reverse-time migration: Presented at the 74th Annual EAGE Meeting Expanded Abstracts, EAGE.

Gassmann, F., 1964, Introduction to seismic travel time methods in anisotropic media: Pure and Applied Geophysics, **58**, 63–112.

Golikov, P., and A. Stovas, 2012, Accuracy comparison of nonhyperbolic moveout ap-

proximations for qP-waves in VTI media: Journal of Geophysics and Engineering, **9**, 428–432.

Grechka, V., 2009, Applications of Seismic Anisotropy in the Oil and Gas Industry: European Association of Geoscientists and Engineers.

Grechka, V., L. Zhang, and J. W. Rector, 2004, Shear waves in acoustic anisotropic media: Geophysics, **69**, no. 2, 576–582.

Hao, Q., and A. Stovas, 2014, Anelliptic approximation of p-wave phase velocity in orthorhombic media: Presented at the 16th International Workshop on Seismic Anisotropy.

Haven, J., and M. Batzle, 2014, Thomsen parameter relationships and estimation from laboratory ultrasonic data: 84th Annual International Meeting Expanded Abstracts, Society of Exploration Geophysicists, 2772–2777.

Helbig, K., 1983, Elliptical anisotropy — Its significance and meaning: Geophysics, **48**, no. 7, 825–832.

———, 1994, Foundations of Anisotropy for Exploration Seismics: Pergamon.

Helbig, K., and M. Schoenberg, 1987, Anomalous polarization of elastic waves in transversely isotropic media: Journal of Acoustical Society of America, **81**, no. 5, 1235–1245.

Helbig, K., and L. Thomsen, 2005, 75-plus years of anisotropy in exploration and reservoir seismics: A historical review of concepts and methods: Geophysics, **70**, 9ND–23ND.

Hepbasli, A., 2004, Oil shale as an alternative energy source: Energy sources, **26**, no. 2, 107–118.

Hill, R., 1965, A self-consistent mechanics of composite materials: J. Mech. Phys. Solids, **13**, 213–222.

Hornby, B. E., 1998, Experimental laboratory determination of the dynamic elastic properties of wet, drained shales: Journal of Geophysical Research, **103**, 29945–29964.

Hornby, B. E., L. M. Schwartz, and J. A. Hudson, 1994, Anisotropic effective-medium modeling of the elastic properties of shales: Geophysics, **59**, no. 10, 1570–1583.

Ivanov, Y., and A. Stovas, 2016, Normal moveout velocity ellipse in tilted orthorhombic media: Geophysics, **81**, no. 6, C319–C336.

Jakobsen, M., J. A. Hudson, and T. A. Johansen, 2003, T-matrix approach to shale acoustics: Geophysical Journal Interntional, **154**, 533–558.

Jakobsen, M., J. A. Hudson, T. A. Minshull, and S. C. Singh, 2000, Elastic properties of hydrate-bearing sediments using effective medium theory: Journal of Geophysical Research, **105**, 561–577.

Jakobsen, M., and T. A. Johansen, 2000, Anisotropic approximations for mudrocks: A seismic laboratory study: Geophysics, **65**, no. 6, 1711–1725.

Johansen, T. A., B. O. Ruud, and M. Jakobsen, 2004, Effect of grain scale alignment on seismic anisotropy and reflectivity of shales: Geophysical Prospecting, **52**, 133–149.

Johnston, J. E., and N. I. Christensen, 1995, Seismic anisotropy of shales: Journal of Geophysical Research, **100**, 5991–6003.

Jones, L. E. A., and H. F. Wang, 1981, Ultrasonic velocities in cretaceous shales from the williston basin: Geophysics, **46**, 288–297.

Mavko, G., T. Mukerji, and J. Dvorkin, 2009, The Rock Physics Handbook, 2 ed.: Cambridge Universiy Press.

Mehrabadi, M. M., and S. C. Cowin, 1990, Eigentensors of linear anisotropic elastic materials: Quarterly Journal of Mechanics and Appllied Mathematics, **43**, 15–41.

Mensch, T., and P. Rasolofosaon, 1997, Elastic wave velocities in anisotropic media of arbitrary anisotropy – Generalization of Thomsen's parameters ϵ, δ, and γ: Geophysical Journal International, **128**, 43–64.

Muir, F., 1990, A modified anisotropic system: SEP, **67**, 41–42.

Muir, F., and J. Dellinger, 1985, A practical anisotropic system: SEP, **44**, 55–58.

Mura, T., 1987, Micromechanics of Defects in Solids, 2 ed.: Martinus Nijhoff Publishers.

Murphy, E., S. R. Barraza, M. Gu, D. Gokaraju, M. E. Far, J. Quirein, and L. Ou, 2015, New Models for Acoustic Anisotropic Interpretation in Shale: Presented at the 56th Annual SPWLA Logging Symposium, SPWLA.

Musgrave, M. J. P., 1970, Crystal Acoustics: Introduction to the Study of Elastic Waves and Vibrations in Crystals: Holden-Day.

Nishizawa, O., 1982, Seismic velocity anisotropy in a medium containing oriented cracks – transversely isotropic case: J. Phy. Earth, **30**, 331–347.

Ponte Castañeda, P., and J. R. Willis, 1995, The effect of spatial distribution on the effective behavior of composite materials and cracked media: J. Mech. Phys. Solids, **43**, no. 12, 1919–1951.

Prasad, M., A. Pal-Bathija, M. Johnston, M. Rydzy, and M. Batzle, 2009, Rock physics of the unconventional: The Leading Edge, **21**, no. 1, 34–38.

Pšenčík, I., and V. Farra, 2007, First-order P-wave ray synthetic seismograms in inhomogeneous, weakly anisotropic media: Geophysical Journal International, **170**, 1243–1252.

Pšenčík, I., and D. Gajewski, 1998, Polarization, phase velocity, and NMO velocity of qP-waves in arbitrary weakly anisotropic media: Geophysics, **63**, no. 5, 1754–1766.

Quirein, J., M. Eid, and A. Cheng, 2014, Predicting the stiffness tensor of a trans-

versely isotropic medium when the vertical Poisson's ratio is less than the horizontal Poisson's ratio: Presented at the 55th Annual SPWLA Logging Symposium, SPWLA.

Rasalofosaon, P., 1998, Stress-induced seismic anisotropy revisited: Rev. Inst[] Français Pétrole, **53**, 679–692.

Rüger, A., 2002, Reflection Coefficients and Azimuthal AVO Analysis in Anisotropic Media: Society of Exploration Geophysicists.

Sayers, C. M., 2005, Seismic anisotropy of shales: Geophysical Prospecting, **53**, 667–676.

Schoenberg, M., 1994, Transversely isotropic media equivalent to thin isotropic layers: Geophysical Prospecting, **42**, 885–915.

Schoenberg, M., and M. V. de Hoop, 2000, Approximate disperion relations for qP-qSV-waves in transversely isotropic media: Geophysics, **65**, no. 3, 919–933.

Schoenberg, M., and K. Helbig, 1997, Orthorhombic media: Modeling elastic wave behavior in a vertically fractured earth: Geophysics, **62**, 1954–1974.

Schoenberg, M., F. Muir, and C. Sayers, 1996, Introducing ANNIE: A simple three-parameter anisotropic velocity model for shales: Journal of Seismic Exploration, **5**, 35–49.

Slawinski, M., 2010, Waves and Rays in Elastic Continua: World Scientific.

Sone, H., 2012, Mechanical properties of shale gas reservoir rocks and its relation to in-situ stress variation observed in shale gas reservoirs: PhD thesis, Stanford University.

Song, X., and T. Alkhalifah, 2013, Modeling of pseudoacoustic P-waves in orthorhombic media with a low-rank approximation: Geophysics, **78**, no. 4, C33–C40.

Sripanich, Y., and S. Fomel, 2014a, Anelliptic approximations for qP velocities in

orthorhombic media: 84th Annual International Meeting Expanded Abstracts, Society of Exploration Geophysicists, 453–457.

———, 2014b, Modified anelliptic approximations for qP velocities in tranversely isotropic media: 84th Annual International Meeting Expanded Abstracts, Society of Exploration Geophysicists, 409–414.

———, 2014c, Two-point seismic ray tracing in layered media useing bending: 84th Annual International Meeting Expanded Abstracts, Society of Exploration Geophysicists, 3371–3376.

———, 2015, On anelliptic approximations for qP velocities in transversely isotropic and orthorhombic media: Geophysics, **80**, no. 5, C89–C105.

———, 2016, Theory of interval traveltime parameter estimation in layered anisotropic media: Geophysics, **81**, no. 5, C253–C263.

Sripanich, Y., S. Fomel, and P. Fowler, 2016, A comparison of anisotropic parameterizations for TI and orthorhombic media and their sensitivity with respect to qP velocities: 86th Annual International Meeting Expanded Abstracts, Society of Exploration Geophysicists, 479–484.

Sripanich, Y., S. Fomel, A. Stovas, and Q. Hao, 2017, 3D generalized nonhyperboloidal moveout approximation: Geophysics, **82**, no. 2, C49–C59.

Stopin, A., 2001, Comparison of $v(\theta)$ equations in TI medium: Presented at the 9th International Workshop on Seismic Anisotropy.

Stovas, A., 2010, Generalized moveout approximation for qP-and qSV-waves in a homogeneous transversely isotropic medium: Geophysics, **75**, no. 6, D79–D84.

———, 2015, Azimuthally dependent kinematic properties of orthorhombic media: Geophysics, **80**, no. 6, C107–C122.

———, 2017, Kinematic parameters of pure- and converted-mode waves in elastic orthorhombic media: Geophysical Prospecting, **65**, 426–452.

Sun, J., and S. Fomel, 2015, Lowrank one-step wave extrapolation for reverse time migration: Geophysics, **81**, no. 1, S39–S54.

Sun, J., S. Fomel, Y. Sripanich, and P. Fowler, 2016, Recursive integral time extrapolation of elastic waves using lowrank approximation: 86th Annual International Meeting Expanded Abstracts, Society of Exploration Geophysicists, 4145–4151.

Thomsen, L., 1986, Weak elastic anisotropy: Geophysics, **51**, 1954–1966.

———, 2014, Understanding Seismic Anisotropy in Exploration and Exploitation, 2 ed.: Society of Exploration Geophysicists and European Association of Geoscientists and Engineers.

Tsvankin, I., 1996, P-wave signatures and notation for transversely isotropic media: An overview: Geophysics, **61**, 467–483.

———, 1997, Anisotropic parameters and P-wave velocity for orthorhombic media: Geophysics, **62**, 1292–1309.

———, 2012, Seismic Signatures and Analysis of Reflection Data in Anisotropic Media: Society of Exploration Geophysicists.

Tsvankin, I., J. Gaiser, V. Grechka, M. van der Baan, and L. Thomsen, 2010, Seismic anisotropy in exploration and reservoir characterization: An overview: Geophysics, **75**, no. 5, 75A15–75A29.

Tsvankin, I., and V. Grechka, 2011, Seismology of Azimuthally Anisotropic Media and Seismic Fracture Characterization: Society of Exploration Geophysicists.

Ursin, B., and A. Stovas, 2006, Traveltime approximations for a layered transversely isotropic medium: Geophysics, **71**, no. 2, D23–D33.

Vasconcelos, I., and I. Tsvankin, 2006, Non-hyperbolic moveout inversion of wide-

azimuth P-wave data for orthorhombic media: Geophysical Prospecting, **54**, 535–552.

Vasin, R. N., H.-R. Wenk, W. Kanitpanyacharoen, S. Matthies, and R. Wirth, 2013, Elastic anisotropy of kimmeridge shale: Journal of Geophysical Research, **118**, 1–26.

Vavryčuk, V., 2003, Generation of triplications in transversely isotropic media: Physics Review B, **68**, no. 5, 054107–1–8.

Vernik, L., and X. Liu, 1997, Velocity anisotropy in shales: A petrophysical study: Geophysics, **62**, no. 2, 521–532.

Vernik, L., and A. Nur, 1992, Ultrasonic velocity and anisotropy of hydrocarbon source rocks: Geophysics, **57**, no. 5, 727–735.

Wang, Z., 2002, Seismic anisotropy in sedimentary rocks, Part 2: Laboratory data: Geophysics, **67**, no. 5, 1423–1440.

Willis, J. R., 1977, Bounds and self-consistent estimates for the overall moduli of anisotropic composites: J. Mech. Phys. Solids, **25**, 185–202.

Wu, T. T., 1966, The effect of inclusion shape on the elastic moduli of a two-phase material: Int. J. Solids Structures, **2**, 1–8.

Xu, X., I. Tsvankin, and A. Pech, 2005, Geometrical spreading of P-waves in horizontally layered, azimuthally anisotropic media: Geophysics, **70**, D43–D53.

Zhang, F., and N. Uren, 2001, Approximate explicit ray velocity functions and travel times for P-waves in TI media: 71st Annual International Meeting Expanded Abstracts, Society of Exploration Geophysicists, 106–109.

Zhang, Y., H. Zhang, and G. Zhang, 2011, A stable TTI reverse time migration and its implementation: Geophysics, **76**, no. 3, WA3–WA11.

Vita

Yanadet Sripanich was born in Bangkok, Thailand in 1990. He graduated from Triam Udom Suksa School, Bangkok in 2008 and earned a full scholarship on the same year from the Royal Thai Government to study Geosciences in the United States of America. He earned two Bachelor of Science degrees with the highest honors in Geophysics and Mathematical Sciences from The University of Texas at Austin in 2013. He also received a special departmental honors for his thesis on "An Efficient Algorithm for Two-Point Ray Tracing in Layered Media" and represented his graduating class as the valedictorian. He is a candidate for the degree of Doctor of Philosophy at the The University of Texas at Austin.

Permanent address: 503/29 Soi.Vipawadee 42 Vipawadee Rd. Ladyao
Chatuchak Bangkok, Thailand 10900

This dissertation was typeset with LaTeX[†] by the author.

[†]LaTeX is a document preparation system developed by Leslie Lamport as a special version of Donald Knuth's TeX Program.